A Study of Ion Beam Sputtering

of Compound Materials with Laser Spectroscopy

Thesis by

Shouleh Nikzad

In Partial Fulfillment of the Requirements

for the Degree of

Doctor of Philosophy

California Institute of Technology

Pasadena, California

1990

(Submitted May 22, 1990)

Acknowledgments

Throughout my graduate studies, I have had the privilege of working and associating with many outstanding scientists and wonderful human beings. For the work presented here, I have acted as the link between the two groups at Caltech and Argonne National Labs. This created an enviable situation for me to collaborate with great people, without whose help this work would not have been possible.

Tom Tombrello, my advisor, provided an environment of freedom for individual growth and independent thinking. With patience and constant support, he helped me overcome the hurdles of graduate work and obstacles associated with being a foreign student. With his incredible scientific insight, he saw through things that were only possible for me after pondering endless days and nights; his patience allowed me to figure things out for myself. For his encouragement and support, and for having me as a student, I express my gratitude.

I am indebted to the staff of Argonne National Laboratories. They were generous with me, both in sharing their fantastic equipment and their guidance. I thank: Dieter Gruen for his invaluable advice and sharing of his vast knowledge, and for being always available to talk to; Mike Pellin for his scientific insight, everlasting and contagious optimism, pep talks, and for his excellent talk at Caltech that made me want to go to Argonne; Wally Calaway for his scientific and technical support, without which I would have been lost in the maze of LFS and SARISA, for his patience and kind nature, for taking questions even at home and at odd hours; for all of his help with one of my many moves while at Argonne; Charlie Young for having answers to my questions even late

at night when I would knock on his office door, for giving me a hand in the lab when I needed more than two, and for helping me fix my car when I was stranded in the snow; Joe Burnett for many helpful and enjoyable discussions, for helping me in and out of the lab, and for putting up with me when we were sharing an office; Alan Krauss for answering my many questions and loaning me an ion gun power supply when mine was taking a break without me; Jerry Hunt for providing the power supply for the turbo pump and for generously lending me his Macintosh so that I could write and work on my data in the convenience of my office; Stephanie Christian for her valuable assistance with the administrative tasks throughout my association with Argonne; Shanna Coon for staying up with me several nights to help me get things done, for her cheery nature to make those hours pleasant, and for sending me home when I was getting too tired; Keith Lykke and his family for generously sharing their home with me, and for letting me keep Hobbes company for the last two weeks of my stay at Argonne; Dan Spiegel for his help in the last days of my stay at Argonne; Goerge Lamisch for keeping the SARISA electronics running and Jim Whitten for his general help.

Of the members of the group at Caltech I'd like to acknowledge: Steve Spicklemire, with whom I have had the fortune of collaborating, the results of which only appear in spirit in this dissertation, for all that I learned just by working around him, friendship, great sense of humor; Alan Rice for his very important technical support and his patience in going through practice sessions when I was getting ready for my candidacy exam; Bob Housley for much of the same in the days of the candidacy exam, and for helpful discussions and his very kind nature throughout all of it.; Michelle Vine for all of the administrative work at Caltech and for making the group feel much more at home and for being

a friend to me; Richard Borup and Steve Stryker for teaching me about design and machining; Brad Werner, for his support while I was writing this manuscript, and for cheering me up when I was in the low points; and all the other Brown Baggers who have had an effect on my technical (and not so technical) education.

I acknowledge the financial support of DOE, NSF, and Caltech without which this work would not have been possible.

I would like to thank Roya Maboudian, for all the good times and hard times she shared with me, and for all the e-mail she sent to me to Argonne so I didn't feel homesick. Many other special friends made these years that at times seemed endless, more bearable, Carlo Carraro, Bob Walker, Soosan Roodbari, Michael Mittelstein and Soheila Mirhashemi, Joan Frye, and Joel Blum.

My sincere love and appreciation goes to my family, who gave me love, support and encouragement, and made it possible for me to come to the States; also to my soon to become new family, for accepting me and for generously finding ways for Michael and I to see each other while I was at Argonne. Finally, I sincerely thank Michael Hoenk, for working very hard with me the last days of getting this document together, for listening to me talk about my work, for many phone calls to Argonne which were a blessing when nothing was working, and for believing in me.

Abstract

Single crystal metal sulfides of ZnS, CdS, and FeS_2 were bombarded with a 3 keV Ar^+ beam. The secondary neutrals sputtered from the suface of the target were interrogated by laser ionization mass spectrometry and laser fluorescence spectroscopy .

The velocity distribution and yield of sputtered Fe from a FeS_2 sample were measured. The velocity distribution of Fe sputtered from the sulfide is qualitatively the same as that of Fe sputtered from the pure metal. The yield of Fe from the sulfide target, after prolonged bombardment, was at most 20% of the yield from the metal. The results are compared with Monte Carlo calculations using the TRIM (transfer of ion in matter) code. Total sputtering yields of ZnS, CdS, and FeS_2 were measured by profilometry and were compared with the same measurements of sputtered metal targets.

We have demonstrated the necessity of measuring sputtered molecules and excited state neutrals for accurate yield evaluation. The population distribution of ground state multiplets of sputtered Fe from FeS_2 is compared with that measured from an Fe target. The excited state population of sputtered Fe is slightly higher in the FeS_2 target (~10%). Molecular yields have also been measured by laser ionization mass spectrometry from ZnS, CdS, and FeS_2 . S is sputtered predominantly as S_2 from all three crystals. Metals are sputtered as the atom, metal sulfide, and metal dimer (except in the case of Fe_2). The yield of the metal sulfide

molecules is about 10% of the yield of the metal. Plausible formation mechanisms of molecules and excited state neutrals are discussed.

Table of Contents

Chapter One

Introduction

Sputtering is the ejection of particles from the surface of a solid due to energetic primary particles impinging on the surface. The primary particles can be positive or negative ions (ranging in energy from hundreds of eV to MeV), electrons, photons, or neutral energetic particles. Sputtering is divided, according to mass and energy of the primary ions, into electronic, collisional cascade, thermal, and spike regimes. This division into the categories also depends on the nature of the sample under bombardment. The yield of the secondary particles and the energy distribution of the sputtered particles can be different for the various sputtering regimes.

Since the potential applications of ion beam sputtering in processing, growth, and analysis of materials have been realized, the ion beam interaction with a solid surface has been the subject of much research. The sputtering phenomenon has been studied extensively for the last 30 years. Sputtering is used for the etching

step of electronic device processing as well as in the growth of thin films. Secondary ion mass spectrometry (SIMS) is used pervasively as a very sensitive analytical tool for trace, compositional, and surface analysis and depth profiling. For a long time the secondary ions produced in sputtering were the main window into the sputtering mechanism. A far more powerful technique, namely laser ionization secondary neutral mass spectrometry has been developed in the last decade. In this technique, the sputtered neutral atoms, which constitute the majority of the sputtered species can be detected. RI(M)S (resonance ionization (mass) spectroscopy) or NRIS (nonresonant ionization spectroscopy), which are distinguished by the ionization scheme employed, are two of the mass spectrometric techniques for detecting sputtered neutrals.

Another method of the detection of neutrals is LFS (laser fluorescence spectroscopy). In this method sputtered atoms are resonantly excited by a laser. The fluorescence from the de-excitation of the sputtered atoms is detected and the light intensity is proportional to the number density of the sputtered atoms. With this technique, relative sputtering yields information and the velocity distribution of the sputtered particles can be determined. Some low resolution angular information is also obtainable.

The two methods of secondary neutral analysis mentioned above were used for the measurements in this dissertation and are discussed in more detail in Chapter 2.

1.1 Sputtering Parameters

For the medium mass primary ions, such as Ar^+, sputtering is in the linear cascade regime where the energy is transferred to the solid through elastic collisions. In the sputtering theory for metals, the maximum energy transferred to an atom from an ion with energy E is

$$TE_{max} = \frac{4m_1m_2}{(m_1 + m_2)^2}E , \quad (1.1)$$

where m_1 and m_2 are the masses of the primary ion and atom, respectively, and TE is the transferred energy. The final ejection of particles from the surface involves a complex series of energy transfers between many atoms in the target. This mechanism is referred to as the 'collisional cascade.' Figure 1.1 depicts the surface of a target (x=0) and an escaped atom from that surface. The outward current of the atoms (J) leaving the surface due to bombardment by ions at an angle (θ) is

$$J(E_o, \Omega_o) \propto \psi F_D(E, \theta) \frac{dE_o}{E_o |dE_o/dx|} |\cos\theta_o| \frac{d^2\Omega_o}{4\pi} \quad (1.2)$$

where θ_o is the recoil angle (inside the cascade) with respect to the normal to the surface, E_o is the energy of an atom in the cascade, ψ is the flux of primary ions, F_D is the density of deposited energy and is defined in equation (1.6), dE/dx is the nuclear energy loss, and Ω is the solid angle. Assuming a planar surface potential of barrier E_b,

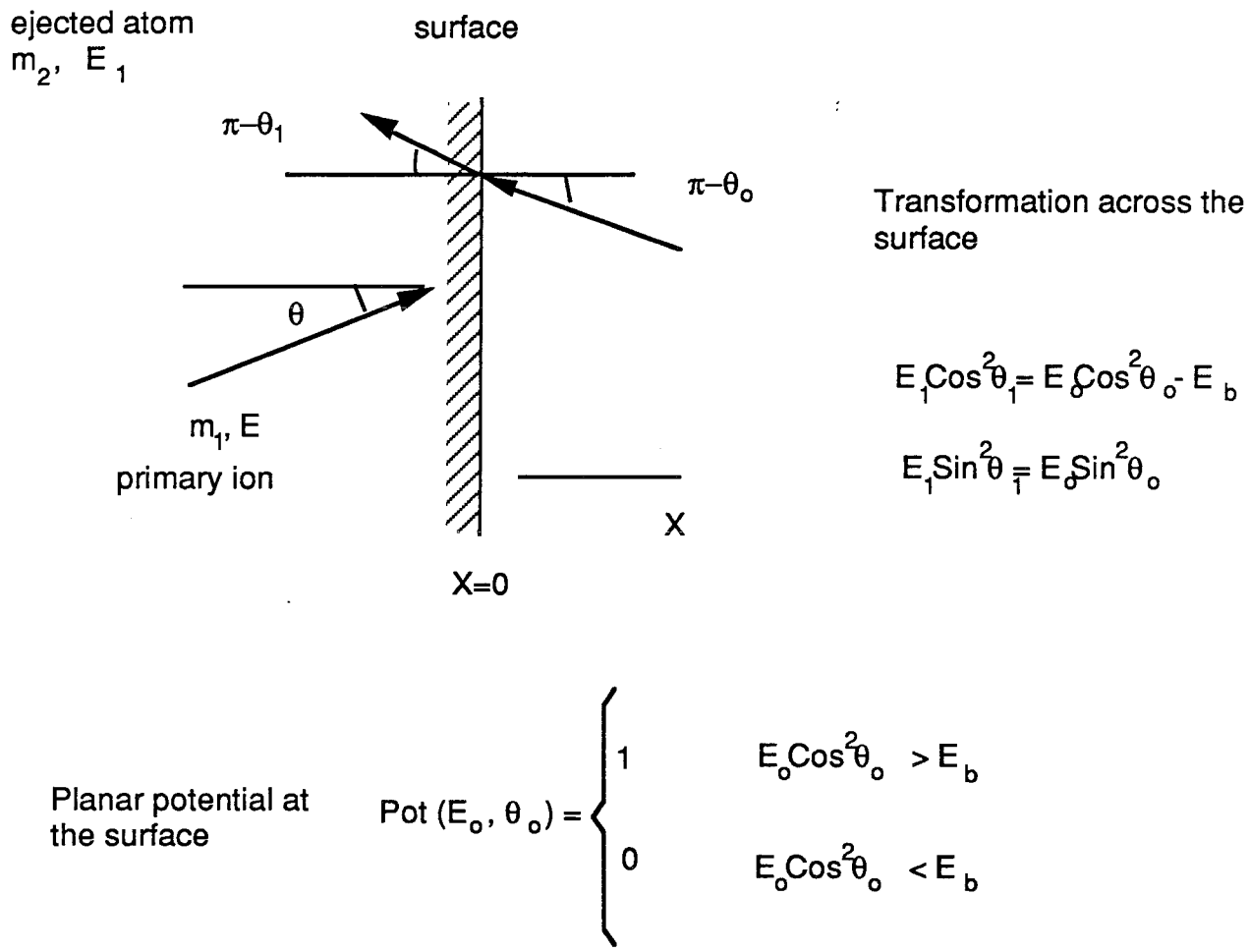

Figure 1.1 The sputtered particle has an energy E_o inside the cascade. As it goes through the surface, the transformation shown above incorporates the surface binding energy.

the yield of the sputtered atoms is given by integrating (1.2) and making the proper transformation for the energy inside and outside the solid, the differential yield of the sputtered atoms can be obtained by

$$\frac{d^3Y}{dE_1 d\Omega_1} \propto \frac{E_1}{(E_1+E_b)^3} |\cos\theta_1| \ . \quad (1.3)$$

Equation (1.3) indicates the energy and angular distribution of the sputtered particles, where E_1 is the energy of the sputtered particles, θ_1 is the angle of ejection, and $d\Omega_1$ is the differential solid angle.

The yield of the ejected particles is defined as the average number of ejected particles per primary particle (ion). According to the linear cascade theory for metals by Sigmund[1,2] the yield is expressed as

$$Y = \Lambda F_D(E_o) \ . \quad (1.4)$$

The first term Λ contains the target characteristics. It defines the cost to the solid of losing an atom, and it is derived from the linear cascade theory as

$$\Lambda \approx \frac{.042}{NE_b} \quad (\text{Å/ eV}) \ , \quad (1.5)$$

where N is the atomic density of target atoms, E_b is the binding energy of the atom to the surface, which is usually estimated to be

equivalent to the heat of sublimation of the solid. The second term in eq. (1.4) contains information on the energy transfer between the primary particle and the solid, i.e., the energy loss as a function of position in the solid. The term $F_D(E_o)$ is called the density of deposited energy at the surface and is defined as

$$F_D(E_o) = \alpha N S_n(E_o) , \quad (1.6)$$

where $S_n(E_o)$ is the nuclear stopping cross section, $NS_n(E_o)$ is the nuclear energy loss, and α is a correction factor.

Sputtering of compound materials, the subject of investigation of this dissertation, is an area of sputtering that, although very important, has not been studied in a comprehensive manner.

There is an abundance of information available in the literature on the sputtering of elemental targets, especially the sputtering of metals. Some understanding of the sputtering of insulators and semiconductors also exists. The information on metal sputtering is in the form of experimental measurements, analytical results, and computer simulations. Due to the complexity of the sputtering of a compound material, theoretical treatments of the problem do not exist, and there are few experimental results. Some of the complexities stem from the mere presence of a second element in the matrix. Sputtering of multi-component targets has been the subject of some investigations such as sputtering of different isotopes[3] or sputtering of alloys[4]. Issues of preferential sputtering and surface

segregation have been demonstrated in these studies. To first order, the particles of lower mass and smaller binding energy will be sputtered more easily, leaving the surface of the material depleted in that species and enriched in the other. This effect will in turn change the sputtering rate until enough material has been removed, and then the sputtered material will be representative of the bulk concentration. In a compound material, however, the chemistry also plays an important role. Some of the energy of the primary ion is spent in breaking chemical bonds. In addition, due to bombardment, the nature of the chemical bonds can change, adding more complexity to the problem. Compound materials also fit into different categories with respect to their electrical properties. Depending on their electronic characteristics, these materials respond differently to bombardment by charged particles.

Although sputtering of compound materials is a difficult problem, there are scientific and technological advantages that make the effort worthwhile. For example, after prolonged bombardment of an elemental sample, the embedded primary ions form a binary target with the sample. In case of using a reactive primary ion beam such as O (for example for SIMS), the binary target would be an oxide of the target. From the application standpoint, almost all the materials used for thin film growth are compound materials (e.g., optical coatings, and oxides grown in semiconductor processing).

There are two major points to the study in this dissertation: The understanding of the sputtering of compound materials and also the

quantitative evaluation of the techniques of detection of sputtered neutral atoms. It is perhaps ambitious to talk about a study of the compound material sputtering, because of the diversity of material properties (for example, in the sputtering of alkaline halides, the halogen is sputtered in thermal sputtering regime, and the metal is sputtered in the collisional cascade regime[5]). Thus, we have chosen a subclass of compound materials, i.e., metal sulfides for this study. The characteristics of sputtering of Fe from FeS_2 are presented in Chapter 3.

1.2 Metastable state population distribution of sputtered atoms

The most important aspect of this study is the quantization of the secondary neutral atom mass spectroscopy technique. There is an abundance of information both theoretically and experimentally regarding the ionization process of the sputtered atoms - especially from a metal target. For most studies, it has been assumed that the sputtered neutrals that are ejected in excited states are formed by the same mechanism as the secondary ions. To that extent some theoretical models also treat the excitation of the sputtered species. Some of these models are described in Chapter 4. There are more experimental data available regarding the sputtered excited neutrals - mainly from metals and alloys. In Chapter 4, measurements of the metastable state population distribution of the ground electronic

state sputtered Fe atoms are described along with some of the measurements in the literature.

Though the models differ in the details of the treatment, they can be separated into three general categories of thermodynamical, quantum mechanical, and collisional statistical treatment.

1.3 SPUTTERING OF MOLECULES

During the period that SIMS has been used as an analytical technique for depth profiling, the background due to molecular sputtering has been regarded an interference. In the same way, sputtered molecules are a source of noise in the detection of neutral atoms. In order to obtain a more precise measure of the sputtered neutral atoms, the fraction of the sputtered molecules needs to be known. To understand the sputtering of molecules, the real question is to determine the mechanism of their formation. The internal energy distribution of the molecules should be studied in addition to the kinetic energy and angular distribution of molecules. Depending on the formation mechanisms, sputtered molecules may be predominantly vibrationally or rotationally excited. The studies suggested above are complicated experiments, due to the fact that the signals from the internal energy states could be quite small. To overcome this difficulty, very sensitive methods of detection should be employed, in addition to a careful choice of samples. To make the problem more manageable, one should study molecules of known spectroscopy, such as S_2. A study with the LFS technique of S_2

molecules sputtered from a frozen CS_2 target and an amorphous S target were conducted by workers at the FOM Institute. Time-of-Flight methods were employed for investigation of the velocity distribution of the sputtered molecules. Internal energy distributions of the S_2 molecule were also measured with LFS.

A few other sporadic measurements on sputtered molecules have used different methods of detection, such as SIMS and light emission from excited molecules.

In order to study the molecular sputtering of a binary target, the sputtered molecules must first be identified. Then, the yield of the molecules should be investigated. In fact, a quantitative study of molecules sputtered from materials of different crystalline structures provides valuable information regarding the formation mechanism of the sputtered molecules. Because sputtering from a compound material entails competition for the formation of different dimers, molecules of lesser known or unknown spectroscopy are also produced. Again, some valuable information can be obtained by probing these molecules using lasers having different photon energies (see Chapter 5).

To summarize the existing theories, two methods of molecular formation have been postulated. In the first method, the molecule is formed above the surface of the sample due to gas phase collisions or interaction with the solid as the third body. The other method suggests the formation of the molecules inside the solid and the

ejection of the molecule from the surface via collisions. There are sub-categories in the second theory regarding collisions leading to sputtering. The ejection mechanism can be best understood by studying the internal energy distribution of the sputtered molecules.

Some molecular dynamics calculations also have been performed for these systems. To date, most predictions by molecular dynamics calculations have supported the theory of molecular formation in the space above the sample surface. Whereas these calculations are purely classical, the formation and ejection of the molecules from a sample under ion bombardment is quantum mechanical in nature. The classical theory is, therefore, incomplete. Until further experimental results are obtained, the classical simulations serve a valuable purpose in providing prediction for the probability of simultaneous ejection of two or more atoms very close together in space, which is one of the criteria for the formation of a molecule.

1.4 References

1 P. Sigmund in *Sputtering by Particle Bombardment I*, R. Behhrisch ed., Topics Appl Phys., **47**, 9 (Springer-Verlag, Berlin, 1981).

2 L.C. Feldmann and J.W. Mayer, *Fundamentals of Surface and Thin Film Analysis* (North Holland, New York, 1986).

3 D.L. Weathers, 1989, Ph.D. Thesis, Caltech and S.J. Spicklemire, 1990, Ph.D. Thesis, Caltech.

4 M.F. Dumke, T.A. Tombrello, R.A. Weller, R.M. Housley, and E.H. Cirlinm, Surf. Sci. **124**, 407 (1983).

5 M.L.Yu, D. Grischkowski, and A. C. Balant, APL **39**, 703 (1983).

Chapter Two

Apparatus

The two pieces of apparatus used for the experiments presented here are SARISA and the LFS instruments at Argonne National Labs., both of which are based on the analysis of the secondary neutrals that result from ion beam sputtering. A brief description of both systems is included in this document to explain the changes made for these particular experiments. A section is devoted to each instrument. Each section is organized in the following way; first the principles of the method are explained, then the instrument is described. Figures are included in each section following the text.

2.1. Laser Fluorescence Spectroscopy

Concept

Figure 2.1 shows the schematic of the experimental arrangement. A 3 keV Ar^+ impinges on the target at an angle 14 degrees to the target normal. A fraction of the sputtered species cross the path of the probe laser. The laser is in resonance with one

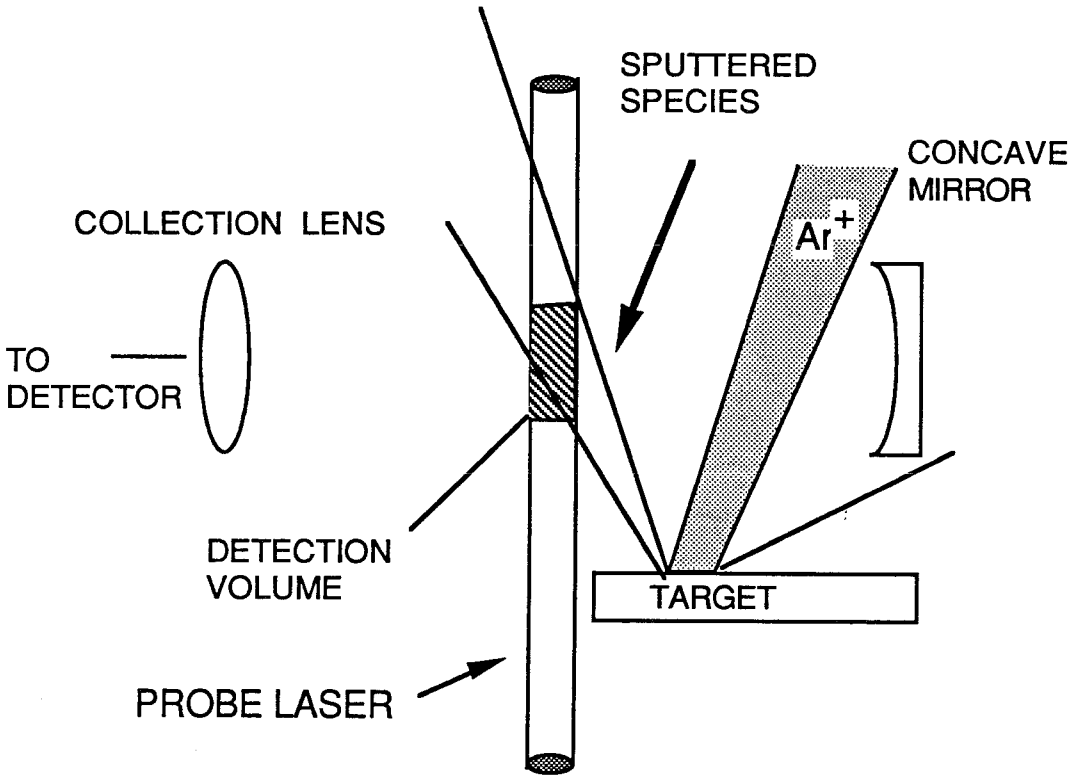

Figure 2.1 A schematic view of the LFS experimental arrangements.

transition from the ground state to an excited state of the sputtered species, therefore causing excitation of some of the particles that cross its path. Fluorescence from the de-excitation of these species is focused into the detector. The signal intensity is proportional to the number of atoms that interact with the laser in the detection volume. The fluorescence contains Doppler shifts, and as the laser is scanned in frequency this Doppler broadened signal is detected. The frequency scan is then converted to a velocity distribution of the sputtered species. This apparatus is element specific and, for a given run, data can be obtained for that element. The information obtained by this apparatus is: velocity distribution; relative population of the energy states; relative sputtering yields; and low resolution angular sputtering distributions.

The efficiency of this method is determined by: (a) the number of sputtered neutrals that are excited; and (b) the fraction of the fluorescence light that is detected. The latter is a simple matter of optimizing the solid angle, and, therefore, the geometry of the optics, the position of the laser, and the angle of ejection of the particles. The former depends on the cross section of the transition, the flux of the photons, the lifetime of the transition, the laser pulsewidth, the velocity of the sputtered particles and therefore the geometry of the target and the laser beam. These factors will be discussed in later chapters[1].

2.1.2 Instrument

a. Ion Beam

The commercial ion gun made by Varian (model 981-2043), can produce about 14 μA of Ar^+ ion current focused to a spot of 2.5 mm in diameter at 5 cm below the tip of the gun. There are two deflectors and a focusing lens in the gun. While running the ion gun, the ion pump, which is the principle pump of the UHV chamber, is turned off and the chamber is back filled with Argon causing the pressure to rise to $6x10^{-5}$ torr. The base pressure of the chamber is $2x10^{-10}$ Torr. The ion beam is pulsed synchronously with the probe laser to minimize the coverage of the light optics by sputtered material, and to reduce damage to the target. The ion beam pulses are about 16 μsec long and the pulser is homemade. The pulsing action is accomplished by deflecting the beam enough so that it misses the target. There are no apertures to stop the beam from being reflected from the walls of the chamber.

b. Laser

There are stringent requirements on the laser, therefore making this part of the instrument the most important one to understand and the most challenging to operate. The laser has to be tunable (for selectivity), UV (to reach ground level transitions), narrow-band (to resolve the Doppler linewidth), and can be scanned uniformly. Figure 2.2 depicts the laser system. A visible cw tunable

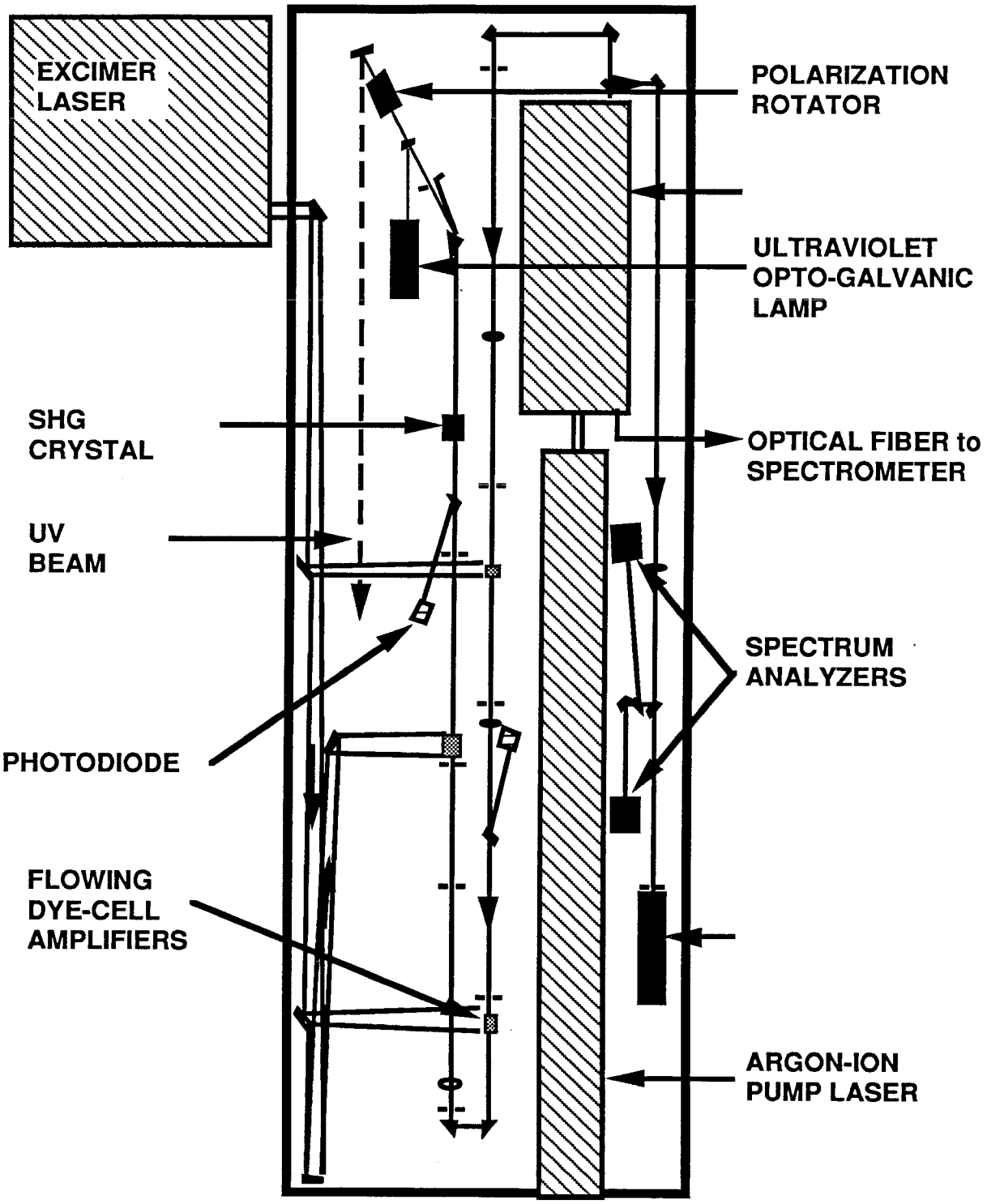

Figure 2.2 The layout of the optics that generate the laser light for the LFS experiments. The laser beam is sent to the UHV chamber by the mirror located after the polarization rotator.

narrow linewidth (20MHz) light is generated by a Spectra Physics ring dye laser model 380A, pumped by a Spectra Physics Ar ion laser model 171. The power necessary to run an experiment is generally 250 to 300 mW from the ring laser. To obtain tunable UV, this visible light (302nm for Fe atom transitions) is amplified before passing through a KH_2PO_4 (KDP) crystal for second harmonic generation (SHG). The three amplifiers are flow-through dye cells that are pumped transversely by a Lumonics excimer laser model TE 181T operating with XeCl at 308nm. The minimum requirement of the pulse energy at 10 Hz is 55mJ/pulse. By using Ne instead of He as a buffer gas in the laser gas mixture, we were able to obtain 90mJ/pulse output. The excimer laser output is divided to 10%, 30%, and 60% onto amplifying cells 1 through 3, respectively. The final amplification is normally about 6 orders of magnitude depending on the ring power, freshness of the dye in the cells, and the excimer gas. The amplified light goes through the doubling crystal followed by a prism to separate the UV and the visible light. The efficiency of the crystals is at best about 20%, resulting in the generation of UV pulses with 0.5 to 1.3 mJ of energy. Since the efficiency of the SHG crystals increases with the input light intensity[2], the amplification takes place before frequency doubling. Arranging the process in this order also reduces the background from amplified spontaneous emission that can be generated by the excimer laser pumping the flowing dyes. The UV pulses are 10 nsec long - the same length as the excimer laser pulses. The linewidth of the laser is estimated at this point to be 200MHz[3]. Part of this broadening comes from the Fourier Transform pulse limit (the flowing dye cells are pumped by a pulsed

laser) and partly due to the doubling crystal. The UV light is sent by a mirror from the optical table into the UHV chamber through a Brewster quartz window and leaves the chamber through a similar window after intercepting the sputtered species. The flight tubes of the laser before and after the UHV chamber are long, blackened baffled tubes and are provided to minimize the amount of scattered light that can leak into the detector.

Before going through amplification, a small portion of the ring dye laser (10%) is picked off for frequency analysis. The ring laser is first coarsely tuned through a spectrometer, then further interrogated by matching the absorption spectra of an iodine cell. The scanning of the laser is monitored with two etalons (3 and 300 GHz) to look for mode hopping. Any irregular scanning or so-called mode hopping of the laser leads to lack of signal in the experiment, so, in an iterative process, the different tuning elements of the laser are adjusted to give smooth scanning. The maximum scanning interval of the laser is one wave-number(cm^{-1}) or 30 GHz. The zero velocity transition frequency (no Doppler shift) of the sample is marked by the optogalvanic signal from a hollow cathode lamp. The cathode of the lamp must be made of the same material as the sample under investigation in the experiment. The lamp is biased at 200V and a discharge is seen. Before sending the UV beam into the chamber, 1-2 % of it is sent into the center of the hollow cathode lamp. The laser is scanned and tuned in frequency until the optogalvanic signal due to the atomic transition of the cathode is observed on an oscilloscope. The scanning start frequency of the

laser is locked to the optogalvanic signal frequency by the ring laser electronics. This completes the frequency requirements of the laser. The power of the UV beam is monitored by a photodiode at the exit from the chamber. The experiments are performed at 35 Hz, usually averaging over 200 to 500 laser shots in 30 GHz scans. The scanning of the etalons, the optogalvanic signal, and the photodiode output are monitored in duration of the experiment and are displayed with the output signal.

c. Detector

The fluorescence light is imaged onto a cooled PMT (EMI model 9659 QB) by a lens and a concave mirror through a bandpass filter of 10 Å spectral width. Because of the fact that the probe laser is narrow linewidth and only excites the atom of interest, high level discrimination is not necessary[4]. It is necessary, however, to suppress stray light - such as light from ion gun filament or scattered laser light. The suppression of light is accomplished by the interference filter mentioned above. The lens and the mirror are inside the UHV chamber and the filter is outside the chamber at the exit port of the fluorescence light. The signal from the PMT is either charge digitized or the individual photo-events are counted - depending on the intensity of the fluorescence. The detector is gated for noise discrimination.

d. Sample and Sample Holder :

Two samples can be loaded at the same time in this apparatus. The sample manipulator has x, y, z, and rotation degrees of freedom. The schematic in Figure 2.3 shows the geometry of the two samples in the chamber.

e. UHV Chamber:

As shown in Figures 2.4, 2.5, and 2.6, the UHV chamber is pumped by an ion pump and the pressure is monitored by an ionization gauge. As mentioned before, the base pressure is $2x10^{-10}$ Torr, and during the sputtering experiments the ion pump is turned off and the chamber is back filled with Argon, bringing the pressure to $5x10^{-5}$ Torr. The roughing stage of pumping is managed by two sorption pumps, which are not shown in the schematics.

f. Data Acquisition:

Data collection and experiment control is performed by LSI 11/23 computer through a CAMAC crate. The data acquisition process starts with the ion beam striking the sample. The laser (15nsec) is fired at the falling edge of the ion beam pulse (16μsec). The signal collection is started by positioning the detector gate at the center of the laser beam. The detector is gated (100nsec) for the reduction of the noise that is the result of any other light besides the fluorescence. The level of this noise or background is measured by

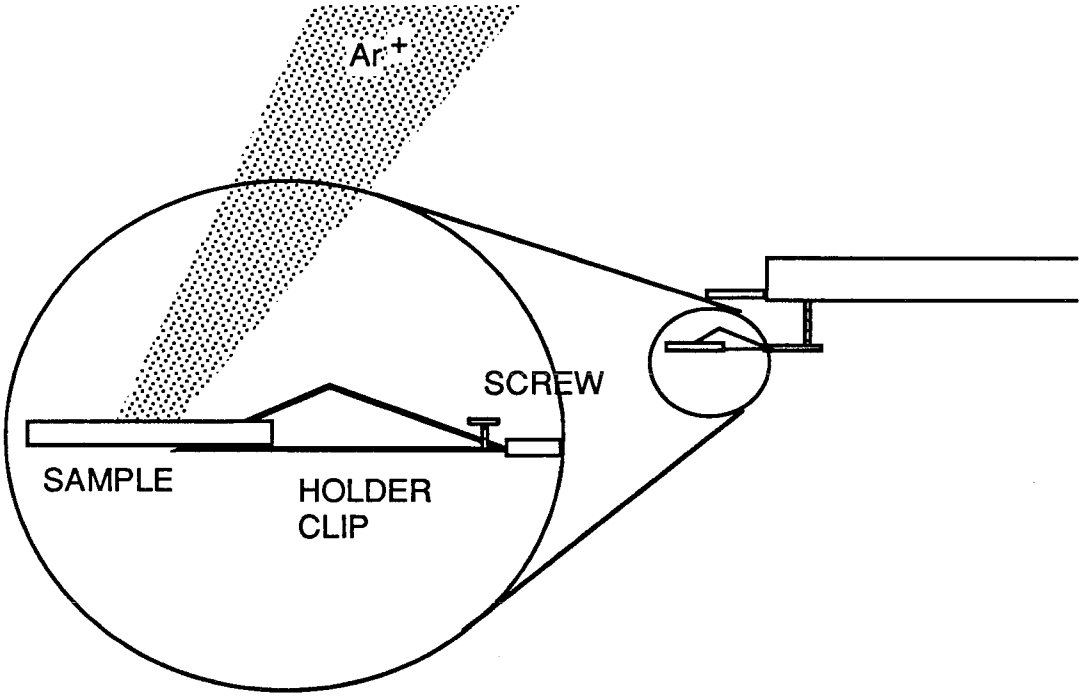

SAMPLE HOLDER SIDE VIEW

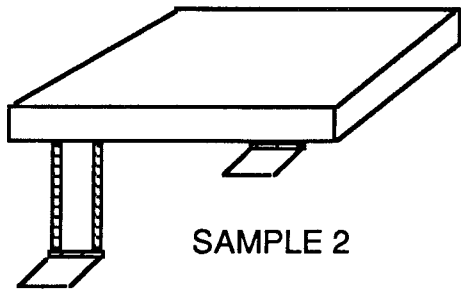

SAMPLE 1

SAMPLE HOLDER FRONT VIEW

Figure 2.3 A close up view of the sample holder. The holder is rotated by the manipulator to position one of the two samples in the beam line.

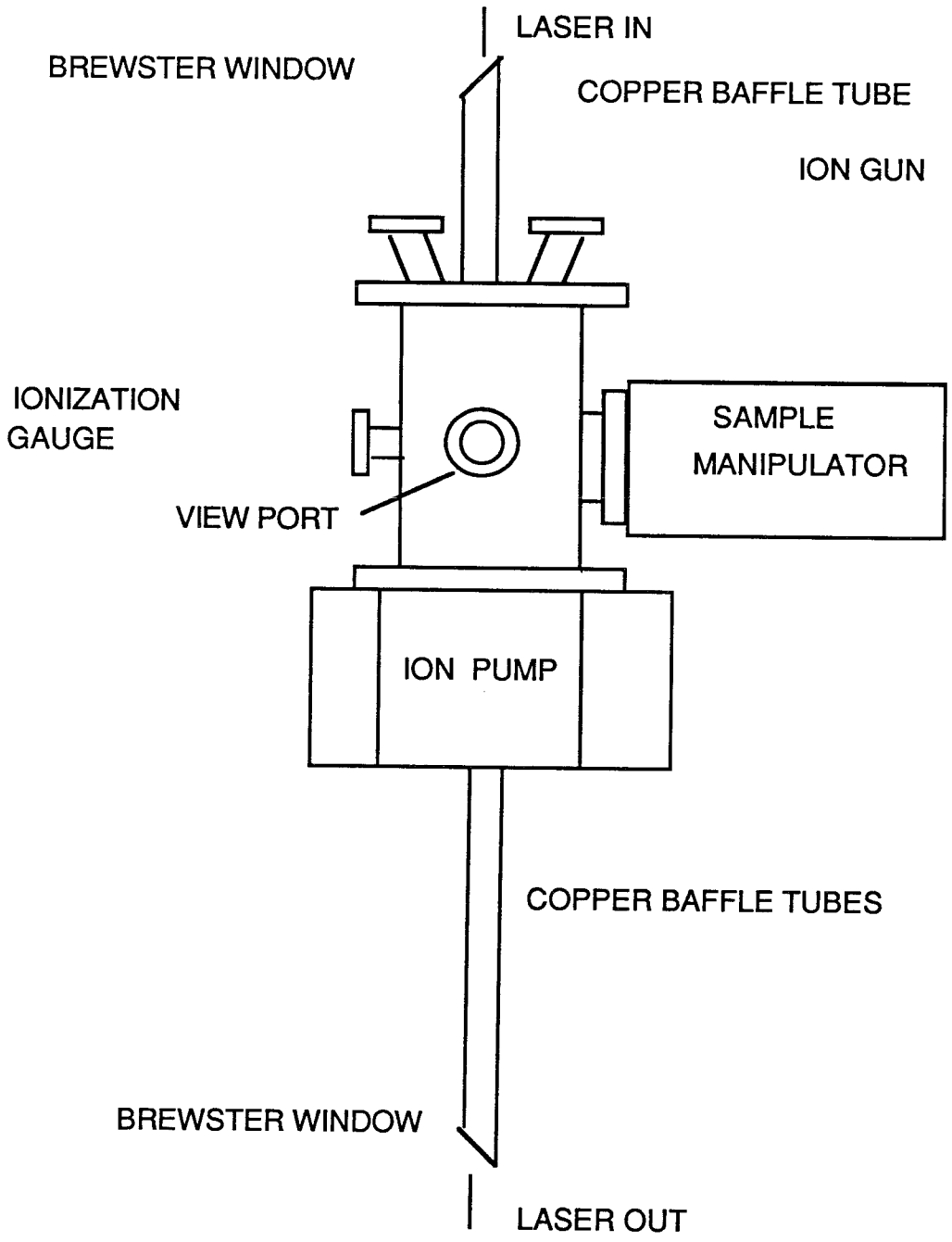

Figure 2.4 Front view of the LFS UHV chamber.

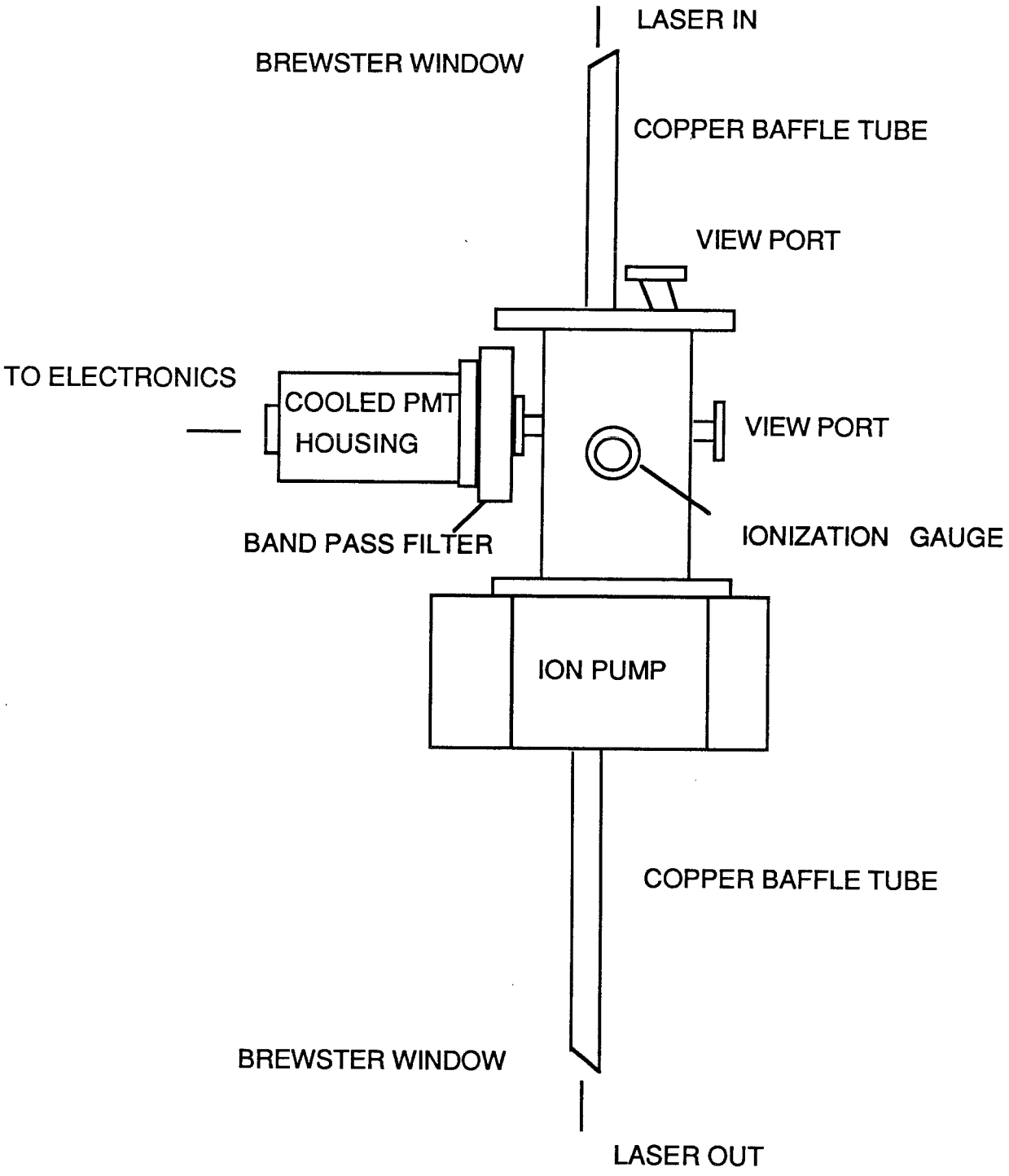

Figure 2.5 LFS UHV chamber side view.

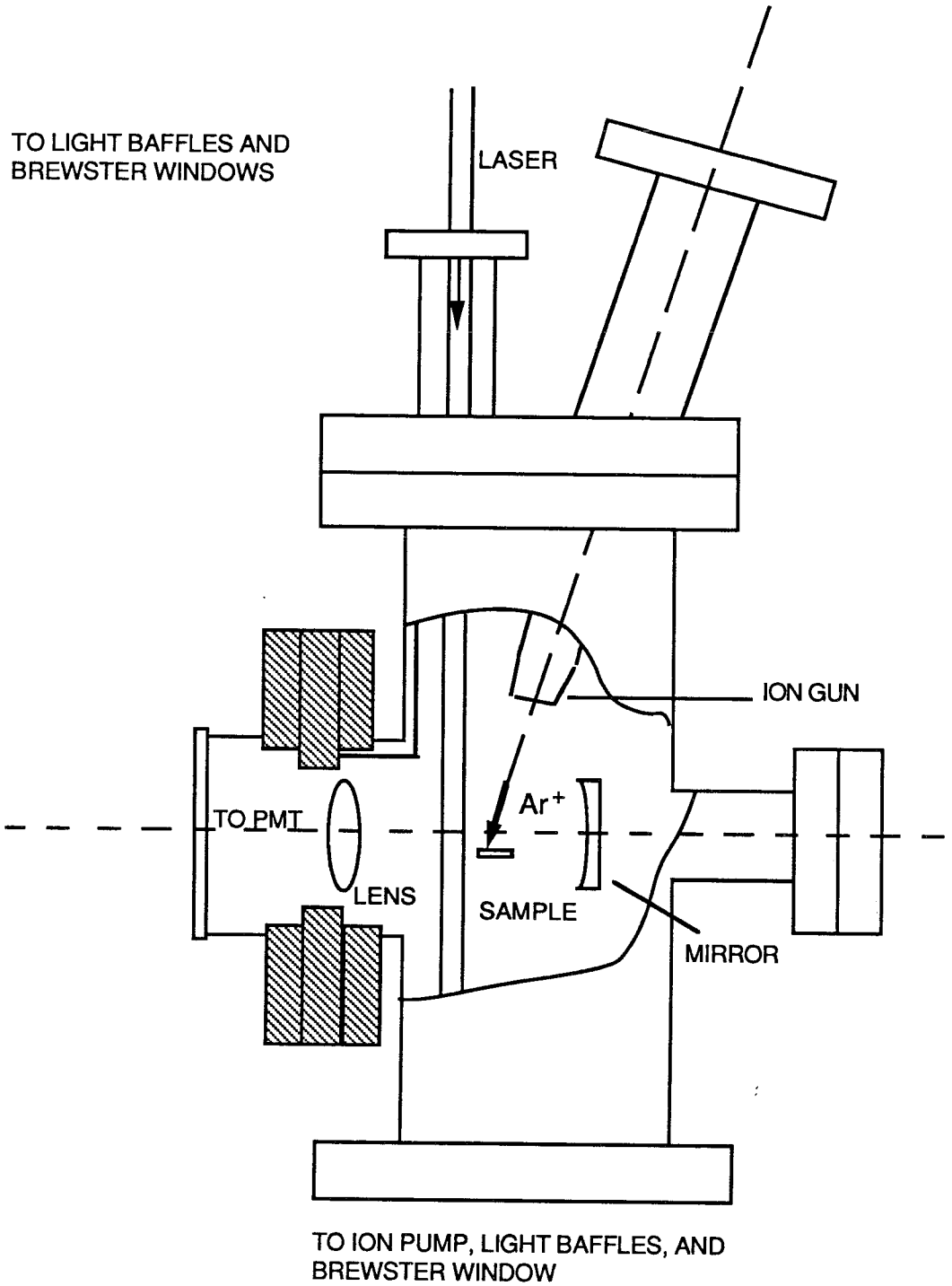

Figure 2.6 The LFS UHV chamber and a view of the experiment in the interior of the chamber. The laser system is described in Figure 2.2. Besides the light baffles, there is a bandpass filter before the detector to reduce the background light into the photomultiplier tube.

another gate at the detector following the signal gate to subtract the background]from the signal. As mentioned before, the pulsing of the ion beam does not influence the timing of the experiment, rather it is a damage-preventive method. For analysis, data files are transferred in ASCII format to a Macintosh computer. The signal obtained from the experiment is a Doppler shifted signal from the atomic transition chosen. This signal is accompanied by the etalons' scan, the optogalvanic signal, and the photodiode output (UV beam power monitor). These allow the extraction of velocity distribution, and relative yields population. Figure 2.7 shows a typical output of an experiment.

2.2 SARISA

2.2.1 Concept

Figure 2.8 shows a schematic view of the SARISA apparatus. The ion beam strikes the sample, generating secondary neutrals and ions in the form of atoms, molecules, and clusters. Sputtered particles are ejected in all directions. The probe laser, which is generally focused for increasing the photon fluence, moves parallel to the surface of the target about 1mm away from the surface. A fraction of the sputtered particles cross the path of the laser. Ionization probabilities of unity are possible if the laser fluence saturates the excitation and ionization transitions. The photoions are

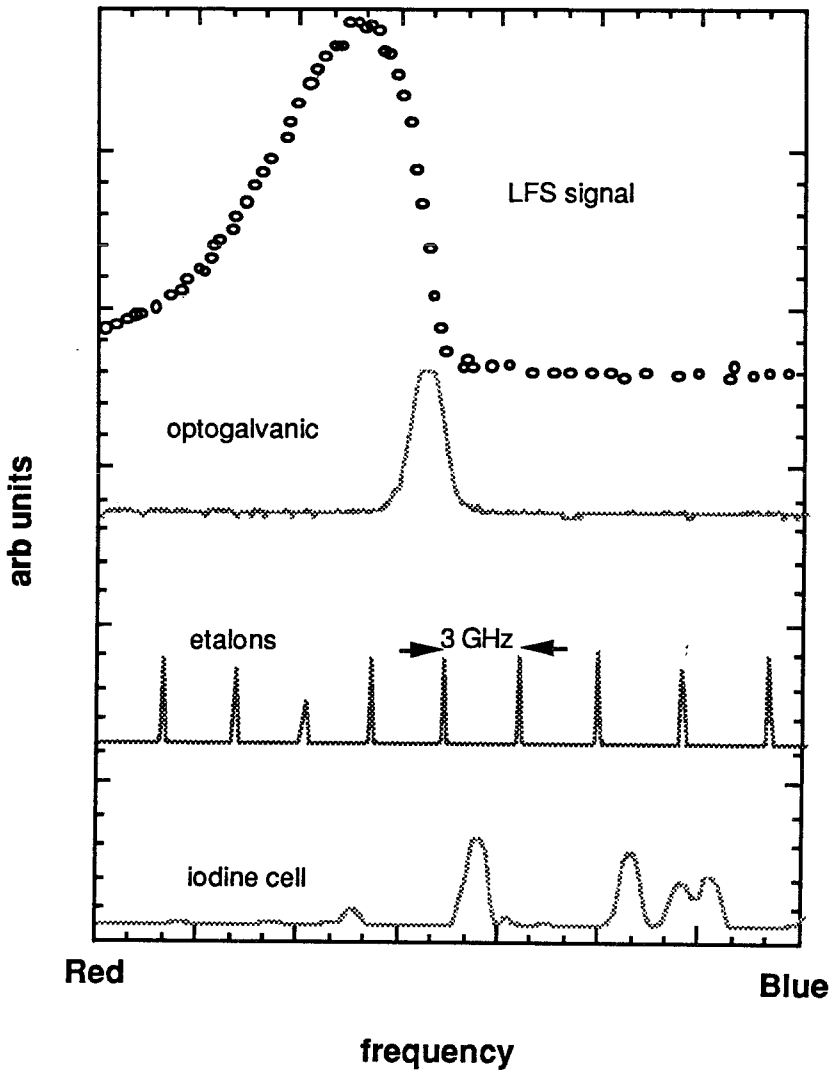

Figure 2.7 A typical output of the LFS experiment for ground state transition of Fe. The optogalvanic signal indicates the Doppler-free transition (zero velocity). The free spectral ranges of the etalons are 3 GHz and 300 GHz. The full frequency range shown here is one scan of 30 GHz. The iodine absorption lines provide means of tuning the laser frequency to the correct transition frequency of Fe.

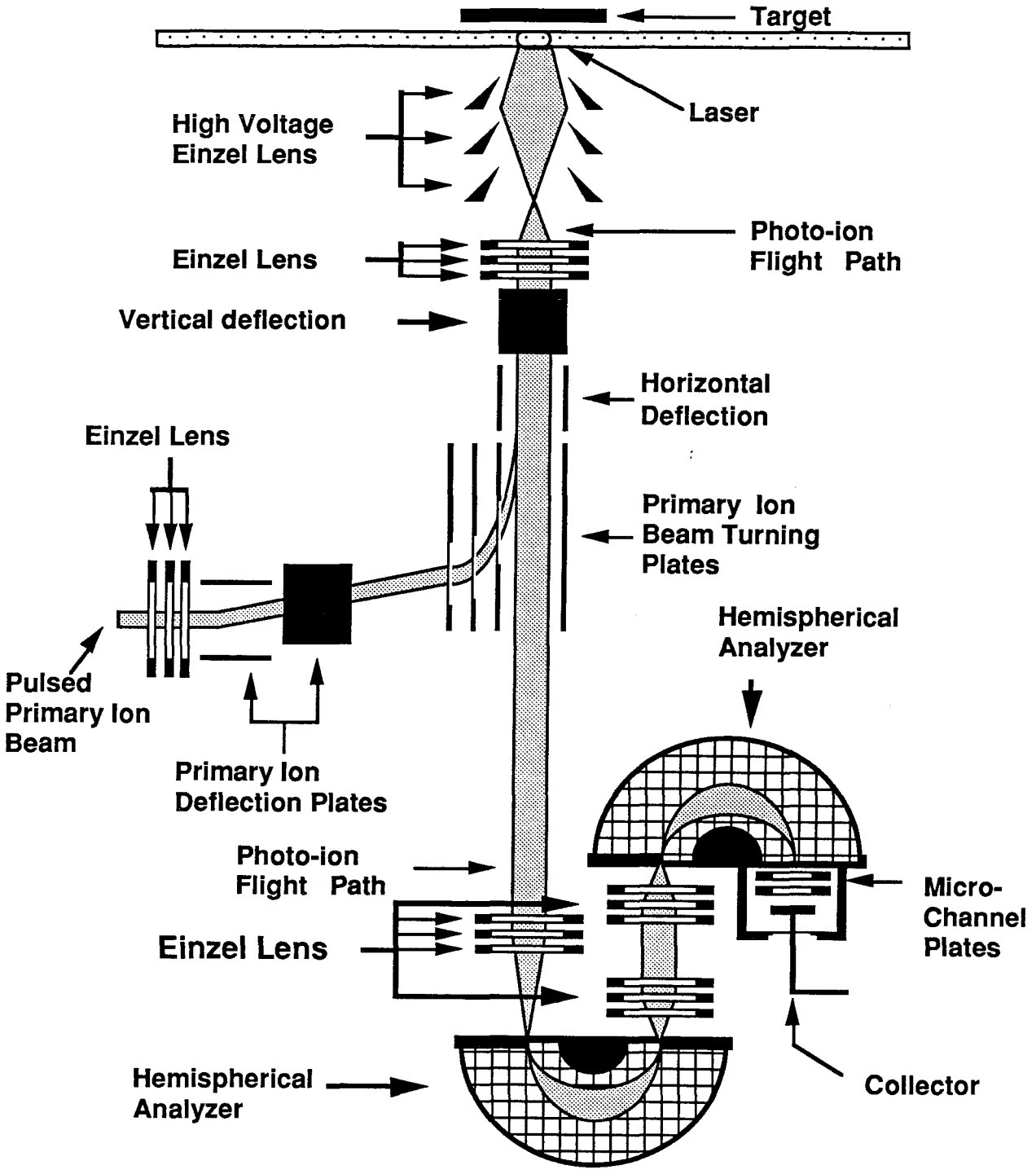

Figure 2.8 A schematic diagram of the SARISA apparatus.

detected with microchannel plates after passing through a time-of-flight (TOF) mass spectrometer. This method of detection gives the apparatus very high sensitivity.

2.2.2 Instrument

a. Ion Source

The primary ion beam, a 5 keV Ar^+ is generated by a commercial Colutron source. The current on sample is about 2 μA, with an ion beam diameter of 200 μm. The ion beam can be pulsed and has a variable pulse width from 100 nsec to 2 μsec. The pulsing of the ion beam takes place by pulsing the voltage on the deflection plates. The ion beam can also be operated in the raster mode where the ion beam scans an area of up to $4mm^2$.

b. Laser

There are two Questek excimer lasers, models 2660 and 2860, two Lumonics, and one Molectron excimer pumped dye lasers available to the SARISA apparatus. This provides a number of combinations of lasers to be used for the resonant and nonresonant ionization experiments. There is one entrance window for the laser in the SARISA chamber. In case of multicolor experiments a view card at the exit port of the chamber is used for alignment of the

multiple laser beams to insure spatial overlap in front of the sample. The same card is used as a beam block during the experiments for safety reasons. For power study experiments, a power meter monitors laser power at the exit port.

i. NRIS

An excimer laser (ArF, XeCl, KrF, KrCl) is used to nonresonantly ionize the sputtered species. For most species, this is a multiphoton process. A very powerful feature of this method is the capability of ionization without discrimination, and therefore allows the detection of a number of species in a given experiment. The ionization efficiency is not the same for all materials, so the information obtained from this process is qualitative. Quantitative information can be obtained by saturating the transitions. Monitoring the signal level while changing the laser power determines the laser power necessary to saturate the atomic (or molecular) transition. Saturating a transition is usually obtained more easily with less laser power using the more selective method of resonance ionization spectroscopy. To overcome isobaric interferences that are a source of noise in the NRIS method, the more selective method of resonance ionization can be employed.

ii. RIS

Tunable dye lasers are used for the resonance ionization of the material. For multiphoton experiments in which more than one dye

laser is used, the pump excimer laser beam is divided according to the power needed for the atomic or molecular transition. As a general rule, ionization transitions have orders of magnitude lower cross sections[5], and therefore require more power than the excitation transition. Lasers used for the ionization process therefore require higher power. The ionization and the excitation processes can be saturated by choosing the right geometry and laser power.

c. Timing

To better understand the description of the post-ionization process and the detection of the secondary particles, the timing diagram should be consulted. Figure 2.9 shows the timing diagram of SARISA. The ion beam is pulsed in order to reduce space charge effects by reducing the number of particles in the detection volume. The time between the ion pulse and the laser pulse determines the energy of the sputtered particles to be detected. In detection of photoions one of the inevitable sources of noise is the secondary ions produced in sputtering. As discussed in the section below, the hemispherical analyzers are designed to detect ions in a certain energy interval[6]. The suppression of secondary ions in this apparatus is achieved by accelerating the secondary ions beyond the transmission windows of the analyzers. To give additional energy to the secondary ions, the target is pulsed 200V on top of its bias voltage. This pulse lasts for the duration of the ion beam pulse to accelerate all the secondary ions generated in the sputtering. The laser is fired at optimum time delay for a given sputtered species.

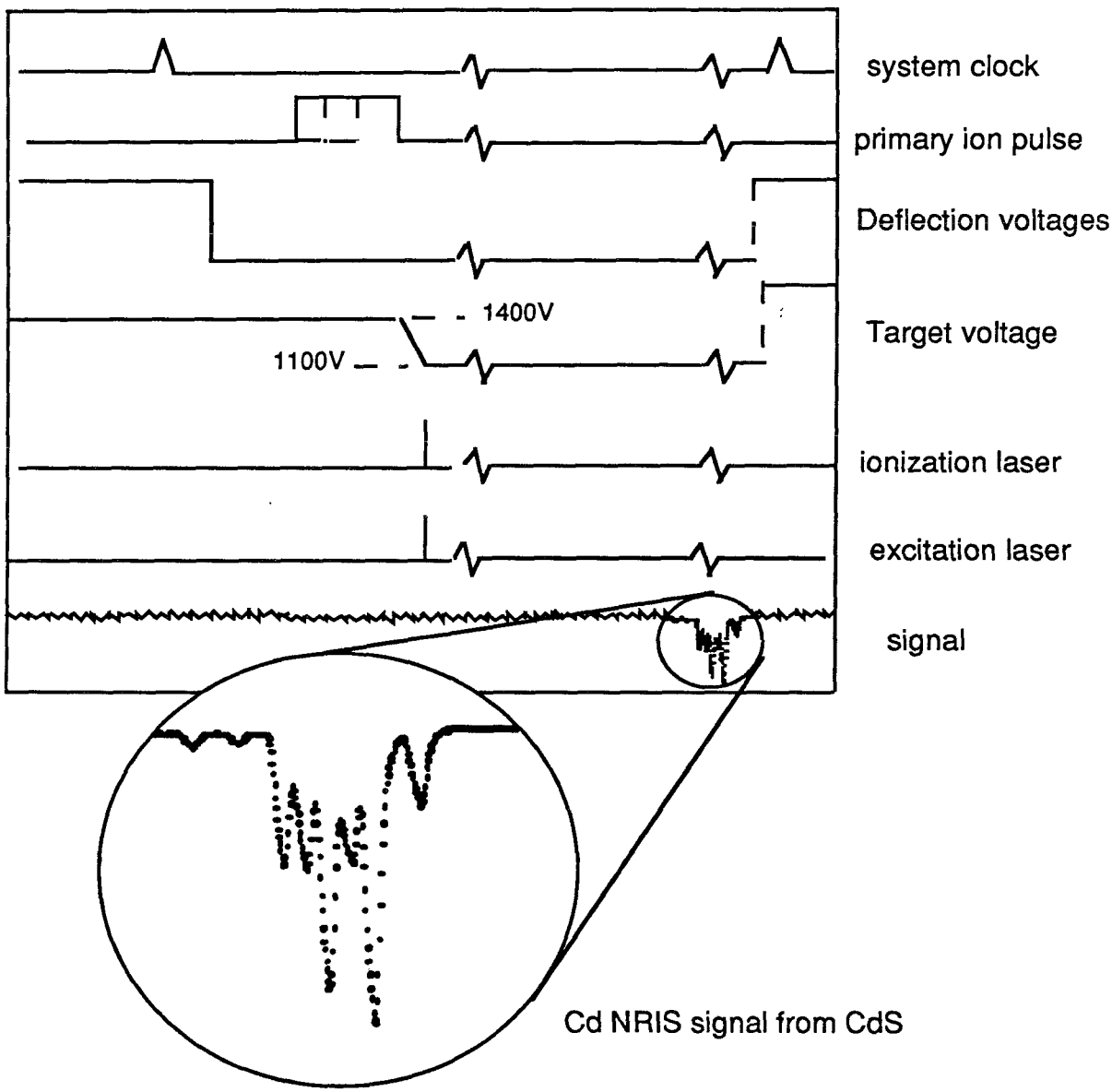

Figure 2.9 Timing sequence of the SARISA.

The ions produced by the laser (photoions) are then focused in the detector. The signal is charge digitized or the individual photoions are counted, depending on the amount of signal available. Particles arrive at the detector at a time that is dependent on their initial energy (before ionization) as well as their m/e. The digitizer's start pulse, therefore, is set accordingly for detection of the particles of interest.

d. Detector and Ion Optics

Figure 2.8 shows the details of the ion optics in SARISA. The high voltage lens close to the target focuses the primary ion beam onto the sample. The existence of the lens close to the target minimizes aberration effects. A smaller lens (-2.8 kV) provides extraction and focusing of the photoions produced by the laser. This lens has little effect on the primary ions. The photoions go through the high voltage lens and the primary ion beam bending plates, which are now held at ground. The photoions are imaged by a set of einzel lenses on the first analyzer. Upon arrival at the spherical analyzers the photoions will experience a 1/r potential. The particles of higher energy have larger orbits[7]. The potential on the hemispherical analyzers is chosen to detect particles of 1000 ± 100eV. This process is used for suppression of the secondary ions by adding a 200V pulse on the target. The machine can be set up for the collection of the secondary ions by turning off the target pulser and decreasing the target potential by 100 volts. In this way the

secondary ions will have lower energies and will be within the threshold windows of the hemispherical analyzers.

To characterize the transmission of the detector, the machine was set up for the detection of the secondary ions of potassium as a function of the target potential. This is shown in Figure 2.10. The other important feature of the double hemispherical analyzers is their role in the reduction of initial energy spread due to the extraction fields of the photoions in the TOF mass spectrometer.

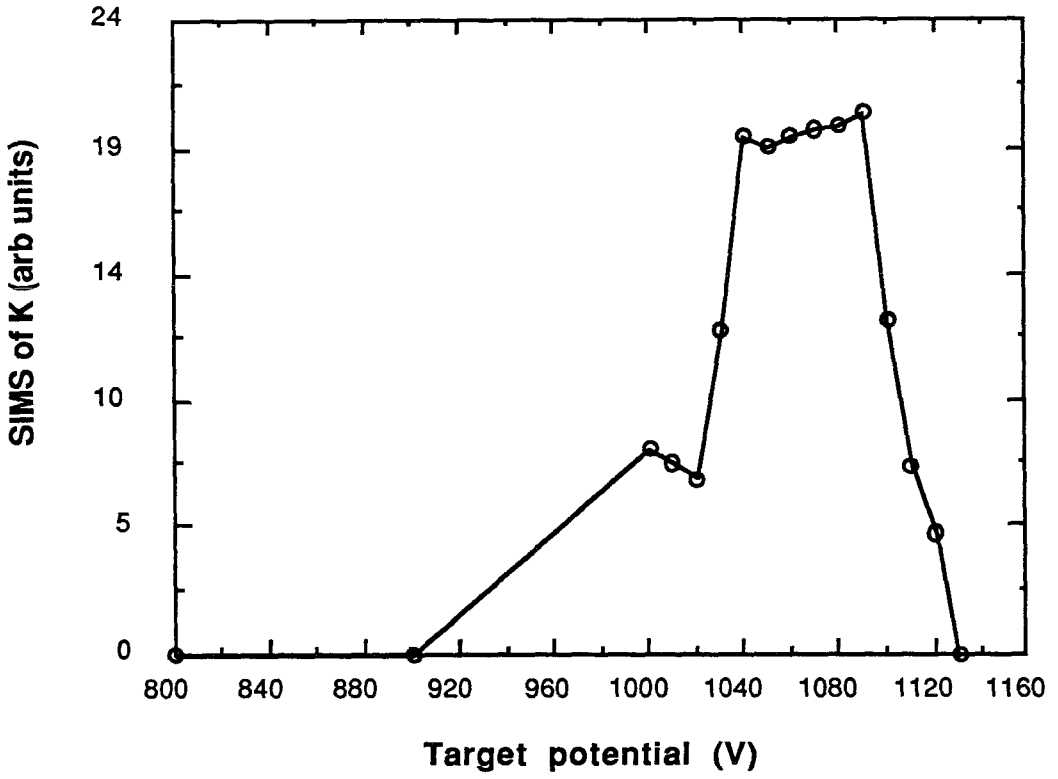

Figure 2.10 The SIMS signal of K was used to determine the transmission of the SARISA detector as a function of the target potential.

2.3 References

1 R.B. Wright, M.J. Pellin, and D.M. Gruen, Surf. Sci. **110**, 151 (1981).

2 A. Yariv, *Quantum Electronics 2nd Edition*, (Wiley, New York, Chichester, Toronto, Singapore, 1975).

3 C.E. Young, D.M. Gruen, M.J. Pellin, and W.F. Calaway, Fusion Technol. **6**, 434 (1984).

4 W.F. Calaway, C.E. Young, M.J. Pellin, and D.M. Gruen in *Ion Beam Desorption , Film Modification, and Synthesis*, J.J. Cuoms, S.M. Rossengel, and H.R. Kaufmann, ed., 1 (Noyes, Park Ridge, NJ, 1988).

5 G.H. Hurst, M.G. Payne, S.D. Kramer, an J.P. Young, Rev. Mod. Phys. **51**, 767 (1979).

6 M.J. Pellin, C.E. Young, and D.M. Gruen, Scanning Microscopy, **2**, 1353 (1988).

7 C.E. Young, M.J. Pellin, W.F. Calaway, B. Jørgensen, E.L. Scheweitzer, and D.M. Gruen, Inst. Phys. Conf. **84**, 163 (1986).

Chapter Three

Ion Beam Sputtering Characteristics of Fe in a Compound Material (FeS_2)

3.1 Introduction

In the first chapter, it was pointed out that the sputtering of a compound material is an important and complex problem. The complexity is due to the fact that the sputtering phenomenon cannot be simply looked at as a collisional cascade. The chemical nature of the material will become a factor in the mechanism of removal of species from the solid. It is conceivable that much of the energy of the primary ion is going to be spent on the dissociation of the chemical bonds that exist in the material. This could make the interpretation of the results quite complicated. The compound materials, however, also have many technological applications (e.g., III-V semiconductors, high T_c superconductors)[1]. We have undertaken the study of compound material sputtering as well as

having put the techniques of secondary neutral mass spectrometry to a test.

To understand the mechanism of sputtering in compound targets, we need to find out the sputtering regime, and the partial yield of the individual constituents, the molecules, and clusters formed by them. We also need to study the angular distribution of the sputtered species. To give a simple example, assume ion beam sputtering is used as a technique for thin film growth of CuO or Y_2O_3 for a high T_c superconducting material. It is important to know about the changes in the stoichiometry, flux as a function of the ejection angle, and the change of sputtering rate due to the dynamics of sputtering. Another example is for analysis with SIMS. The usual probe beam used in SIMS is oxygen, and after prolonged sputtering of the material the embedded oxygen can have a chemical reaction forming an oxide of the target. Again, the rate and the distribution of sputtered species could be affected by the formation of the oxide that will in turn could change the results of the analysis.

In this chapter we discuss the nature of sputtering of a metal sulfide as an example of a compound material. We have chosen a single crystal of FeS_2 for this study for the following reasons : (1) It contains Fe, which has been studied in pure metallic form and in different matrices (such as stainless steel); (2) S atoms are adjacent in crystalline FeS_2. The S_2 molecule is a stable molecule (D=4.4eV) with abundant spectroscopic data; (3) The FeS_2 compound also contains FeS (D=3.3 eV) bonds, which are weaker than those of S_2.

This material, therefore, is very desirable for studying molecular sputtering (see Chapter 5). In order to understand the nature of the sputtering regime of FeS_2 under 3 keV Ar^+ bombardment, we have measured the velocity distribution of sputtered Fe from the FeS_2 target. The velocity distributions were measured by the method of Doppler-shift laser fluorescence spectroscopy (DSLFS) in the LFS apparatus. The total sputtering yield of FeS_2 was measured by profilometry (see appendix) to give perspective to the partial measurements of Fe. The partial yield (Fe partial yield) measurements were conducted as a function of the primary ion dose and were compared with results from a pure Fe target. These measurements were performed both on SARISA (RIS, NRIS) and the LFS apparatus (described in Chapter 2). In addition, these experimental measurements were compared with TRIM[2] Monte Carlo calculations of the sputtering yields. TRIM code was used to estimate the yield and angular distribution of the sputtered species. For sputtered species of a multi-component target may have different angular distribution than the same species has from an elemental target. This becomes a concern when the signal from the two targets is compared for characterization of the multi-component material. The angle of detection of SARISA was also examined in relation to this effect.

3.2. Velocity Distribution

The velocity (energy) distributions of the sputtered species contains some valuable information. Besides being indicative of the sputtering mechanism, it also can help estimate the yield of the sputtered species[3]. According to the sputtering theory for elemental targets (metals) in the collisional cascade regime, the sputtering yield and the surface binding energy are inversely proportional. The peak of the energy distribution is reached to the binding energy of the atom to the target, which in turn is inversely proportional to the total sputtering yield.

The velocity distribution of Fe from Fe and FeS_2 targets was measured by Doppler-shift laser fluorescence spectroscopy (DSLFS) in the LFS instrument. The sample was cut from a natural single crystal with a diamond saw, was cleaned ultrasonically with trichloroethylene, acetone, and methanol, and placed in the UHV chamber. The method and the apparatus were explained in general terms in Chapter 2, but specific details for this measurement will be described below.

Figure 3.1 shows a partial energy diagram for Fe including its ground multiplet states. The transitions used were from a^5D_4 to y^5D_4, requiring excitation photons of 302nm wavelength. The dye used in the ring dye laser is Rhodamine 6G (R6G) and the amplifier cells contained Rhodamine B (RhB). The first amplifying cell

Fe

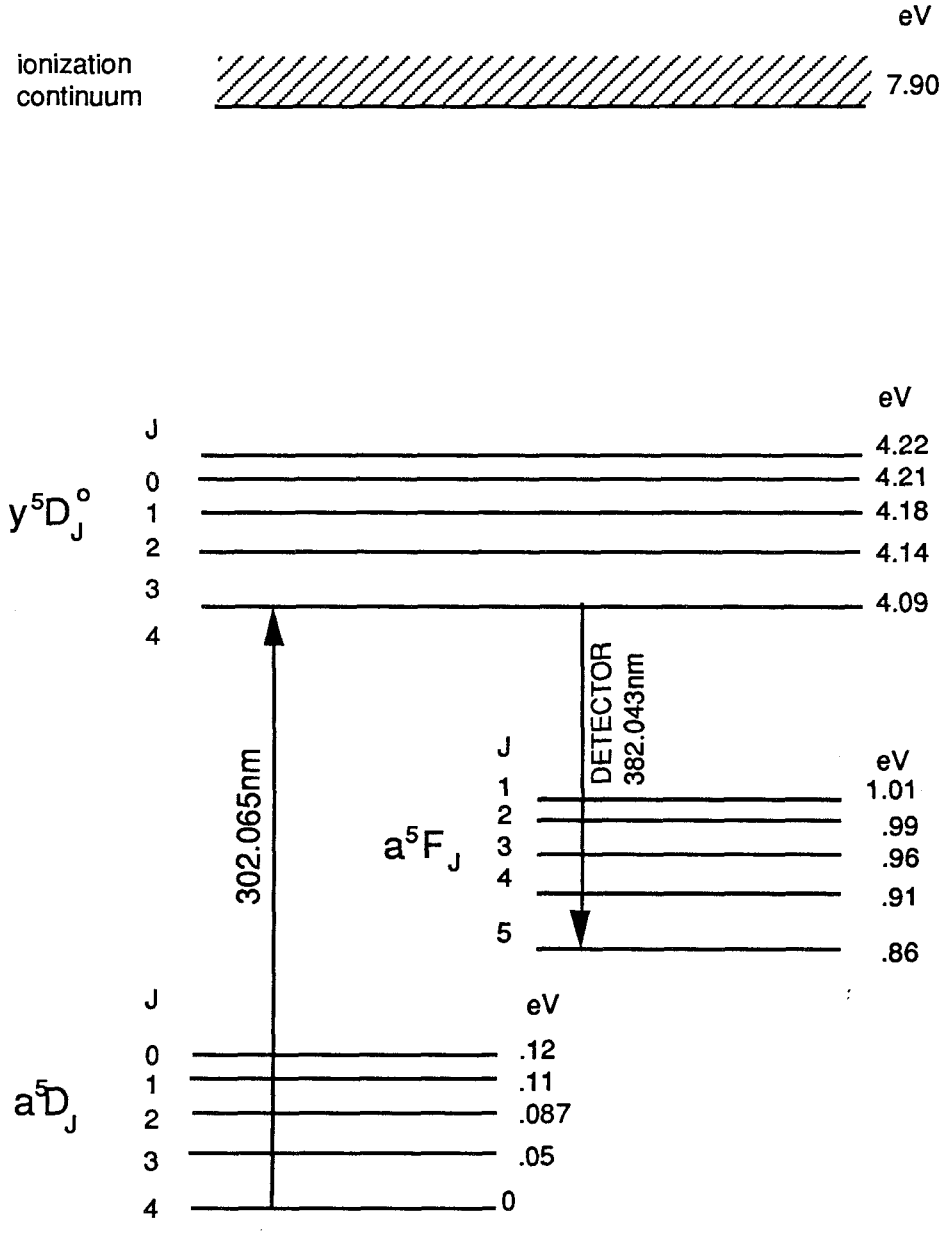

Figure 3.1 A partial energy diagram of the Fe atom. The arrows show the transitions that were used for the excitation and the fluorescence reaching the detector.

contains Kiton Red as well. The excimer laser used in this experiment, as usual, was XeCl.

The details of the conversion and interpretation can be found in the reference section[4,5]. It has been shown by Young et al. and Wright et al. that the LFS signal measured is proportional to the number density of the atoms in the detection volume. The number density is defined as the number of atoms in the detection volume per unit velocity interval integrated over a solid angle (determined by the collection optics of the apparatus). This signal is Doppler-shifted because of the motion of sputtered atoms relative to the collection apparatus. During each run, the laser is scanned in a 30GHz interval and the fluorescence signal is obtained as a function of the frequency. Using the Doppler broadening relation,

$$\nu \propto \nu_0 \ (1+v\cos\theta/c), \qquad (3.1)$$

the LFS signal is converted to the number density in the normal component of the velocity. The velocity distribution of Fe from FeS_2 target is plotted in Figure 3.2. There were 50 laser shots for each point and the signal is the running average of the data. The solid line is the Sigmund-Thompson distribution, which has the following form:

$$N(v) \propto v^2/ (v^2+v_b^2)^3, \quad (3.2)$$

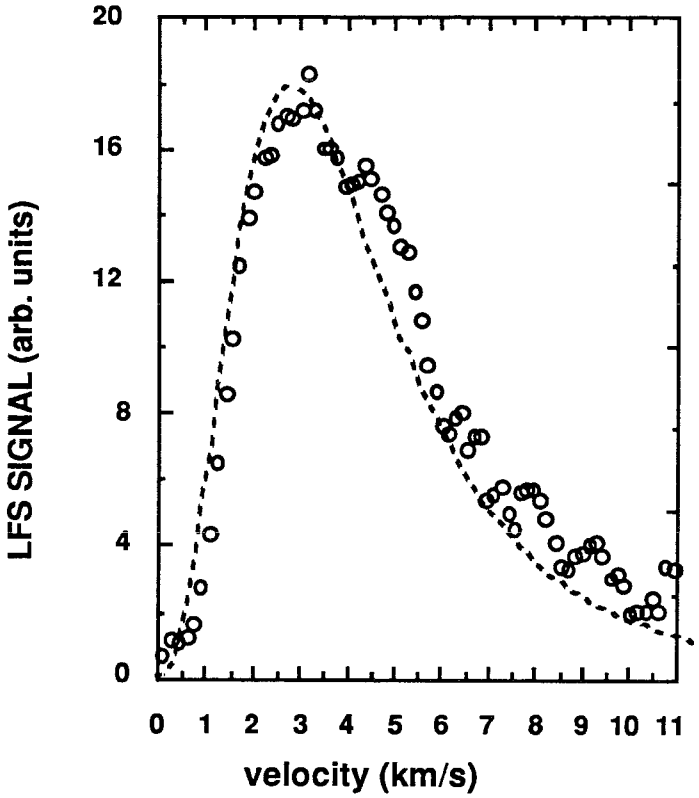

Figure 3.2 Velocity distribution of sputtered Fe from an FeS_2 target. The solid line is a Sigmund-Thompson distribution, normalized to the signal amplitude, with the peak velocity chosen according to the binding energy of Fe from an Fe target.

where v_b is a constant velocity that corresponds to the binding energy of the sputtered material to the surface of the target. This surface binding energy is usually estimated by the heat of sublimation of the material for an elemental target. As seen in Figure 3.2 there is very good agreement between the Sigmund-Thompson distribution and the data. The distribution peaks at $v_b/\sqrt{2}$. In the Sigmund-Thompson distribution shown in the figure, v_b corresponds to the binding energy of Fe from a pure Fe target (E_b=4.315eV)[4]. According to the measurements shown in Figure 3.2, the distribution peaks at about 4 km/s, which corresponds to the binding energy difference of ~0.2 eV between Fe sputtered from Fe and FeS_2.

The structure observed at the high velocity end of the spectrum of Figure 3.2 is attributed to single-crystalline effects of the sort exhibited in molecular dynamics calculations by Shapiro et al. of the single crystal-targets such as Cu[6].

The above result reveals two significant facts about sputtering of FeS_2. First, the sputtering of FeS_2 is in the collisional cascade regime and second, the binding energy of Fe is very similar for the two targets of Fe and FeS_2.

3.3 Yield Measurements

One of the important parameters of any sputtering phenomenon is the yield of the sputtered species. In a binary

compound target, the yield is somewhat more complicated since there are two constituents. The sputtering yield of a metal sulfide can be described as

$$Y_{tot}=Y_{met} + Y_S + Y_{mol}, \qquad (3.3)$$

where the Y_{met}, Y_s, and Y_{mol} are the partial sputtering yield of the metal, sulfur, and molecules, respectively, and Y_{tot} is the total sputtering yield of the material. Each term in the above equation contains the different electronic states of the species. Due to the differences in mass and binding energies of each constituent, preferential sputtering of one of the components of the target might occur. This changes the stoichiometry of the sample. Steady state conditions should be reached after prolonged bombardment of the sample. We have estimated the partial yield of Fe from FeS_2 as a function of the primary ion dose, using the LFS, RIS, and NRIS techniques. The measurement techniques will be described in the following sections. In order to relate the partial sputtering yield of Fe, we obtained the total sputtering yield of the FeS_2. This result and the total yield measurements of some other metal sulfides are presented in the appendix. The yields of Fe and FeS_2 are given in Table 3.1.

3.3.1. LFS Yield Measurements

The samples used for this measurement were pure polycrystalline Fe and natural single crystals of FeS_2. The signal

Total Yield Measurements

sample	profilometry	TRIM	literature
FeS_2	1.1 ± 0.3	1 ± 0.4	------
Fe	2.4 ± 0.5	2.2 ± 0.8	3.1

Table 3.1 The profilometry measurements and the TRIM calculations compared with the results reported in the literature. There is no reported total yield measurement of total yield of FeS_2 in the literature. The yields here are the yield of a molecule of FeS_2 per primary Ar^+ ion. There are large uncertainties that propagate into the ratio of the yield of the two targets.

obtained is the same as the one described in section 3.2. The LFS signal is proportional to the number density of sputtered atoms. By keeping the geometry constant when switching between the two samples, taking into account the laser intensity and the primary ion current, the LFS signals obtained from the two targets of Fe and FeS_2 can be compared. The fluorescence signal is proportional to the $\sqrt{I}$ where I is the probe laser intensity. The primary ion current is directly proportional to the LFS signal obtained, and the LFS signal is scaled accordingly so that the results of the two targets could be compared. The ratio of the two signals after the above normalization is about 18% after the FeS_2 target has been bombarded for a long time ($\approx .5 \times 10^{17}$ ions/cm^2).

3.3.2. RIS Yield Measurements

The polycrystalline Fe and the single crystal of FeS_2 were sputtered in the SARISA apparatus, and RIS was used for the interrogation of the sputtered Fe. The energy diagram of Fe and the scheme of ionization are indicated in Figure 3.3.

The Fe sample was first sputter-cleaned prior to the RIS measurements. An FeS_2 sample was moved into the beam line and was examined by RIS. The sample was raster-sputtered for 1 minute followed by a RIS measurement, again rastered for a 2 minute interval, followed by a RIS measurement. The raster current was 3 μA and the raster area was (1mm)x(1mm). The FeS_2 was removed

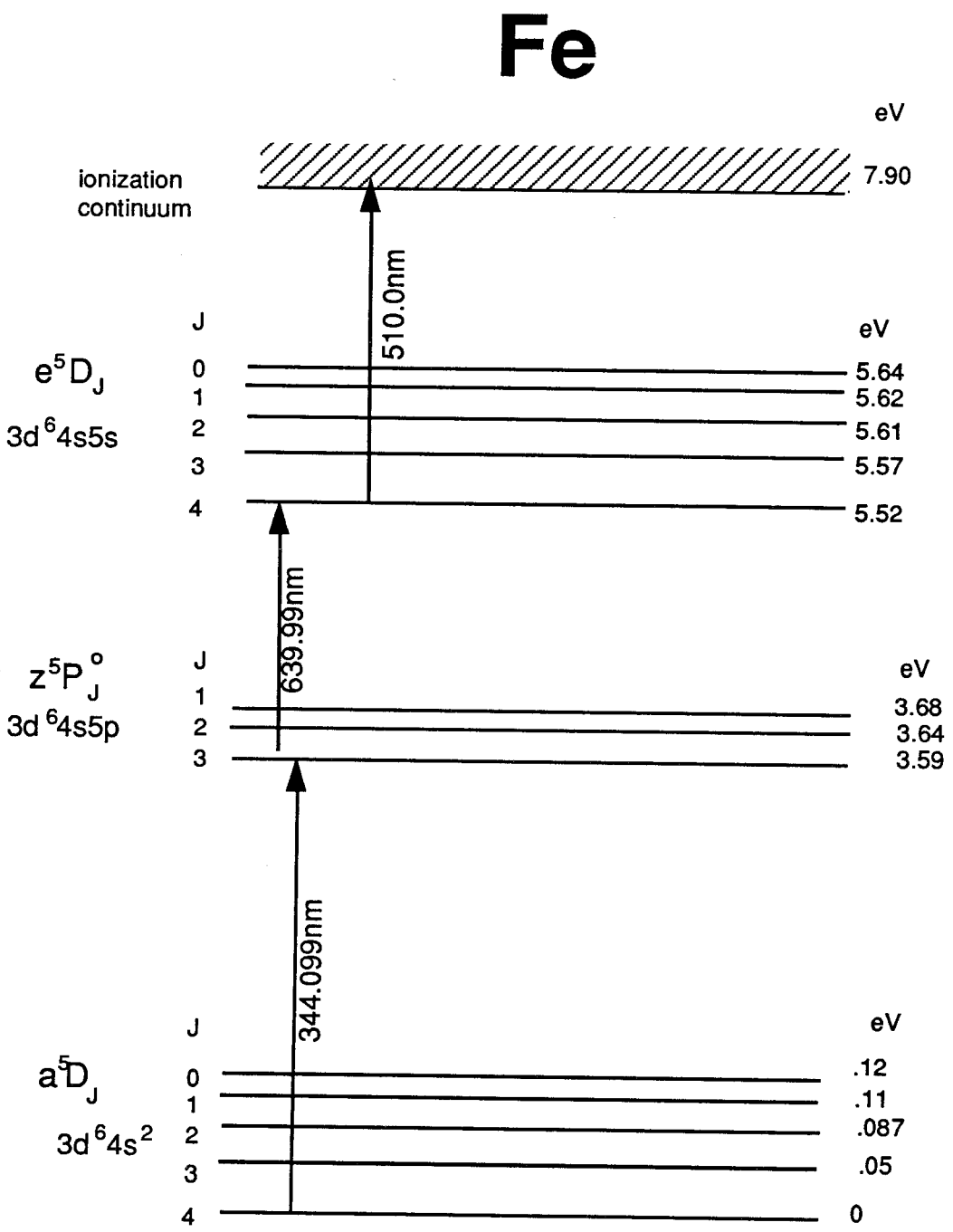

Figure 3.3 A partial energy diagram of an Fe atom. The arrows show the transitions that were used for the excitation and ionization of the ground state along with the wavelength of excitation. A three-color ionization scheme was used.

from the beam line and the Fe sample was brought back to the beam line, and the RIS measurement on the Fe sample was repeated to check reproducibility.

The RIS measurements were three-color experiments. The source of photons for the three colors of the transitions is provided by three dye lasers pumped by an excimer laser. XeCl excimer laser (Questek) beam was divided equally among the three dye lasers. Two Lumonics dye lasers, (Coumarin 510nm, and PTP dye 344nm) and the Molectron dye (DCM) laser were used. Saturation of each transition was studied as a function of the laser power. With the exception of the ionization transition, all transitions were saturated.

3.3.3 NRIS Yield Measurements

Sputtering yields from Fe and FeS_2 were examined by NRIS measurements. This method of measurement was used for monitoring simultaneously the signal level of different sputtered species.

The partial yield of Fe was measured as a function of the primary ion dose in order to observe the dynamics of sputtering. The primary ion dose was increased by rastering the ion beam for different time intervals followed by NRIS measurements. Throughout these rastering and measurement intervals, changes in the parameters of the machine might occur. To separate the

apparatus effect from the sputtering mechanism, a reference point on the sample was chosen and data was collected from this point periodically to ensure that no changes occurred from run to run due to the machine.

The Fe target was sputter-cleaned and then NRIS measurements were performed. An FeS_2 sample was then situated in the beam line. The FeS_2 sample was moved up from the center position and the measurements on this point were used as a reference. The sample was moved down from the center by 2mm and raster-sputtered for various lengths of time. The raster time intervals were from 1sec to 5min. After each raster interval the NRIS signal was measured and the measurements on the reference point were performed after two or three raster and measurement intervals. Figure 3.4 shows the geometry of the sample and the reference and rastered point on the surface.

The Questek excimer laser was used with KrF(248nm) as the ionization laser. The laser was power locked for 200mJ/pulse and the experiments were run at 20Hz. The ion beam current was 1.4μA. The laser beam size was reduced by apertures and collimated by two pairs of telescopes to a (1mm)x(3mm) spot in front of the target. The laser power was monitored at the exit window of the experimental UHV chamber (10mJ/pulse) and was estimated to be unchanged during the measurements.

SCHEMATIC OF THE NRIS EXPERIMENTAL PROCEDURE

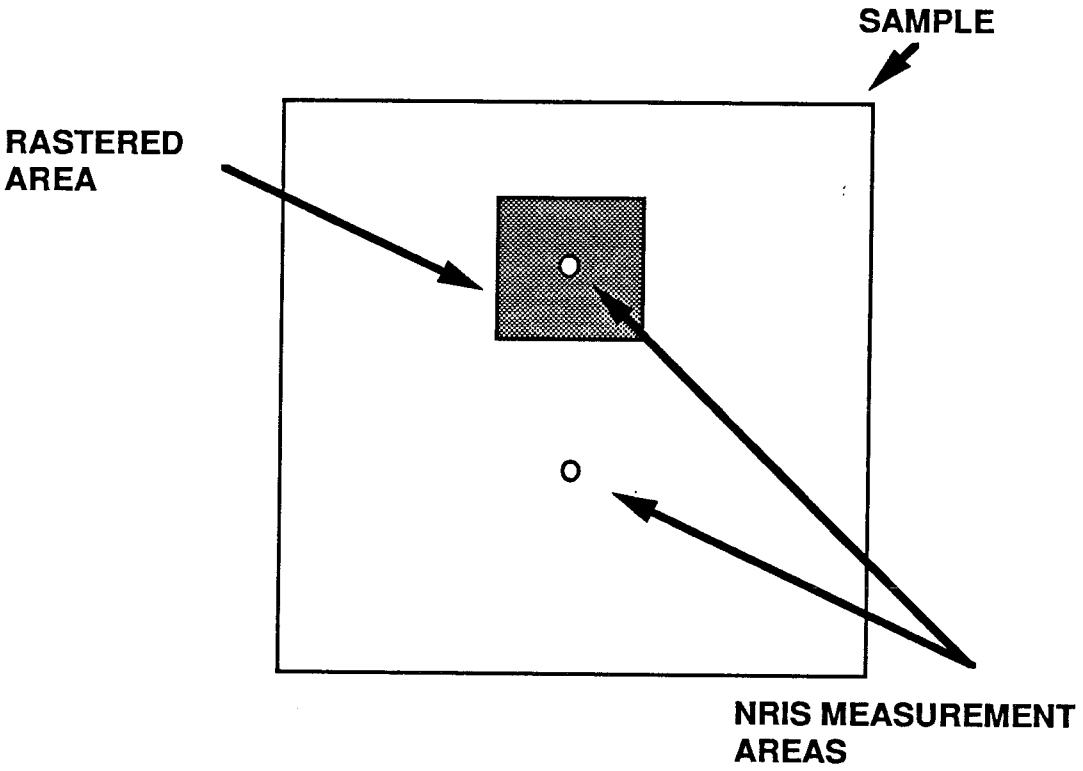

Figure 3.4 One millimeter below the center of the target was chosen as the reference point and was periodically checked for stability of the apparatus. The primary ion dose was increased by rastering a 1mm by 1mm area above the center of the target. Data was taken following each raster period.

The signals from the two targets were scaled for the detector gain. A simple integration was used to determine the signal levels. Although in most data analysis from the signals obtained by SARISA apparatus it suffices to use the peak height of the signal for comparison purposes, it was essential in this case to take into account the width of this signal. As will be discussed later in the section, it appears that Fe signals from FeS_2 obtained by the NRIS method may not be entirely from the sputtered atomic Fe. The photo-dissociated molecules seem to be a possible source, which can be observed from the shape of the signal as well. The signal from the FeS_2 target is normalized to the signal from the Fe target. The result is plotted in Figure 3.5 as the ratio of the two signals vs the number of monolayers removed. This represents the partial yield of Fe from FeS_2 as a function of primary ion dose. The results from the RIS measurement are also plotted in the same figure. The LFS measurements have high uncertainty in terms of the primary ion dose prior to the measurement and are not shown in Figure 3.5.

3.3.4 TRIM Calculation:

a. Yield Measurements

TRIM calculations were conducted to estimate the total yield of the target and the partial yield of the target constituents. TRIM is a Monte Carlo calculation that involves binary collisions, with no consideration of crystal structure. Thus, the sputtering products are

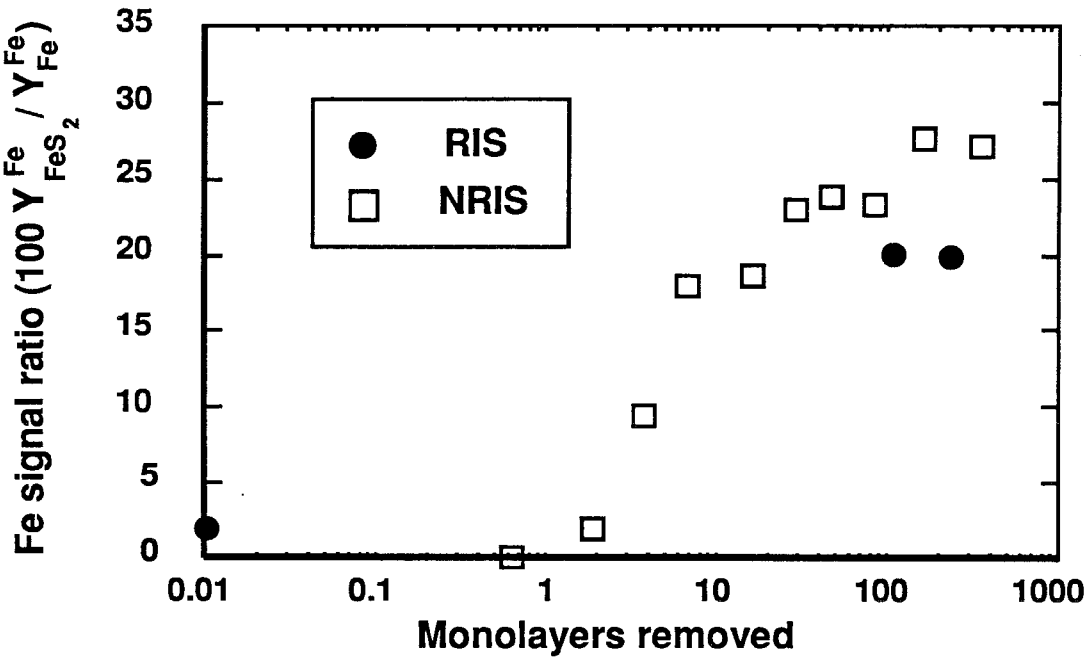

Figure 3.5 The partial yield ratio of Fe as a function of the primary ion dose. The RIS data was obtained by a three-color experiment and the NRIS was performed with a KrF excimer laser. The signal of Fe obtained from sputtering from an FeS_2 target is normalized to the sputtered Fe from an Fe target. The first two or three points of the NRIS data are indicative of cleaning of the target. The change in the ratio demonstrated here is only due to the changes of the Fe signal from the FeS_2 target. The partial yield of Fe saturates at two different levels when obtained by the two different techniques of RIS and NRIS.

only in the form of elemental Fe or S from FeS_2. The other difficulty in these calculations was the estimation of the surface binding energies of the two components. Several different binding energies were chosen for S and Fe. The binding energies for which, the yield obtained for the metal sulfide were more than the pure targets, were rejected. The results of some of these calculations are summarized in the Table 3.2. Table 3.1 shows the results of TRIM yield calculations along with the total yield measurements and the values quoted from the literature[7].

b. Angular Distribution Calculations

The angular distribution of the Fe was obtained using the TRIM code for sputtering a 10^4 Å thick layer of FeS_2. This output is normalized to have a peak value of unity, and is plotted as a function of angle of ejection to the target surface normal (Figure 3.6a). A cosine distribution of the ejection angle is also plotted in Figure 3.6a for comparison. A two layer target was also used in a separate TRIM run where the first layer was 10 Å of Fe and the second layer was a 10^4 Å thick FeS_2 (Figure 3.6b shows this result, and a $\cos\theta$ distribution is plotted in the same figure). The second of the calculations was performed to simulate the surface enrichment in Fe. The effect of enrichment of Fe, (which was observed experimentally in the partial yield measurements and also in the velocity distribution measurements) is simulated by having a layer of Fe over FeS_2.

TRIM YIELD CALCULATIONS OF FeS_2

Fe SE_b(eV)	S SE_b(eV)	TOTAL YIELD	S YIELD	Fe YIELD
4.32	4.0	.6	1.55	0.6
5.5	4.0	.5	1.54	0.5
2.6	4.0	1.0	1.6	1.0
2.6	2.88	1.0	2.1	1.0

Table 3.2 Some of the results of the TRIM runs for the yield calculations from FeS_2 for with different surface binding energies (SE_b). The total yield number presented here is the sputtering yield of the FeS_2 as a molecule. This way, these results cab be compared directly to the profilometry measurements. The cohesive energy of Fe is 4.32 eV and that of S is 2.88 eV. The dissociation energy of S_2 is 4.4eV. The ion beam used in all the calculations is 5keV.

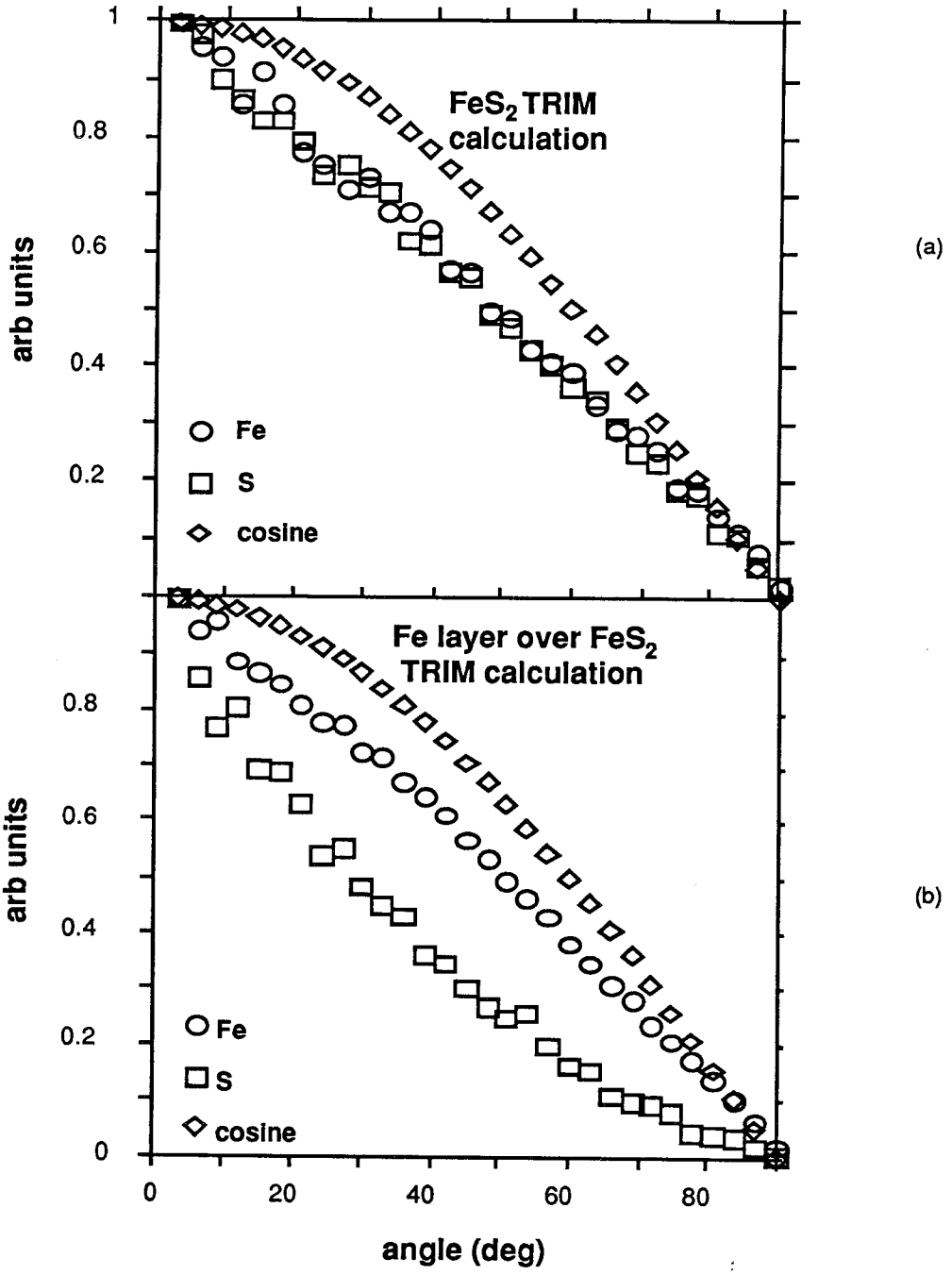

Figure 3.6 a) Angular distribution of sputtered Fe and S from FeS_2 target njormalized to unity amplitude. A cosine distribution is also plotted for comparison. b) Angular distribution of sputtered Fe and S from FeS_2 target after prolonged bombardment. Fe enrichment in the surface has been simulated by having a layer of Fe over the target.

The ejected Fe and S from FeS_2 have the same angular distribution, which is slightly sharper than a cosine distribution. By adding a layer of Fe to the surface, the Fe angular distribution remains unchanged, but the sputtered S will have a super-cosine distribution even more sharply peaked toward normal. Figure 3.7 is a close up look at the detection volume and the angle of detection of the SARISA apparatus. The laser is usually about 1mm away from the target and the 3mm detection length is due to the ion beam optics solid angle. This geometry provides a ±60° acceptance angle which is demonstrated in the figure. This high efficiency detection setup would only lose ≈5% of the sputtered Fe in the plane of detection. According to the TRIM calculations, the angular distribution of sputtered Fe is not any different for Fe and FeS_2. Since the instrument's detection efficiency is the same for both cases, and sputtered Fe appears to have the same angular distribution, any difference observed in the signal level is due to the difference in the nature of sputtering. It should be pointed out again that TRIM calculations involve amorphous targets and will not reveal any single crystal effects.

3.4 Results and Discussion

In Figure 3.5 the two measurements are plotted vs the primary ion dose in units of monolayers removed (10^{15} ions/cm^2). An important result of these measurements becomes apparent by comparing the partial yield measurements obtained by RIS and NRIS measurements. In both sets of measurements the partial yield of Fe

SARISA DETECTION SOLID ANGLE

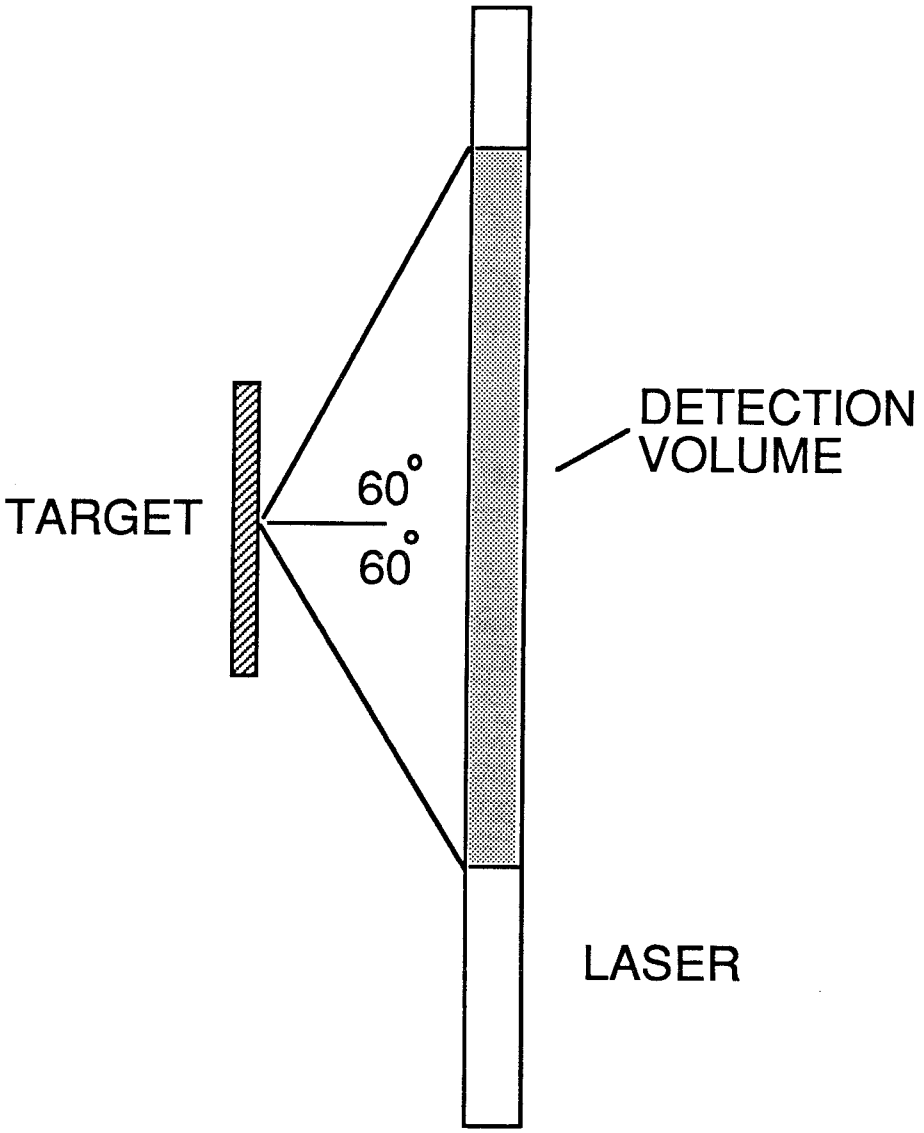

Figure 3.7 A schematic of the target and the ionization laser in SARISA apparatus. The detection angle is determined by the distance of the laser from the target and the solid angle of the ion optics, determining a 120° total angle of acceptance.

starts from a very low value, and after removal of many monolayers of the target via ion bombardment, the partial yield saturates at a certain percentage of the Fe sputtering yield for a pure Fe target. The saturation level for the FeS_2 target is different for the two techniques of measurement. By using the NRIS technique, the partial yield of Fe is about 27% of Y_{Fe}^{Fe} (sputtering yield of Fe from Fe target), and in the RIS measurements this number is about 19% (these results agree with the LFS measurements). It should be pointed out again that the technique of RIS is a state-specific technique and only represents the partial yield of ground state Fe from FeS_2. The difference in the two levels could be due to this characteristic of the measurement. That is to say that the difference in the signal level is due to the difference in the population distribution of the two targets for the excited state neutral Fe. The other possibility is the generation of Fe from photo-dissociated molecules, which would remain undetected by the RIS method. If the sputtered Fe from the FeS_2 target has a higher population in the metastable states, then the NRIS signal level could be higher than the RIS. The metastable population distribution of sputtered Fe was measured for the two targets and is described in detail in the next chapter. Briefly, it was found that the ground state fraction of the sputtered Fe was 10% lower for FeS_2 than for the Fe target. By taking into account the slight difference in the fraction of the ground state sputtered Fe from the two targets, the saturation of the partial yield measured by RIS will be increased to 22%. The rest of the difference, we believe, is in the Fe produced by the photo-dissociated

sputtered molecules. Another evidence for the existence of the sputtered molecules is seen by close examination of the spectra of Fe obtained from the two techniques. The NRIS spectrum has a larger width, which suggests a greater spread in the initial velocity of the sputtered species. The spectrum has a sharp rise time, and the fall time is slower than ones observed from the Fe target. Since molecules are more massive, they will be slower sputtered species, and the Fe signal due to the dissociation of these molecules will arrive at the detector at a later time. This can cause the larger width of the spectrum obtained by the NRIS technique.

The other point about this result is that the saturated level differs from the total yield ratio for the Fe and FeS_2 target. According to the values reported in Table 3.1, the partial yield ratio of Fe for the two targets is

$$R=0.5 + .24 /- .22. \qquad (3.4)$$

Since there is a large uncertainty associated with this ratio, it is difficult to draw a hard conclusion from this measurement. The uncertainties may be overestimated. But even at the low end of the estimated ratio (28%), the partial yield of Fe from the NRIS measurement is lower than expected from the profilometry measurements. This is especially interesting in light of the similar binding energies of the two targets. The angular distributions calculated by TRIM did not show any difference for the sputtered Fe from the two targets. This suggests that, in the absence of crystal effects, the detection efficiency of the detector remains the same for

the two targets. Another explanation for the lower than expected level of the signal is that the Fe is sputtered in forms that even the nonresonant technique is not ionizing efficiently. There are, of course, some molecules that are either not photo-dissociated or are not ionized after photodissociation. This could account for the difference in the saturation level obtained by the total yield measurements. In Chapter 5 the sputtered molecules are discussed in more detail.

3.5 References

1 A. I. Kingon, O. Auciello, M. S. Ameen, S. H. Rou, and A. R. Krauss, App. Phys. Lett **55**, 301 (1989).

2 J. P. Biersack and W. Eckstein, Appl. Phys. A **34**, 73(1984).

3 P. Sigmund, in *Sputtering by Particle Bombardment I*, R. Behrich, ed., 9 (Springer-Verlag, Berlin, 1981).

4 C.E. Young, D. M. Gruen, M. J. Pellin, and W. F. Calaway, Fusion Technology **6**, 434 (1984).

5 R.B. Wright, M. J. Pellin, D. M. Gruen, and C. E. Young, Nucl. Instrum. Methods **170**, 295 (1980).

6 M. H. Shapiro, P. K. Haff, T. A. Tombrello, D. E. Harrison, Jr. and R.P. Webb, Radiation Effects **89**, (1985).

7 N. Matsunami, Y. Yamamura, Y. Itikawa, N. Itoh, Y. Kazumata, S. Miyagawa, K. Morita, R. Shimuzu, and H. Tawara, At. Data and Nucl. Tables **31**, 1 (1984).

Chapter Four

Metastable States Population Distribution of Sputtered Fe from FeS_2 and Fe Targets

4.1 Introduction

In previous chapters, three different experimental methods that have been employed to detect sputtered neutral Fe were presented. Two of these methods are state-specific (RIS and LFS) and the other (NRIS) is not. The results of two different types of measurements can only be compared if one of two conditions is satisfied. First, the resonant lasers have a large enough linewidth that the simultaneous excitation of several states is possible, or second, the relative population of the states containing appreciable population is known. This is why the measurement of the multiplet ground states of Fe is important. In order to use RIS as a reliable and quantitative measurement method for sputtering phenomenon, calibration of the method is required. One step in calibrating this technique is to measure the relative population of the metastable excited states for the sputtered species. Such measurements have been performed for sputtered Fe species for pure Fe, Fe as impurity in Si and Mo,

stainless steel, or Ni_3Fe alloy samples[1-4]. The results from these measurements show that the distribution of the ground state multiplets of sputtered Fe are nearly the same for the different samples and that the distribution is therefore independent of the matrix. There also exists low-lying state population distribution of other elements with clean surface or controlled oxygen coverage of the surface. Since metastable state population distribution of Fe has been measured in different matrices, it is a particularly good candidate for our measurements.

We have repeated the same measurements of the ground state multiplet distribution of sputtered Fe in a compound material (FeS_2) where a chemical bond exists between Fe and the other constituent of the target. What can be learned from this measurement is the effect of the chemical nature of a surface on the distribution of the metastables. This could have a strong impact on the sputtering yield measurements by the state selective methods such as LFS and RIS.

An example of the need for such calibrated measurements was presented in the comparison in sputtering yield of Fe from FeS_2 and a pure Fe target in the previous chapter. The partial sputtering yield measurement of Fe from FeS_2 was unexpectedly lower than the stoichiometric sputtering yield when compared with the yield from a metallic Fe sample. Thus, this excited state measurement in a sense was also a search for the Fe that seems to be missing when sputtered from FeS_2.

4.2 Background

With the onset of the ion-atom collisions in a solid, atoms will move in all directions. Some of these species in motion in the right direction will have sufficient energy to escape the surface of the solid. The molecules and atoms are ejected as ground or excited state (neutrals and ions). The final state of the ejected species is strongly influenced by the nature of the solid surface. It has been demonstrated that the ionic yield of the sputtered species is increased by oxygen flooding of the surface of the target.[5-8] In the case of metals the effect of the work function (Φ) and its relation to the ionization potential (I) of the ejected species in determining the final state of the sputtered particle has been worked out analytically[9] and confirmed experimentally by Yu[10].

There have been numerous attempts, with reasonable success, to understand the origin of the secondary ions and the sputtered excited neutrals both experimentally and theoretically. Most of the effort has been focused on the sputtering of metals with primary ions that have energies of ~10 keV[6]. Formation of secondary ions and neutral atoms in higher energy excited states has received more attention than in low-lying energy levels. In general these metastable states will have the same electronic state as the ground state but differ in the orientation of orbital and spin angular momentum. Optical emission detection, which is normally used for the excited neutrals, is not possible in this circumstance.

The attention received by the secondary ions is understandable both because detection of ions is relatively straightforward and also because the use of SIMS as an analytical tool is widespread. For neutral emission, however, the accurate measurements of the low-lying states are important in order to know the yield of the sputtered species in all the possible channels and to quantify more accurately the yield of the secondaries.

There have been some measurements of yield of the fine structure multiplets of Fe and in the a^5D_J from pure metallic targets and for Fe in an alloy and as an impurity in Si and Mo[7]. The a^3F_J states population distribution for Zr has also been measured.[11]

As mentioned above, the majority of the work in this area has been with metals. However, some work has been done on semiconductors. The effect of change of the work function on the secondary ion yield of Si has been examined by Yu.[12]

Some experimental findings that are established in this field are: a) The yield of negative and positive secondary ions for metals can be enhanced through the use of suitable primary ion beam and by some adsorbates. Oxygen for the positive ions and Cs for negative ions help increase the yields. The excited neutrals, especially in the low-lying states, are affected to a lesser degree by the above factors; b) The yields of the secondary ions and excited neutrals are orders of magnitude smaller than the ground state neutrals. c) The probability

of ionization and excitation is dependent on the normal components of the velocity of the sputtered atom.

We will briefly mention some of the models describing the mechanism of ionization or excitation of sputtered species and will outline two that are more consistent with the experimental results and thus represent the major points of view. This is, of course, not meant to be an exhaustive survey of all the theoretical and experimental efforts in this area. Our attention is more focused on the models that describe the excited states, due to their relevance to the measurements presented later in this chapter.

Some of the approaches start from the assumption that there can be a local thermodynamic equilibrium (LTE) and calculate the probability of ionization and excitation. The microscopic approach involves a quantum mechanical treatment and gets quite complicated. In some studies oversimplifications have taken place.

4.2.1 The statistical model of Kelly:[13]

This model is based on Firsov's[14] idea of electronic excitation due to inelastic energy transfer of the last collision. This is a purely statistical study and the nature of the surface does not play a role. The basic assumptions of this model are:

1. The sputtered particles are all from the outermost or next outermost layer of the solid. They are ejected due to collision with an atom from the solid that has a distribution :

$$f(E) \propto E^{-2}dE\ \sin\theta\cos\theta d\theta \quad .(4.1)$$

There are different possibilities resulting in the ejection of an excited neutral atom. These possibilities are depicted in Figure 4.1.

2. The elastic energy transfer is in the following form

$$\Delta E_e \ll KE \quad .(4.2)$$

In this equation ΔE_e is the transferred energy in the inelastic collision, E is the kinetic energy of the cascade particle and K is a constant with very small values ($K<<1$).

3. The probability of excitation only scales with the degeneracy g_i (and not the transition rate).

4. The excitation due to the inelastic energy transfer is not necessarily a resonant transition ($\Delta E_e = \varepsilon_i$), but for any $\varepsilon_i \leq \Delta E_e$ the excitation is possible, where ε_i is the energy of the excited state. This probability of the excitation is weighted by the degeneracy of the level. This so-called 'degeneracy-proportional probability' is introduced in the form of a degeneracy ratio factor, which is the degeneracy of the excited level divided by the cumulative degeneracy.

$$R_{ik} = \frac{g_i}{G_k} \quad (4.3)$$

$$\text{where} \quad G_k = g_0 + g_1 + g_2 + g_3 + \cdots\cdots g_k \quad (4.4)$$

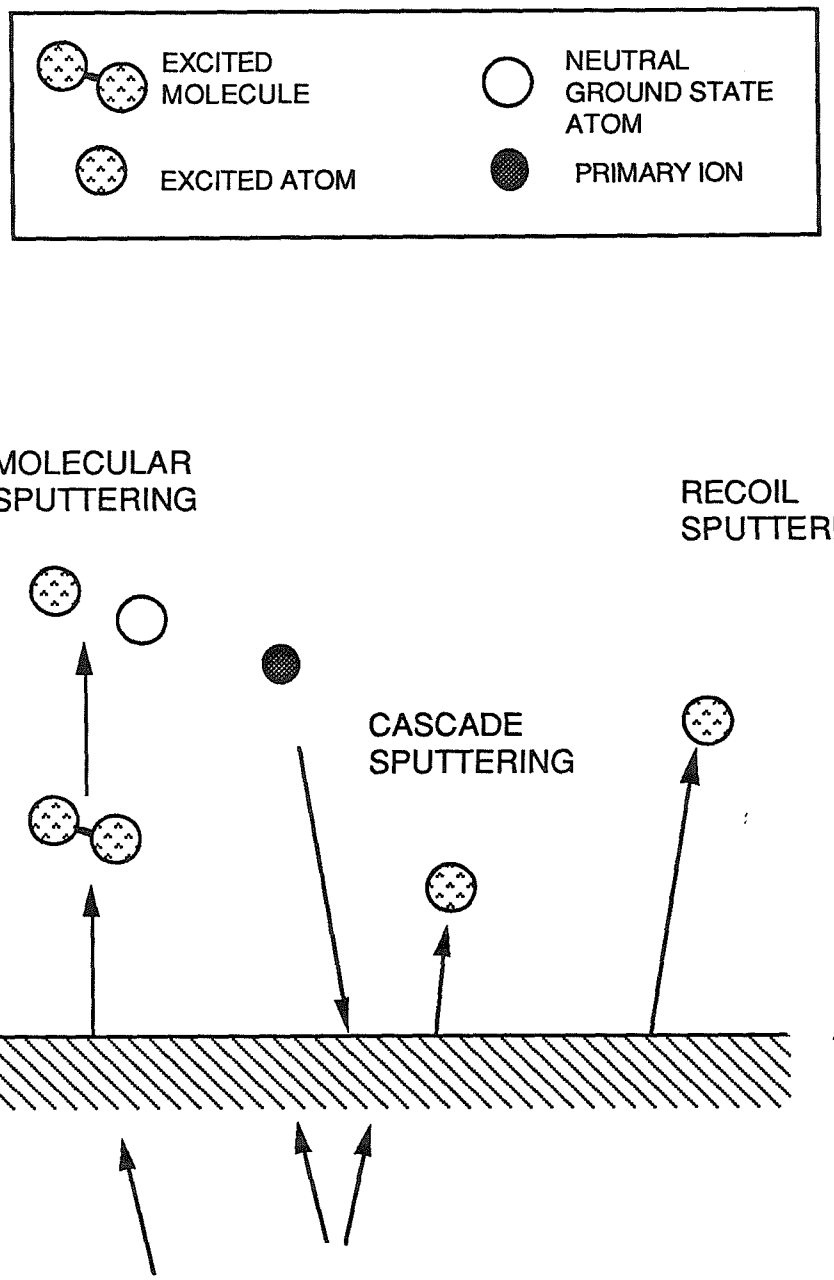

Figure 4.1 Possible situations for formation of excited state atoms due to surface-atom interaction.

G_k is the cumulative degeneracy and g_0 is the ground state degeneracy.

5. The atom in the solid is assumed to be the same as the free atom as far as the g_i and ε_i are concerned, and the shift and broadening due to other atoms or the solid surface are neglected. With these assumptions the yield of the excited states is calculated from:

$$S^* \propto g_i/G_i \int_{\frac{\varepsilon_k}{K}}^{\frac{\varepsilon_{k+1}}{K}} E^{-2}\, dE \qquad .(4.5)$$

This is true if $\varepsilon_i^{-1} < \Delta E_e < \varepsilon_{i+1}^{-1}$. If the $\frac{\varepsilon_k}{K}$ is smaller than the binding energy E_b, then the angular part of the distribution in the cascade becomes unimportant and the yield can be reduced to the following expression.

$$\frac{S^*}{g_i} = K \sum_{k=i}^{\infty} G_k^{-1} (\varepsilon_i^{-1} - \varepsilon_{i+1}^{-1}) \qquad (4.6)$$

The result is that the $\ln(S^*/g_i)$ vs ε_i has a Boltzmann-like behavior. This model has been consistent with some experimental results[14]. It should be noted that one of the assumptions that is important to this model is that the kinetic energy of the sputtered atoms in the excited states is higher by one or two orders of magnitude when compared

with ground state neutrals and even the secondary ions. This is supported by some experimental results[15]; other groups, however, have observed that for the excited state the most likely kinetic energies are still similar for those of the ground state sputtered neutrals. This is true for both low-lying spin-orbit fine structure levels[11] and electronically excited states[16].

4.2.2. The quantum mechanical approach:

All the models that deal with this approach start from an Anderson Hamiltonian. This Hamiltonian describes the atom and the solid system. There are three parts to this Hamiltonian, the first part describes the atom, the second the conduction band electrons of the solid, and the last term is the interaction of the solid with the atom. A time variant perturbation is applied in this mode in order to solve for the final state of the atom. The varous existing quantum mechanical models in the literature differ in the third term. Electrons from the surface can tunnel to and from the moving atom. The eigenstates of the system have to be a linear combination of the eigenstates of the conduction band and the free atom energy states. The Hamiltonian of the system is given by:

$$H= \sum_{k<k_f} (\varepsilon_k C^{\dagger}_k C_k + \varepsilon_a(t) C^{\dagger}_k C_k) + \sum_{k} (V_{ka}(t) C^{\dagger}_k C_k + \text{h.c.}); \quad (4.7)$$

where the ε_a is the localized state energy of the atom, V_{ka} is the interaction between the solid conduction electrons and the electrons

in the localized state $|a\rangle$, and $C^{\dagger}_{k}C_{k}$ are the fermion creation operators.

There are two different views on the role of the surface in the atom-surface interaction. In one model[17] it is proposed that the sputtered species start in an ionic state in the solid and are neutralized to the ground state or an excited state due to electron transfer from the surface. In measurements by Veje[18] it is concluded that the moving species start in the ionic state.

The ionization probability for positive ions, and the effective temperature, are given in (4.8) and (4.9):

$$R^{+} = (\frac{2}{\pi})\exp[\frac{-(I-\Phi)}{h\gamma v/2\pi}]; \quad (4.8)$$

$$T_{e}=h\gamma v/2\pi k_{B} ; \quad (4.9)$$

where v is the normal velocity of the sputtered atom and γ^{-1} is the distance from the surface at which the level broadening of the sputtered atom starts decreasing. In other words, it is the effective surface in the interaction. k_B is the Boltzmann constant and h is Planck's constant.

The second model developed by Nørskov[19-24], using the same microscopical formalism, attacks the problem by assuming that the

atom leaves the surface as a neutral atom and picks up (or gives off) an electron from (to) the surface. As a consequence it will be ejected as a negative (positive) ion in excited or ground state. The reason behind this assumption is that in order to have large probability of survival of an excited state neutral or secondary ion, the role of the surface must be excitation. The probabilities of the excitation and ionization and the effective temperature are given for positive ions in (4.10,11,12). The final state depends on the work function of the surface (Φ), ionization potential (I), and electron affinity (A) of the sputtered atom; and the energy of excited state.

$$R^* = (\frac{2}{\pi})\exp[\frac{\pi(\varepsilon_a-\varepsilon_f)_{eff}}{h\gamma v}], \quad (4.10)$$

$$R^+ = (\frac{2}{\pi})\exp[\frac{-\pi(I-\Phi)}{h\gamma v}]\ \exp[\frac{-\pi c_1}{h\gamma v}], \quad (4.11)$$

$$\text{and } T_e = hav/\pi c_1 k_B\ , \quad (4.12)$$

where $(\varepsilon_a-\varepsilon_f)_{eff}$ is the effective energy difference indicating that the ε_a is changing with time (or position) and c_1 is the constant relating the effective energy difference to ($I-\Phi$) linearly. The rest of the parameters are defined above. In the second equation the ionization potential, I, has been substituted for ε_a, which leads to a more successful result compared to the prediction of other models of 10^{-6}-10^{-3} for the secondary ion yield. If the wrong choice is made for V_{ka}, and it is not recognized that ε_a is a time varying parameter, then one would predict a much lower yield: 10^{-15} for a kinetic energy of 40eV,

and 10^{-21} for kinetic energies of 20 eV. The drawback in these models is that the state of the atom as it travels from near the surface to far away from the surface is not well-determined.

4.2.3. Other Models:

Another model based on local thermal equilibrium (LTE) by Andersen[25] starts from the basic thermal equilibrium between the neutrals and the ions. Based on this assumption, one naturally ends up with a Boltzmann distribution. The excited states in this case are generated in the solid and are ejected from the cascade. The problem with this assumption is that the lifetime of the excited state in the solid will be quite short due to level broadening.

Another possible model also has been suggested by Williams[17]. In this model, it is proposed that the excited atom can be formed in the following fashion. Simultaneous sputtering of a pair of atoms from the solid form an excited molecule and go through gas-phase binary collisions to form an excited atom.

4.3 Experimental

The measurements were done with the SARISA apparatus; the targets used were natural single crystal of FeS_2 and polycrystalline Fe. A detailed description of the setup is given in Chapter 2 while the details particular to this experiment are presented here. Figure 4.2 shows a schematic layout of the experiment.

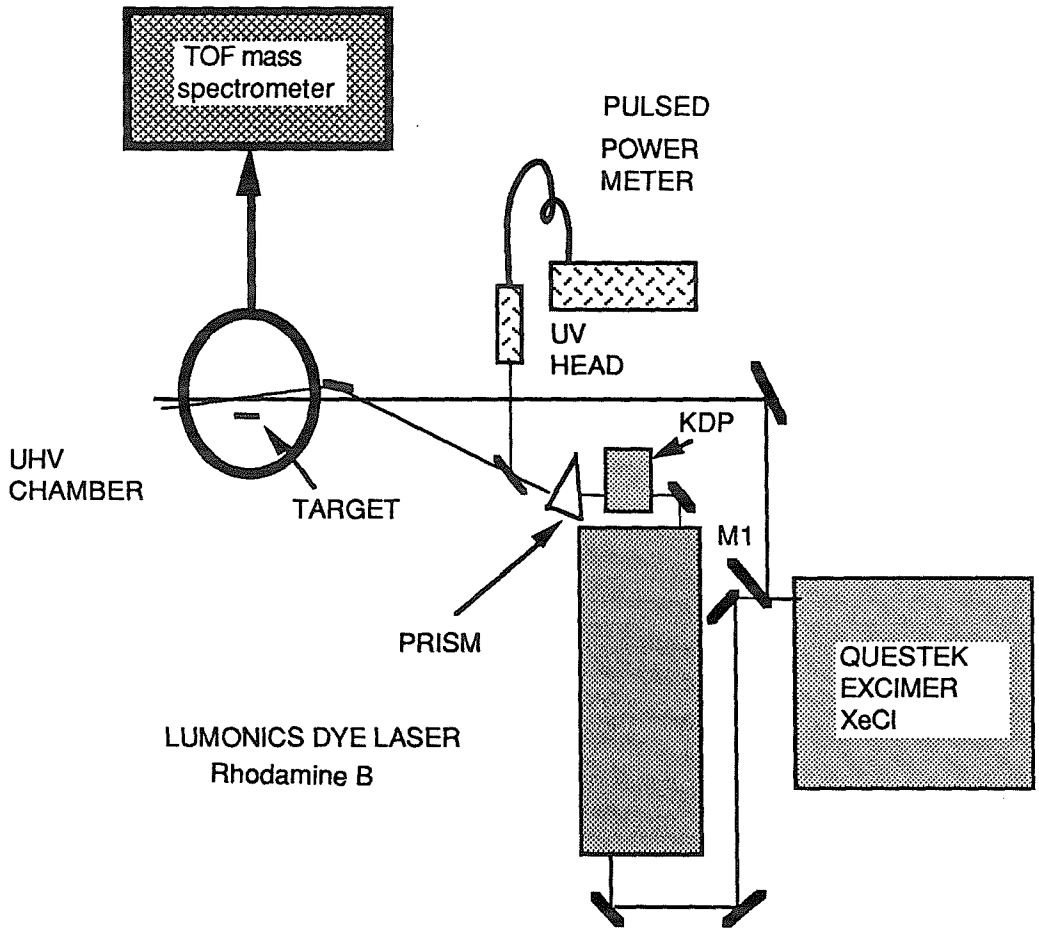

Figure 4.2 Schematic of the experimental arrangement for the measurement of the distribution of the ground state multiplet states of sputtered Fe. Note that since the excimer laser has a large rectangular beam, part of it (70%) is picked off by mirror 1 (M1) and the rest is used to pump the dye laser.

The ionization scheme was a two-photon, two-color ionization of the following type. An excimer laser operating with XeCl was divided into two beams, 30% of which was used to pump a dye laser operating with Rhodamine B dye, and the remaining 70% was used to ionize the excited atoms formed by the first photon absorbed. The output of the dye laser is frequency doubled to generate UV light. The two UV laser beams, the excimer laser and the doubled dye laser output overlap in front of the target inside the UHV chamber. It can be seen from Figure 4.3 (a partial energy level diagram of Fe) that there are many different ionization schemes for Fe to choose from. This method was used for the reasons below. It is a relatively simple scheme, since we can use a high gain dye with which it is easy to saturate the excitation transitions of Fe chosen. In addition, in this method, two different photons provide the excitation and ionization photons, thus the saturation for each step of the ionization transitions can be easily verified. The disadvantage of this scheme is that the XeCl laser could cause a nonresonant signal (NRIS) from Fe that interferes with the measurements. This is especially important for higher energy states that have lower populations and otherwise do not contribute to the NRIS background. To overcome this problem, the NRIS signal could be treated as a background and be subtracted from the signal. Alternatively, the excimer power can be reduced to minimize the NRIS noise at the cost of not saturating the ionization step. The excitation transitions of Fe are from a^5D_J to y^5D_J states with nominal wavelength at λ=302nm. To shorten the notation we shall denote J and J' for the a^5D_J and $y^5D_{J'}$ states, respectively. The

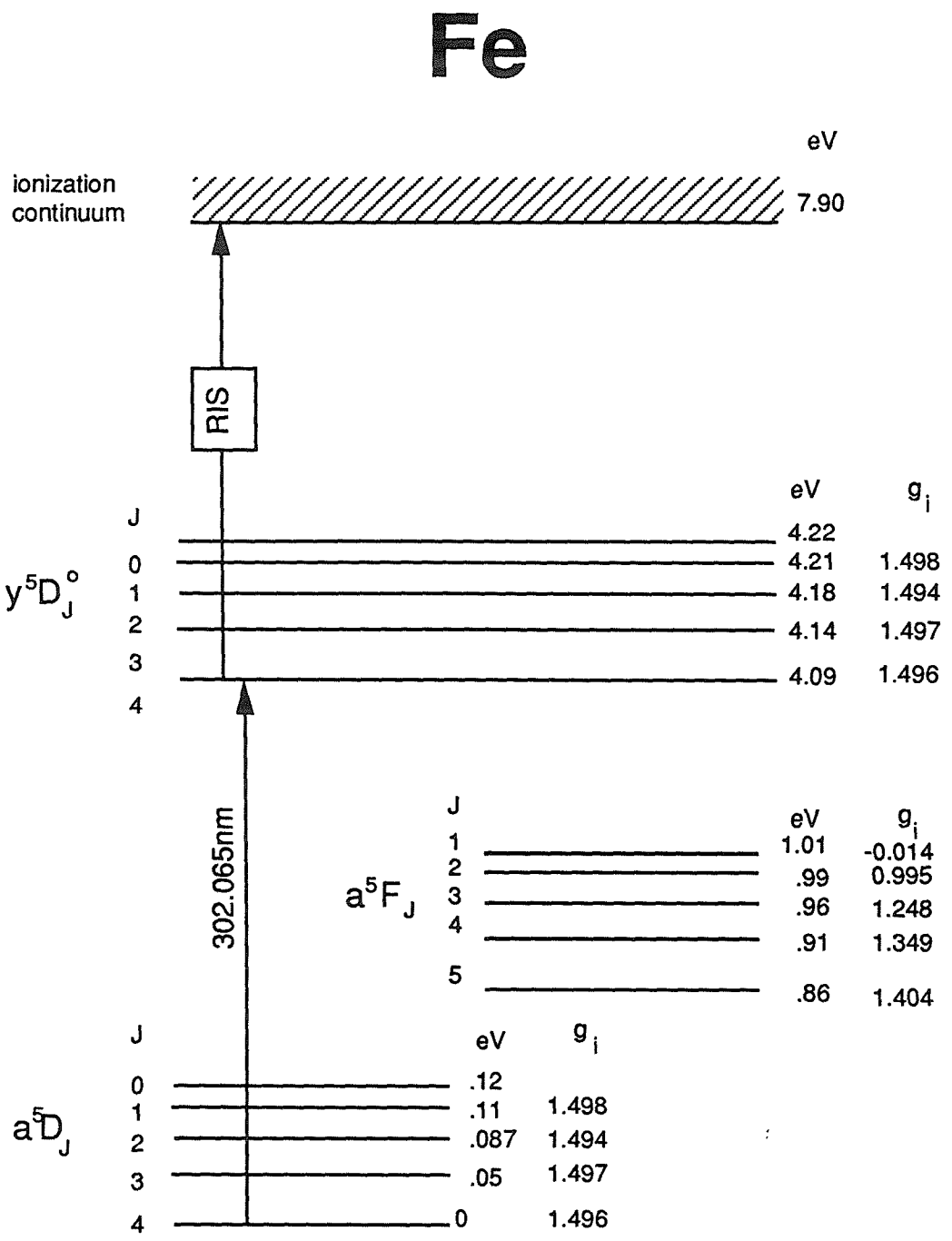

Figure 4.3 A partial energy diagram of the Fe atom. The energy separation of each state from the ground state and the degeneracy of the level are also depicted. The arrows show the transitions that were used for the ionization of Fe in the ground state with a two-photon, two-color scheme.

exact transition wavelength, transition rates, and the energy corresponding to the states involved in these transitions are presented in Table 4.1. It should be noted that these states are metastable and that radiative decay to each other and to the ground state is forbidden. Thus, the signals measured here do correspond to the population of these levels when the transition is saturated. These transitions were identified and the dye laser was calibrated prior to the measurements with an optogalvanic signal of an Fe hollow cathode lamp. The separations in energy from the ground state for these metastable states are from 0.05eV to 0.12eV. The dye laser is tuned to each transition and the signal is detected at the same gain for the detector for the cases where that was possible. The signals due to the ground state and the J=3 state were large enough for the same detector gain. In the case of the J=2 level, although a reasonable signal was detectable, the less acceptable signal-to-noise ratio required increasing the detector voltage by 100V. As will be discussed in the next section, the gain of the detector increases by a factor of ~4 for each 100V. Figure 4.4 shows the gain of the detector as a function of the detector applied potential. The gain had to be increased even further for the last two energy levels. Later the signal from each transition was normalized according to the detector gain. This produces a source of error that will be discussed later. The doubling crystal and the positioning mirrors were aligned to maximize the signal of each transition. The power of the excimer laser and the dye laser were monitored during the experiments. The excimer laser power was measured at the exit window of the SARISA apparatus. The change observed in the

J	J'	$\lambda_{JJ'}$ (nm)	E_J (eV)	$E_{J'}$ (eV)	$A_{JJ'}$ ($10^7 s^{-1}$)
4	4	302.065	0	4.09	6.7
3	3	302.107	.05	4.14	.4.6
2	2	302.050	.087	4.18	.1.9
1	1	300.814	.11	4.21	10.7
0	0	302.584	.12	4.22	3.5

Table 4.1 The metastable states of Fe in the two multiplet states of $a^5D^o_J$ and $y^5D^o_J$ with their decay rates, the transition wavelengths, and the energy separations.

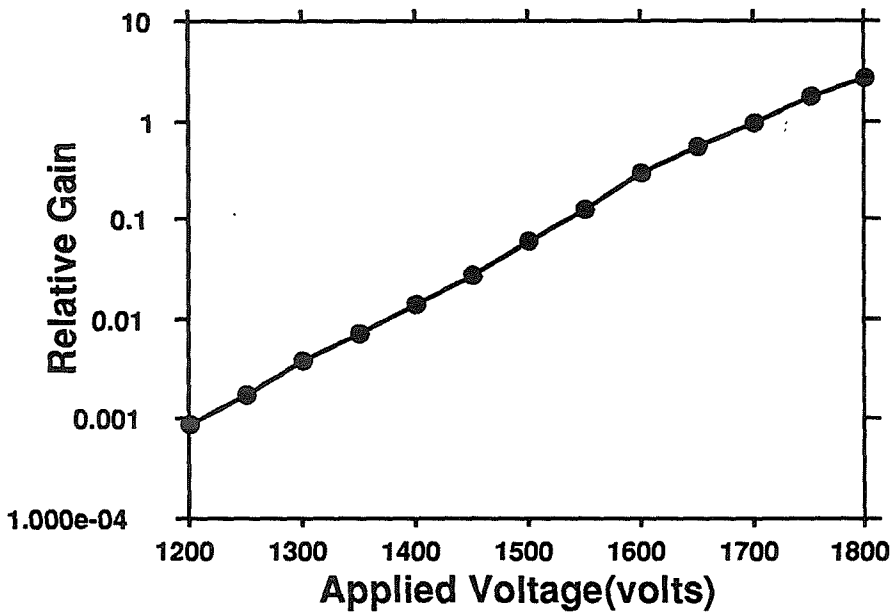

Figure 4.4 The gain of the channel plates is plotted as a function of the applied voltage. There is some uncertainty in this curve, which introduces an error to measurements that are obtained by two different voltages.

excimer power was very small, in fact within fluctuations of the power-meter, the laser power was a constant value. A beam splitter was placed in the doubled beam of the dye laser and sent to a pulsed power meter. The UV power was constant for the time the data was taken. Of course the power was reduced the longer the dye was used. The dye was changed when laser power was too low, and the transition was no longer saturated.

The measurements were performed for the targets of Fe and FeS_2. While the experiments on the Fe samples were conducted, the saturation for the excitation transition was confirmed. However there was only partial saturation of the ionization step. Considering the fact that the cross section of the excitation transition ($\sigma_e \sim 10^{-15}$ cm^2) is orders of magnitude larger than the ionization cross section ($\sigma_I \sim 10^{-18}$ cm^2)[26], this is an expected result for the laser power available and the beam size of each laser. Although ideally both transitions would be saturated, it is still possible to determine relative populations without saturating the transition, if the laser power can be kept constant.

The excimer laser was operated in the power lock mode, and its power was constant during the experiments. Furthermore, the ionization cross section from all levels of y^5D_J is the same. The cross sections are dependent on the wavelength of the transition. Within the range of the the wavelengths for these transitions and to the first order of approximation, the cross sections of the transitions are identical. These facts justify using the signal level from a transition

as a good representation of the population of the starting level. The signal from each transition was compared to the ground state, and they are presented relative to the ground state, a^5D_J. The results of each sample were compared to the results from the literature for an Fe sample. The Fe sample was run first and then the experiments on FeS_2 were performed. For each set of measurements, the sample was rastered prior to the run to sputter-clean the surface. The Fe sample was rastered for 5-10min and the FeS_2 sample for 2sec to minimize the FeS_2 surface modification due to ion bombardment. The measurements of the J=4 state were then performed. Some measurements were repeated 3 to 5 times. For both samples, after all transitions were investigated, the laser was tuned back to the 4-4 transition frequency and the ground state measurement was repeated. The data collection for the J=4 state of Fe sample was repeated again after the measurements of the FeS_2 were completed. This was to confirm the stability of the apparatus and repeatability of the measurements.

The measurements of the FeS_2 target were repeated after the sample was rastered by the Ar^+ ion beam until the primary ion dose in the sample was about 10^{18} ions/ cm^2. The same procedure described above was followed for these measurements. The experiments performed after prolonged bombardment will be referred to as the 'high dose.' The measurements on FeS_2 that were done just after a few seconds of rastering for sputter-cleaning will be called the 'low dose' measurements.

For each transition there is some contribution from an NRIS signal of the other levels. The size of this contribution was measured by tuning the dye laser away from the resonance frequency of the transition and also by blocking the beam. It was determined by alternatively blocking the two laser beam paths that all of the contribution of NRIS was from the two photon absorption of the excimer laser (308nm, 4eV). Although it was not a very large percentage of the signal for the a^5D_4 level, the percentage of the contribution due to the NRIS signal is significant (14% of the signal) for the higher energy level (a^5D_0). For both samples the NRIS signal was regarded as a background and subtracted from the signals of all the levels. It must be kept in mind that J=4 is the most highly populated level and is the source of the observed NRIS signal; it also introduces some systematic error in our measurements since it causes less precision in measurements involving the least populated state. However, as will be discussed later, the contribution of this source of error is almost negligible. This problem had been avoided in the previous measurements by reducing the excimer power level so that the NRIS signal would only account for 1% of the lowest signal[1].

4.4 Results and Discussion

Table 4.2 summarizes the data obtained from the two samples of Fe and FeS_2 sputtered by 3 keV Ar^+. Some of the results reported in the literature on the Fe sample are also tabulated. As mentioned in

METASTABLE STATES (a^5D_J)POPULATION OF SPUTTERED Fe

DISTRIBUTION NORMALIZED TO THE GROUND STATE

J	a FeS (RIS) Low Dose	b FeS (RIS) HIgh Dose	c Fe (RIS)	d Fe (RIS)	e Fe (RIS)	f Fe (LFS)	g SS (LFS)
4	1	1	1	1	1	1	1
3	.51 ± .1	.36 ± .05	.34 ± .05	.34 ± .01	.30 ± .03	.30 ± .06	.43
2	.18 ± .05	.12 ± .05	.11 ± .05	.13 ± .01	.13 ± .01	.09 ± .03	.21
1	.04 ± .03	.03 ± .01	.03 ± .03	.08 ± .01	.05 ± .01	.04 ± .02	.097
0	.02 ± .02	.01 ± .0	.02 ± .01	.02 ± .01	.02 ± .01	.02 ± .01	.029

Table 4.2 Relative population of the metastable states of Fe:

a. Natural single crystal FeS_2 sample only sputter cleaned for a few seconds.

b. Natural single crystal FeS_2 sample, after prolonged ion bombardment.

c. Polycrystalline Fe sample, sputter cleaned.

d,e. Fe samples previously measured by RIS[1,2].

f. Fe sample, measured by LFS[4].

g. Stainless steel, measured by LFS[3].

the previous experimental section, these levels a^5D_J (J=0,3) are metastable states. In addition, the electronically excited states have a short lifetime (< 8nsec), therefore the signals for transitions starting in each level represent the population of that level.

Figure 4.5 shows a typical spectrum obtained from an FeS_2 sample for the J=4 to J'=4 transition. The signals from the other transitions are similar with typical lower peak heights. In this study, the peak height of ^{56}Fe was chosen to represent the signal for each transition. The peak height was obtained by subtracting the minimum in the peak from the base line. Due to fluctuations in the peak height in cases of lower signal transitions (JJ': 0 to 1 and 1 to 0) the minimum value in the peak was estimated by averaging the value's fluctuation at the peak. This has a possible error of 1% of the ground state signal. Another source of error could result if the mass resolution is not optimized and the signal from ^{57}Fe could contribute to the ^{56}Fe peak height. This is estimated to contribute about 1%. For most measurements, however, the resolution is quite good and capable of separating the two peaks.

Some of the measurements were repeated two or three times and the mean value of the results was used. The signal could change from run to run by 30 to 50% in the SARISA apparatus if the measurements are close in time, and by a factor of 2 if the measurements are several hours apart. For most of the measurements here the change is estimated to be about 4 to 5% of the ground state signal. The uncertainties occur due to the

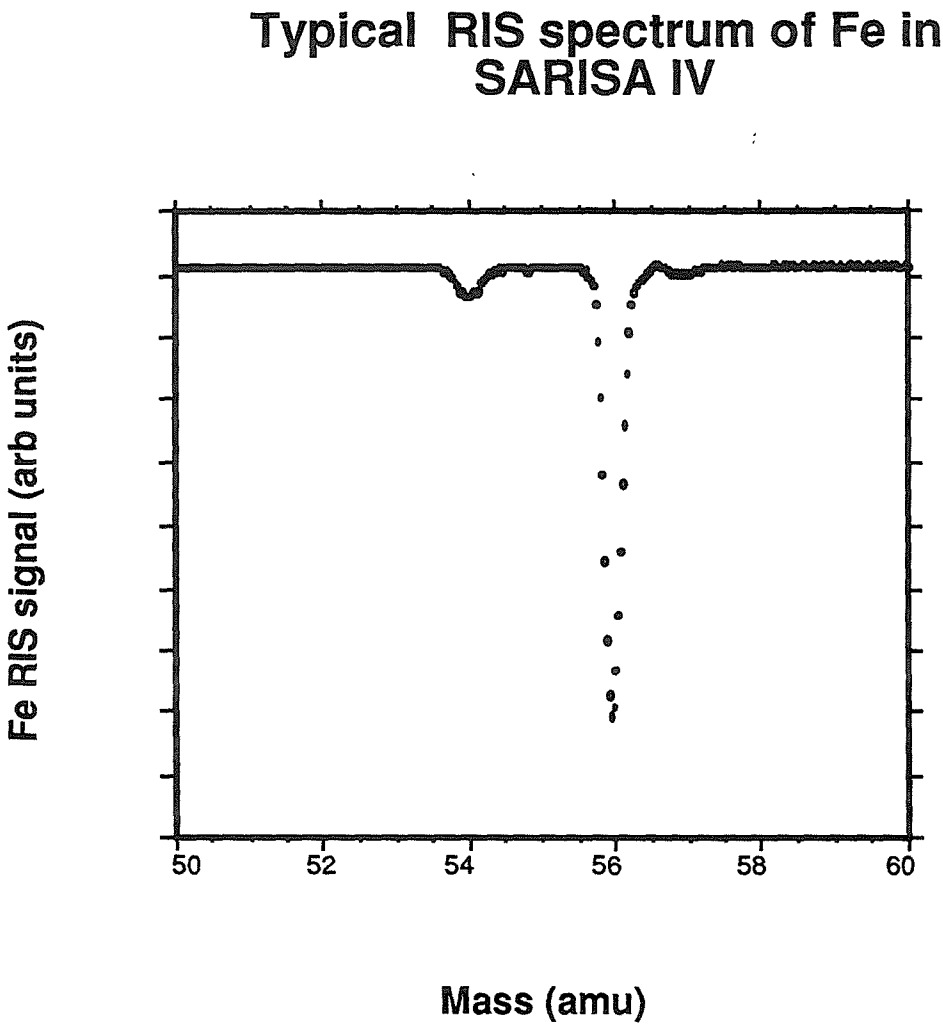

Figure 4.5 A typical spectrum of the Fe RIS signal in SARISA apparatus. The large peak of mass 56 is used as the signal level for comparative analysis.

movement of the laser beams that are caused by vibrations or warming of the doubling crystal, this changes the ionization volume and constitutes a major uncertainty. Another source of error, shift of laser timing with respect to the ion beam pulse which in this case has almost no contribution. The rest of the sources of uncertainty are due to the drift in the rest of the system, i.e., drift in the biases of the ion optics causing a change in the transmission of the detector.

For the low dose measurements of the FeS_2 target, following our procedure described earlier, we repeated the ground state (J=4) measurement after all the other transitions were run. This measurement (of 4 to 4 transition) showed a factor of 3 increase in the signal level, which is outside the regular fluctuations of the apparatus. In the previous chapter we have shown that the Fe signal of the FeS_2 is altered as a function of the primary ion dose. This was confirmed in these experiments as well. This suggests that the signals from the other transitions should be compared with the ground state signal obtained immediately after or before their measurements. For the intermediate measurements (such as the '2 to 2' transitions), the ground state signal level was interpolated by assuming the same rate of change in the sample.

The data reduced from each metastable level was normalized to the ground state signal. To do this, the signals obtained from the different transitions were adjusted to the gain of the detector accordingly. Data from all transitions is adjusted to the detector gain used while taking measurements of the J=0 set according to Figure

4.4. The accuracy of this curve is about 5% of the ground level signal. The errors mentioned above are considered to be of uncorrelated sources and therefore the final uncertainty in the measurements δS is shown is equation 4.13 :

$$\delta S = \sqrt{(\delta A)^2 + (\delta B)^2 + (\delta C)^2}\ , \qquad (4.13)$$

where A, B, and C are the errors mentioned above along with the error associated in the NRIS background. The normalized data were fitted to a Boltzmann distribution using a χ^2 fit. Since the number of data points for the fit are small (only 5 energy levels), the amplitude of the Boltzmann distribution was not normalized to 1 and was used as a parameter in the fit. Figures 4.6-8 show the results of this fit. The data from the measurements reported in the literature were also fitted to a Boltzmann distribution using the same method with the uncertainties that were reported in the literature, which are only the statistical errors.

Table 4.3 shows the temperature obtained from these fits and the corresponding primary ion energy used in the experiments. The temperatures tabulated here are different from the ones reported in the literature because of the fit parameters described above. It should also be noted that there is no physical explanation for a Boltzmann distribution of the sputtered Fe. For convenience, the data presented here use one parameter (the "Boltzmann temperature," T_B) to describe the distribution, which is certainly different from the "effective temperature" of 10^4 K mentioned in the

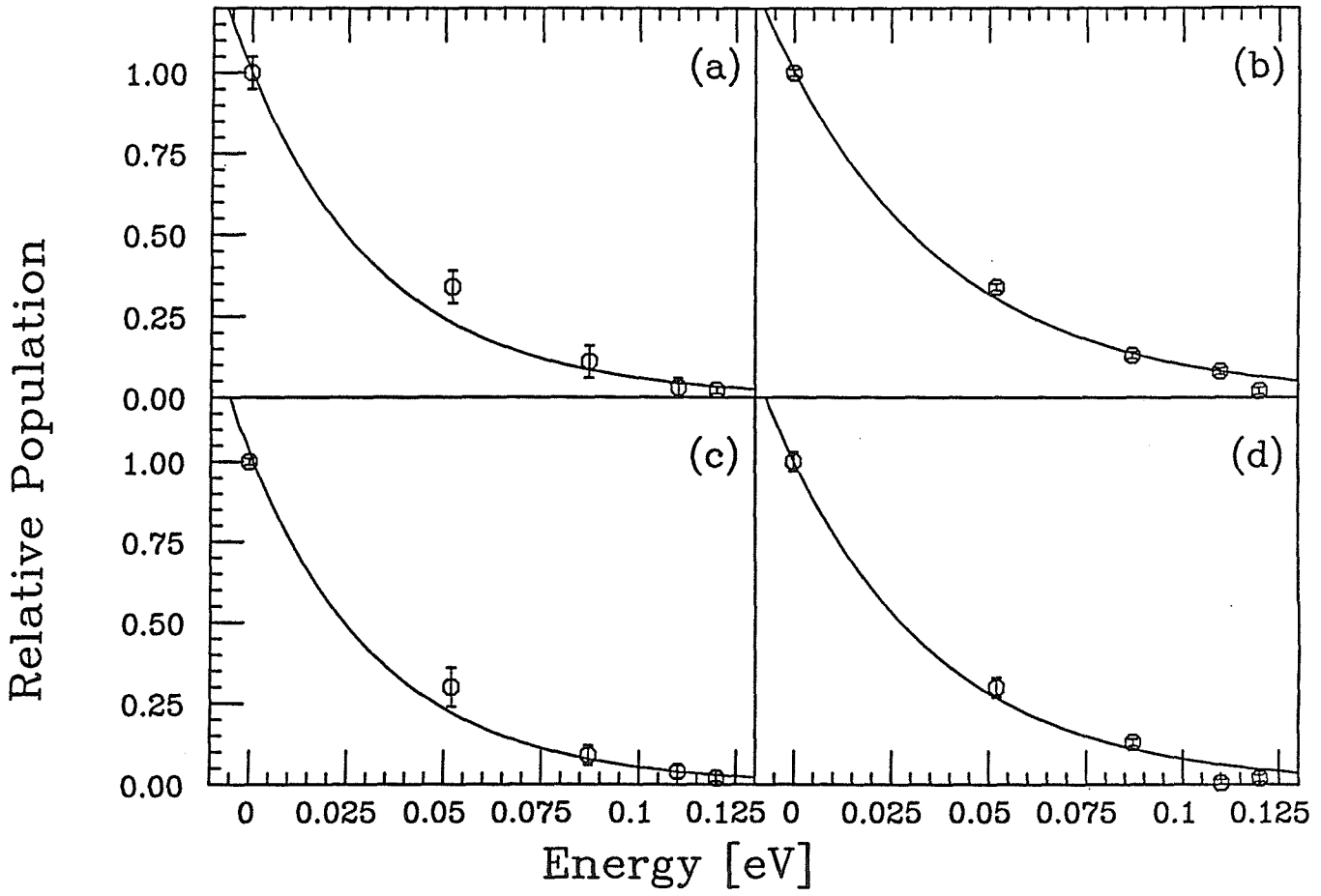

Figure 4.6 a) Measurement of a clean surface of Fe sample by RIS (this study). b) Measurement of clean Fe reported in literature (RIS)[1] c) LFS measurements[2] d) Another RIS measurement by Kimock[4]. Data presented in table 4.2, were fitted to a Boltzmann distribution using amplitude and tempreture as variables.

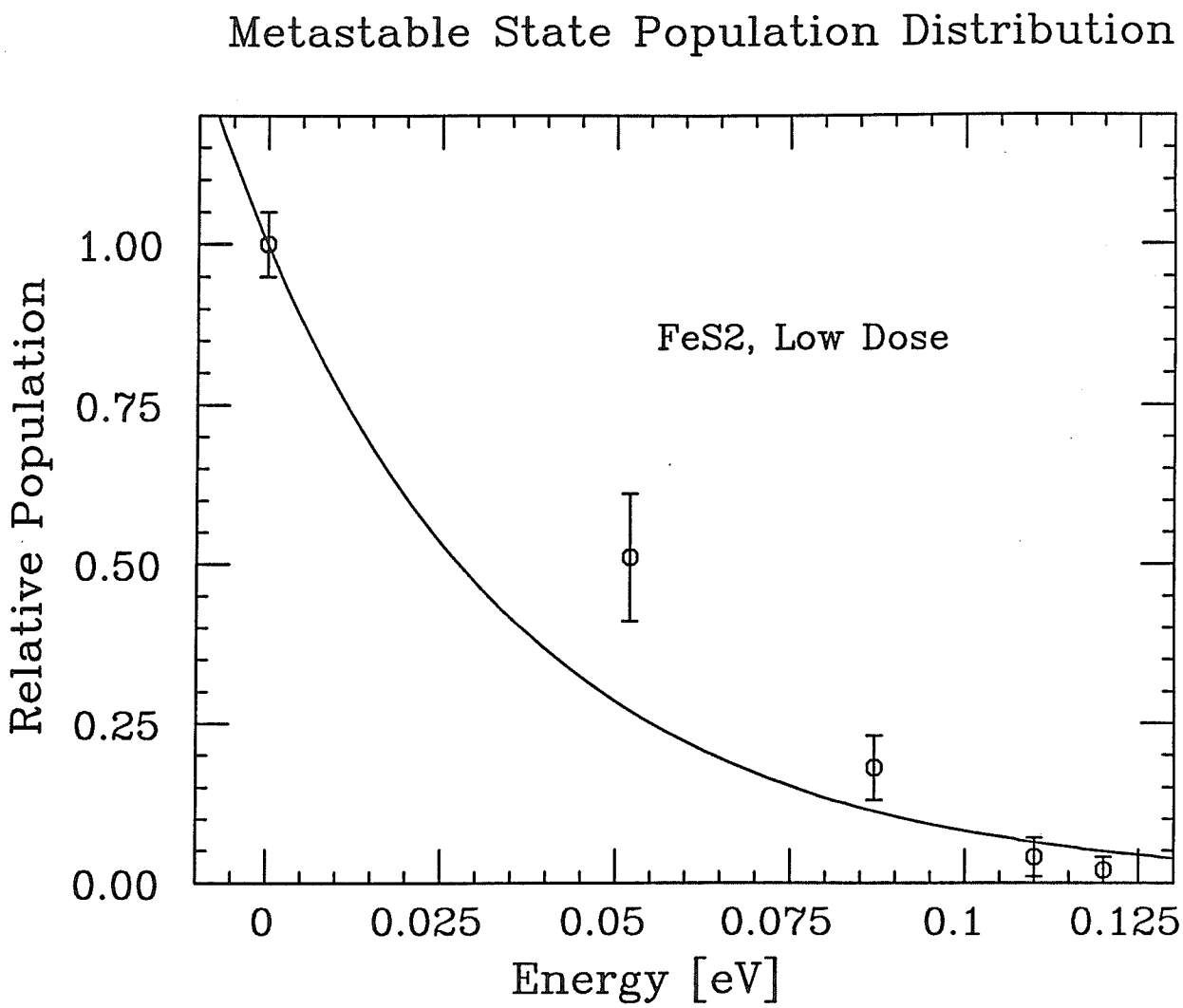

Figure 4.7 The FeS_2 measurements after the sample was sputter-cleaned for a few seconds. This measurement was labeled 'low dose' in table 4.2.

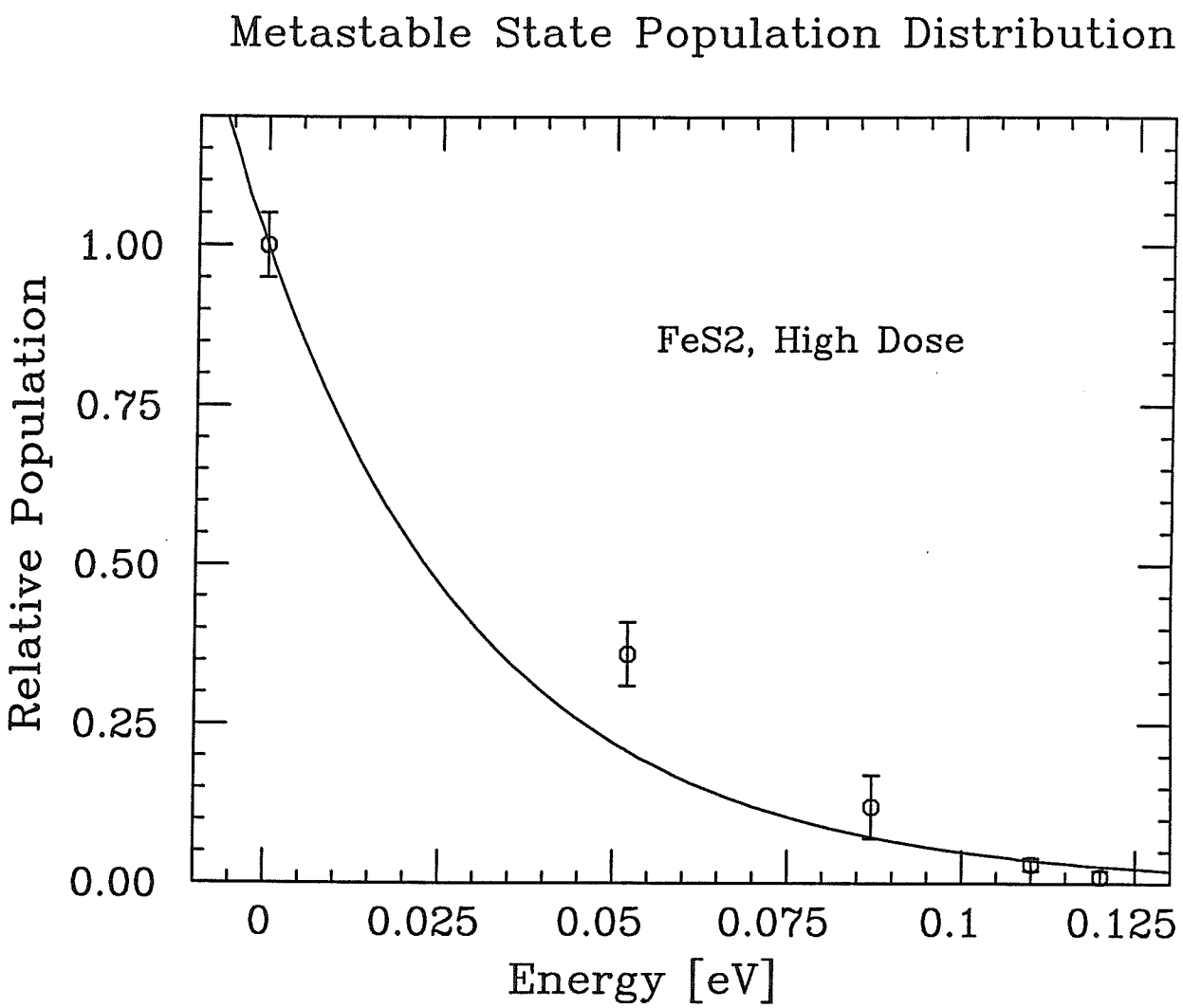

Figure 4.8 The FeS_2 measurements after prolonged bombardment of the sample. This measurement was labled 'high dose' in table 4.2.

SAMPLE	primary ion energy (KeV)	T°(K)
FeS_2	3	461 ± 22
FeS_2^*	3	384 ± 22
Fe	3	408 ± 22
Fe^{19}	3	392 ± 40
Fe^{1}	3	511 ± 40
Fe^{2}	0.9	457 ± 40

* This sample has been bombarded by 10^{18} (ions/cm^2) prior to the measurement.

Table 4.3 The temperatures resulting from the Boltzmann fit for each sample. Within the uncertainties of the measurement, the temperatures of the damaged FeS_2 are close to that of the Fe sample. The temperatures do not seem to be affected by the primary ion energy. The errors in the temperature is calculated by the 'least square fit' program.

background section for the ionization probability of the sputtered species. It would be interesting to understand the meaning of this temperature.

As seen in tables 4.3 and 4.4, the results of the FeS_2 targets are in agreement with the distribution and temperature obtained for the Fe sample. There is, however, a decrease of the Boltzmann temperature from T_B=461K before rastering to T_B=384 K for the FeS_2 sample after it has been rastered. This is closer to the Fe sample temperature T_B=408 K. This change is more apparent when we compare the fraction of the sputtered Fe that is in the ground state. Table 4.4 shows that in the low dose case there is more excited state Fe sputtered from the surface (40%), while the high dose has about 10% less sputtered in the metastable states.

We only have observed a slight change in the population distribution of sputtered Fe due to the presence of S in the target. Experiments using the same target with well-defined surfaces could shed further light on the mechanism of formation of the excited states. This suggests that further measurements of this material are desirable, in which in situ annealing of the crystal surface takes place before the measurements is performed.

Although the results of these experiments are not sufficient to prove or disprove the models described earlier, some qualitative comments about the models can be made. In most of the quantum mechanical models that exist in the literature and are surveyed in

BOLTZMANN TEMPERATURE

Sample	T°(K)	J=4 state population fraction
FeS_2	461 ± 22	57%
FeS_2 (high ion dose)	384 ± 21	66%
Fe	408 ± 22	67%

Table 4.4 The temperatures resulting from the Boltzmann distribution fit for each sample, along with the population of the J=4 state, are summarized. Within the uncertainties of the measurement, the temperature for the damaged FeS_2 is closer to that of the Fe sample. More Fe is sputtered in the excited state from the FeS_2 sample prior to its exposure to the high primary ion dose. The FeS_2 sample that was bombarded by 10^{18} Ar^+ ions/cm^2 prior to the measurements is designated by `(high ion dose).'

the Background section, the information about the spin was left out to simplify the Hamiltonian. There are a few exceptions such as one proposed by Cini[27]. Our measurements deal strictly with excited states that differ in spin-orbit orientation only from one another, so spin could prove to be quite important. Two suggestive trends can be recognized here: first, the role of the surface seems to be important in the population distribution and second, the electronic state of the Fe in the solid does not seem to be very important since the sputtered Fe population distribution of FeS_2 (high dose) is more similar to Fe than the low dose case. In the quantum mechanical models, the most important part of the Hamiltonian is the part that describes the interaction of the solid and the atom, this interaction part or the 'hopping matrix' element is to some extent empirical and the concern has been to predict a realistic secondary ion yield. In dealing with neutrals, the need for a more universal model exists, and data on the metastable states are necessary for the development of such models. It would be useful to know what the final collisions of the Fe are as it leaves the surface of FeS_2. A molecular dynamics simulation of ion bombardment of FeS_2 is a good way to study this problem. In such a calculation, one can follow the history of the collisions experienced by the particle that lead to its ejection from the surface. This could clarify whether or not the presence of S in the target should have a major effect in the metastable state population. This could add to the understanding of any role played by inelastic collisional excitation as suggested in Kelly's model. The investigation of the formation of the excited sputtered atoms from the excited state molecules has not been refuted and should be

investigated further. Molecular dynamics calculations could help in this problem as well.

The role of the primary ion beam energy is negligible in these measurements when compared with the results available in the literature with primary ion energy of 900eV. A previous study by Pellin[1] shows a similar trend, but that study is also within the range of ion beam energy presented here. Further investigation with a wider range of primary ion energy is suggested.

As for the sputtered Fe from FeS_2 that seems to be missing (Chapter 3), we conclude the following. The results of the metastable population distribution have a small ramification on the partial yield of Fe measured by the two methods of NRIS and RIS. That is to say if the ratio obtained with RIS is multiplied by 7/6, the ratio of the partial yield of Fe is increased by 2-3%. The number 7/6 is the ratio of the ground state fraction of the sputtered Fe from the two targets. The metastable population distribution accounts for some of the discrepancy, but it does not explain the observed aberration from the stoichiometric ratio. The evidence still suggests the ejection of Fe in other forms that are not detected. A very possible explanation is sputtered molecules or clusters.

Studying the population distribution of the metastable states in the binary compound has shed some light on the question of how the metastables are formed in sputtering. Comparison of the low dose and high dose FeS_2 measurements indicates that the metastable

states are formed in the interaction with the surface, and the original electronic state of the species is of less importance.

4.5 References

1 M. J. Pellin, C.E. Young, W. F. Calaway and D. M. Gruen, Surf. Sci. **144**, 619 (1984).

2 C.E. Young, W.F. Calaway, M. J. Pellin, and D. M. Gruen, J. Vac Sci. Technol. **A2(2)**, 693 (1984).

3 B. Schweer and H. L. Bay, Vide Couches Minces **201**, 1349 (1980).

4 F.M. Kimock, D.L. Pappas, N. Winograd, Anal. Chem. **57**, 2669 (1985).

5 M.J. Pellin, C.E. Young, M.H. Mendelsohn, D.M. Gruen, B. Jørgensen, R.B. Wright, and A.B. Dewald, J. Nucl. Mat. **111&112**, 738 (1982).

6 G. Slodzian, Phys. Scripta. **T6**, 54 (1983).

7 D. M. Gruen, M.J. Pellin, C.E. Young and M.H. Mendelsohn, Phys. Scripta. **T6**, 42 (1983).

8 G. Betz, and W. Husinsky, Nucl. Instr. Meth. in Phys. Res. **B13**, 343 (1986).

9 See for example:

J.K. Nørskov and B.I. Lundquist, Phys. Rev. B **11**, 5661 (1979).

K. Wittmack, Phys. Scripta **T6**, 71 (1983).

10 Ming L. Yu and N.D. Lang, Phys. Rev. Let. **50**, 127 (1983).

11 M. J. Pellin, R. B. Wright, and D. M. Gruen, J. of Chem Phys., **74**, 6449 (1981).

12 Ming L. Yu, Phys, Scripta. **T6**, 67 (1983).

13 Roger Kelly, Phys. Rev. B **25**, 700 (1982).

14 B. Firsov, Soviet Physics JETP, **36**, 1076 (1959).

15 I.S. Tsong and N.A. Yusuf, Nuclear Instr. Meth. **170**, 357 (1974).

16 Ming L. Yu, D. Grischowsky, and A.C. Balant, Phys. Rev. Lett. **48**, (1982).

17 P.A. Williams, Surf. Sci. **90**, 588 (1979).

18 E. Veje, Surf. Sci. **110**, 533 (1981).

19 Z. Sroubek, J. Zavadil, F. Kubek and K. Zandsky, Surf. Sci. **77**, 603 (1978).

20 Z. Sroubek, K. Zandsky, and J. Zavadil, Phys. Rev. Lett. **45**, 580 (1980).

21 Z. Sroubek, Sur. Sci. **44**, 49 (1974).

22 C.A. Andersen, J.R. Hinthorne, Anal. Chem., **45**, 1421 (1973).

23 A. Blandin, A. Nouriter, and D.W. Hone, J. Phys. (Paris) **37**, 369 (1976).

24 J.K. Nørskov and B.I. Lundquist, Physical Review B **11**, 5661 (1979).

25 C.A. Andersen, J.R. Hinthorne, Anal. Chem., **45**, 1421 (1973).

26 G.S. Hurst, M.G. Payne, S.D. Kramer, and J.P. Young, Rev. Mod. Phys. **51**, 767 (1979).

27 M. Cini, Surf. Sci. **54**, 71 (1976).

Chapter Five

Sputtering of Molecules from Metal-Sulfide targets: FeS_2, ZnS, and CdS

5.1 Introduction

The ejection of molecules has been an area of dispute for as long as sputtering has been used for analytical work. For accurate quantitative yield measurements, the molecular sputtering yield needs to be known and taken into account. It has been the general consensus that, from a clean metal surface, molecules are sputtered in much smaller quantities than atoms. According to some of the existing models for sputtering of molecules, the sputtering yield of molecules should be even lower from a compound material, because the constituents of the molecule may not be on neighboring sights. It will be demonstrated in this chapter that the fraction of sputtered molecules is actually larger than previously believed from the results

of SIMS experiments, and that the molecules are not necessarily formed from adjacent atoms in the solid.

The understanding of the sputtering mechanism for molecules is, at best, in its infancy. Much of the effort of the analysis of sputtered molecules has, for historical and practical reasons, been focused on metallic targets. Moreover, because of the lack of techniques to analyze neutral molecules[1-3], the emission of excited state molecules has been used for yield measurements.

Due to competing processes of formation, fragmentation, and ejection, the sputtering of molecules is a much more complicated process than the sputtering of atoms from a solid surface. When lasers are used for analysis, there is always the possibility that sputtered molecules may be photo-dissociated, which complicates the interpretation of the data.

To get a complete picture of the sputtering of molecules (i.e., to understand the mechanism of their formation), the kinetic energy and internal energy distributions of the molecules should be studied. To make the problem more managable, both theoretical and experimental studies of sputtered molecules have started from diatomic homonuclear molecules. A study of the internal and the kinetic energy distributions of the sputtered diatomic molecules has been done by the group at FOM[4]. This study was done on the sputtering of S_2 from an amorphous sulfur target or frozen CS_2. Theoretical treatments also have been given by Urbassek[5],

Snowdon[6], and Konnen[7]. Molecular dynamics calculations of sputtered molecules have been performed primarily by Garrison[8].

The first question of concern is on the origin of the molecules. The models by Urbassek suggest that the diatomic species are sputtered as a unit, via a single or double collision, and the internal energy and kinetic energy of the molecules are influenced by the orientation of the molecule on the surface (see Figs. 5.1,4). The surface binding energy of a sputtered molecule is also dependent on its orientation. This in turn affects the kinetic energy of the sputtered molecules.

It remains an open question in molecular sputtering as to whether molecules form as a result of simultaneous ejection of neighboring atoms from the solid. This is best examined by sputtering of a binary target, where the constituents of the sputtered molecules do not occupy nearest neighbor sites in the crystal. Answering this question was the primary goal of this study. What we have learned from this study, however, has gone beyond that. We have observed molecules, such as Zn_2, that are not stable in the ground state and only exist in the form of excimers. The yield of these molecules is about 10% of the yield of sputtered atomic Zn, higher than predicted by conventional theory.

There are three major objectives to the understanding of the molecular sputtering. (1) To reduce the number of unwanted sputtered molecules that interfere with the analysis of sputtered

atoms. In SIMS analysis this problem has been dealt with by timing, using the fact that sputtered molecules have lower velocities than the sputtered atoms. In laser ionization processes, the interfering molecules can be rejected in detection. One can exercise more selectivity in the ionization scheme (i.e., the number of excitation steps can be increased). This way, the laser power in each step can be reduced, in order to decrease the probability of nonresonant ionization of molecules. This is not always possible, and it is a rather laborious procedure. (2) For a better quantitative measure of the sputtered particles, it is very important to know the fraction of the neutrals that are ejected as molecules or in other forms. (3) Understanding molecular sputtering sheds light on the nature of the collisions, and the desorption of molecules from a solid surface.

5.2 A Survey of Previous Studies of ZnS, CdS, and FeS_2

5.2.1 Theoretical Models for the Formation of Sputtered Molecules

There are some simple models that describe possible mechanisms of formation and ejection of molecules from the surface of a solid. These models can be divided into two major categories. (1) Direct Emission, in which the molecule is formed in the solid and is ejected via different collisions (a) Single Collision Model[9,5] and (b) Double Collision Model[5,7](2) Recombination method[6] (a) Radiative Association (b) Associative Ionization (see Figures 5.1-5).

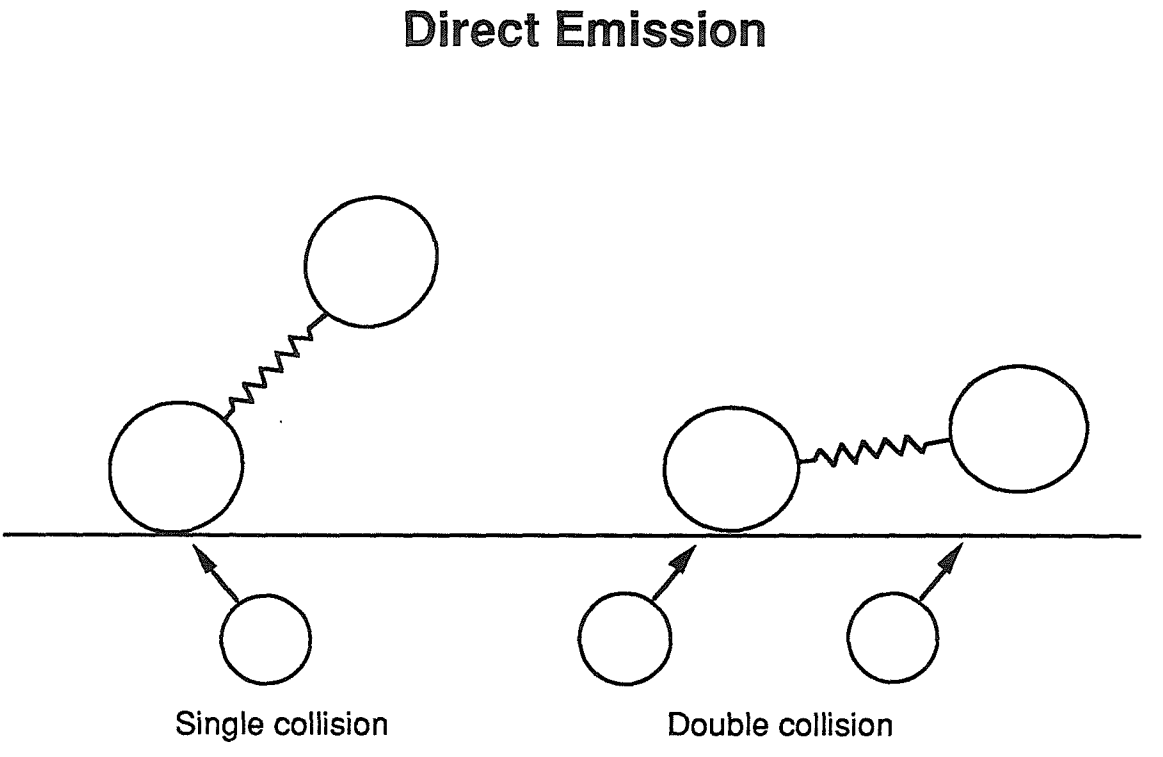

Figure 5.1 The two possible ejection mechanisms for molecules already formed in the solid. The process of ejection is not necessarily orientation dependent as illustrated here.

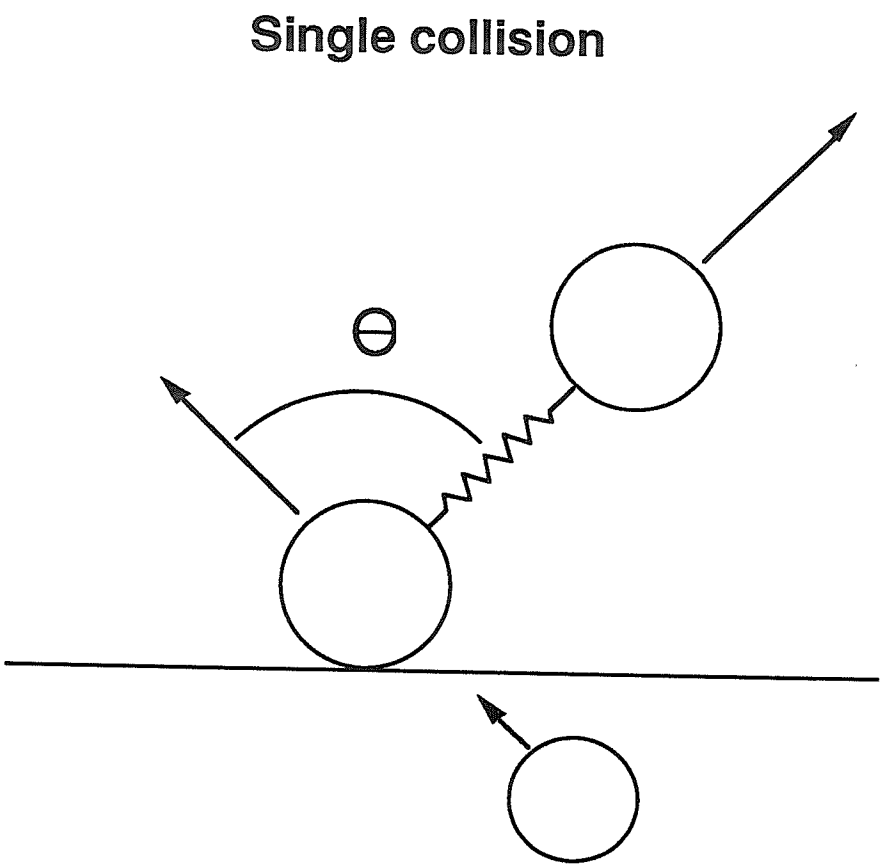

Figure 5.2 The single collision is more probable for stronger molecules that are loosely bound to the surface. As in any other process of ejection, the influential parameters of sputtering are the cascade statistics, dynamics of atom-molecule collision, and passage through the surface barrier.

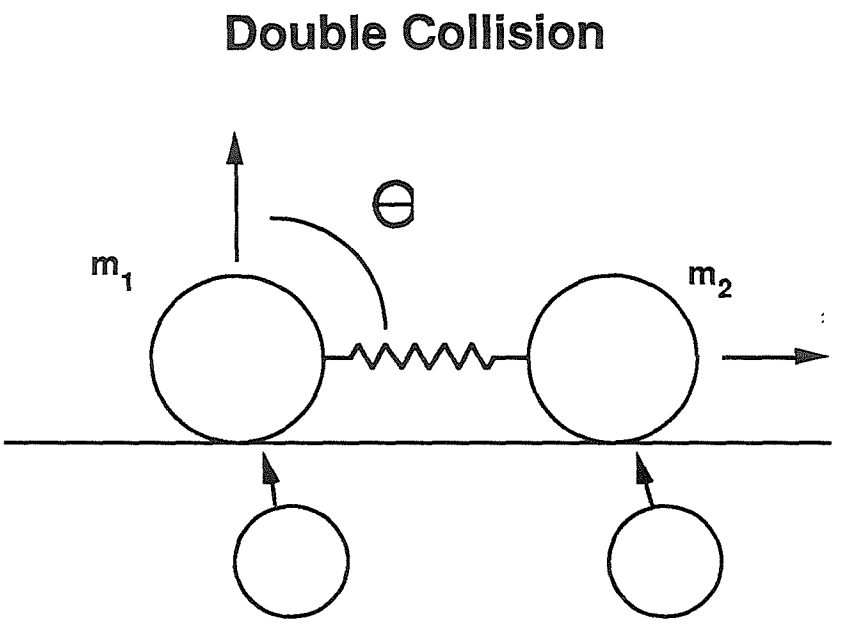

Figure 5.3 The double collision is more probable if more energy is deposited on the solid. Depending on the energy transfer from the individual collisions, the internal energy distribution will be more rotationally or vibrationally excited.

$$E_{vib} + E_{rot} = E_{int}$$

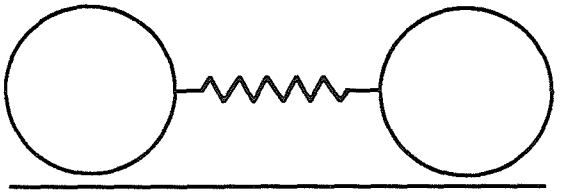

$$E_{rot} = E_{int} \sin^2 \theta$$

$\theta = 90°$

E_{rot} is maximum

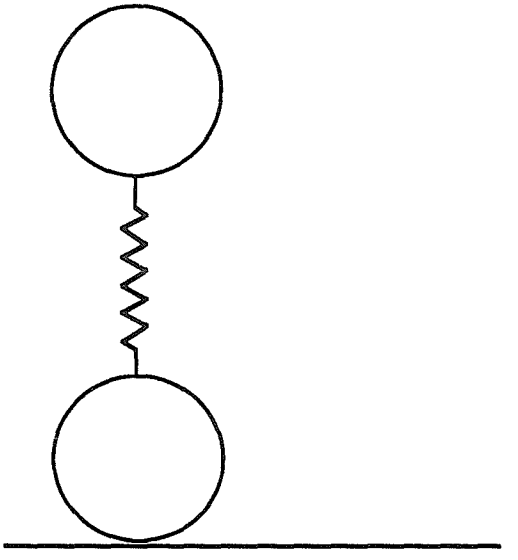

$$E_{vib} = E_{int} \cos^2 \theta$$

$\theta = 0°$

E_{vib} is maximum

Figure 5.4 A simple view of the molecule on the solid assigned by Urbessak. The two extreme orientations of the molecule on the solid surface are shown. In the ejection process, in the first case all of the internal energy would be in the form of rotational energy. The molecule is mainly vibrationally excited through collision, in the second case.

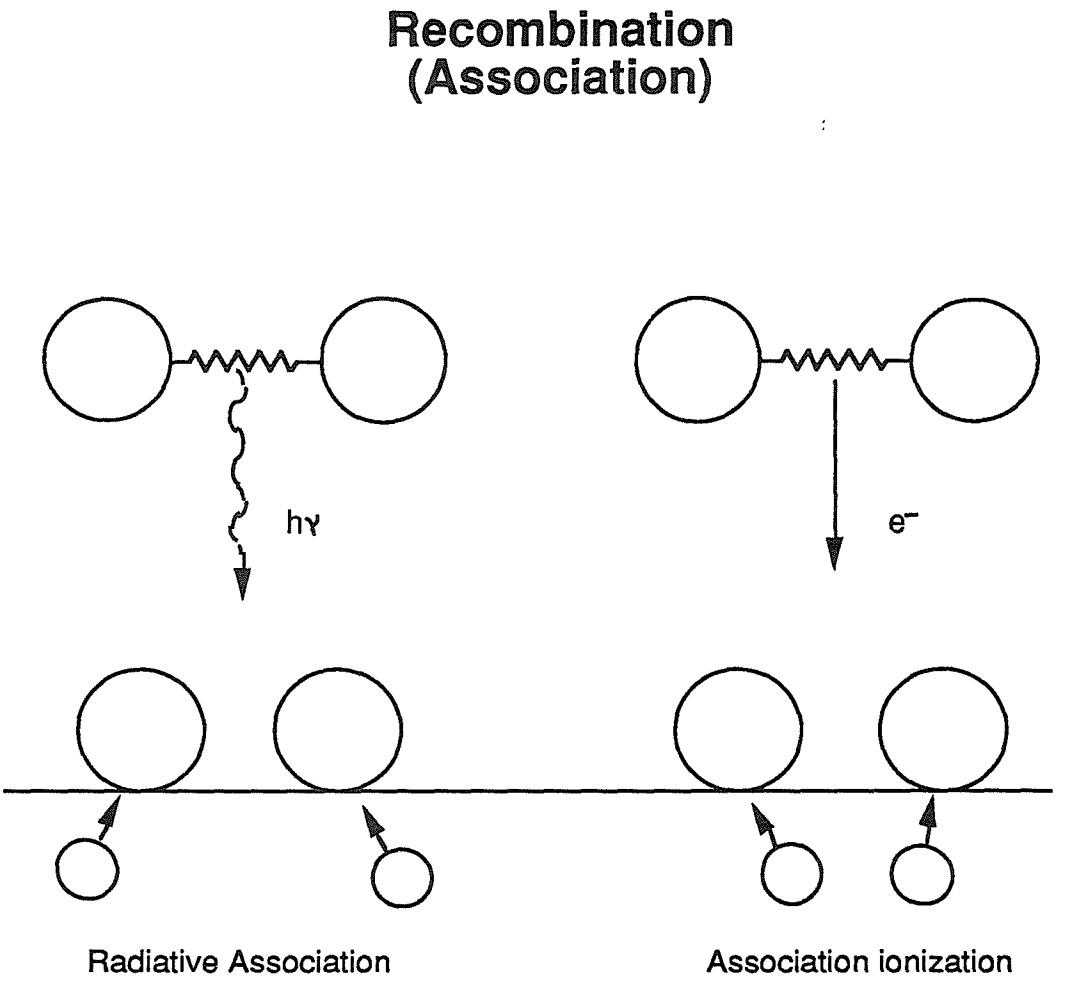

Figure 5.5 Two possible ways of formation of molecules above the surface of the solid, as suggested by Snowden. Simultaneous ejection of two atoms from neighboring sites should occur for this process.

Experimental efforts have been made to determine the mechanism of formation of the sputtered molecules. These experiments have mainly studied secondary molecular ions, for which the yield is dependent on the ionization probability of the sputtered species. Since there is no definite theoretical prediction of ionization probability, it is difficult to determine the absolute yield of molecules. For this reason, it is difficult to determine the mechanism of formation of the molecules. In addition, the sputtered ionic molecules probably form a small fraction of the sputtered molecules. Other techniques have used the optical emission of the excited molecules. There are experiments of S_2 sputtered from amorphous S target and frozen CS_2[10]. There are still no definite models accepted for the sputtering of molecules, but some experimental evidence exists regarding the dependance of the rotational distribution on the vibrational number and the velocity of the molecules. The vibration distribution is independent of the velocity[11,12]. The distribution of the internal energy does not follow a Boltzmann distribution[13].

5.2.2 SIMS Studies of Metal Sulfides

There are a few SIMS studies on the sputtering of metal sulfides that are used in the experiments described here.

In the SIMS studies of a single crystal of ZnS[14], an attempt has been made to show the crystal structure dependence of the yield of the sputtered molecules. In this study, the low energy, low current density Ar ion bombardment shows only those molecules (in enough

abundance for detection) that exist in the solid as neighboring atoms (i.e., ZnS molecules). The fluence and energy of the primary ion is purposely low, to reduce the effect of the ion beam collisions on the structure of the crystal. Because experiments are normally performed with more energetic ion beams, the low energy results are not relevant to the usual experimental conditions. However, the result of this particular work serves as good evidence for the fact that, while sputtering compound materials, the yield of molecules is not dependent on the crystal structure. In this report, SIMS of CaF_2 is reported with $\frac{Ca_2^+}{Ca+}$ of 10^{-3}. This ratio is compared with the ratios of 10^{-1} for targets of metals such as Fe and Cu. This difference is attributed to the fact that, in metal targets, each metal atom is surrounded by similar atoms. The energy of the primary ion beam used for this set of experiments is stated to be 3keV.

Another SIMS measurement on thin film ZnS was an attempt to make quantitative analysis of SIMS data from a compound material[15]. In this work, a 7keV Ar^+ ion beam, with a current density of $0.01mA/cm^2$, is used. No secondary molecular ions were reported in this work. Furthermore, since the assumption has been made that the ions are only sputtered in elemental form, all of the signal at mass 64 is considered to be Zn. This leads to some unexpected phenomena that could otherwise have been explained by secondary S_2^+.

To the authors' knowledge, there has been only one SIMS study of single crystal FeS_2[16]. This single crystal, like the one used in our experiments, is of natural origin. In these experiments, the primary ion beam used is 5keV Ar^+, with current densities as low as 14 nA/cm^2. Ions, in polyatomic, diatomic, and atomic forms, are observed in the SIMS analysis. The observed molecules are positive ions of S, Fe, S_2, FeS, Fe_2, FeS_2, Fe_2S, and Fe_2S_2. The negative ions are S, S_2, and FeS_2. The largest signal in the positive ion yield belongs to the Fe signal and the smallest is S_2. Since the ionization efficiency of the different species is not the same, this was not a quantitative comparative analysis. The mass resolution of the system ($\frac{m}{\Delta m}$) is less than 50.

5.2.3 An overview of thermodynamic studies of Metal Sulfides

The three metal sulfides that are used in the molecular sputtering experiments had been previously investigated for thermodynamic purposes. Crystal structure and thermodynamic data for each sample are presented here, in order to give the information necessary to make conclusions about the data.

a. ZnS and CdS

The Knudsen cell studies of these two metal sulfides[17] have shown that the intensities of the ZnS and Zn_2 molecules in the gas

phase are very small. The ZnS/Zn ratio is less than 10^{-2}, and a similar result is true for the case of CdS.

b. FeS_2

The Knudsen cell studies of FeS_2 have not observed molecular FeS_2 in the vapor; FeS, on the other hand, has been observed in very small amounts[18]. The ratio of FeS to S_2 is less than 10^{-4}. Thermodynamic calculations of the FeS molecule have been based on assumptions about the rotational constant and the properties of the molecule.

In the above studies, the sulfide molecules occurred in such small quantities that parameters such as the appearance potentials in the mass spectrometer are not reported in the literature.

5.3 Materials and Methods

The results presented in this chapter are all from NRIS experiments performed with the SARISA apparatus, operating with an excimer laser. There are three different samples and three operating wavelengths for the lasers. Each sample, and the laser employed for ionization, will be described separately.

5.3.1 ZnS

The single crystal used for this experiment has the Wurtzite structure. The crystal was purchased from Eagle-Pitcher, and polished by LLNL. The sample was ultrasonically cleaned with

acetone and methanol, and was inserted in the SARISA chamber. The sample was sputter-cleaned for two minutes prior to the measurements.

In ZnS crystals, there are no Zn-Zn or S-S bonds, and each element is surrounded by four atoms of the other kind.

The NRIS technique, with an ArF (193nm, 6.4eV) excimer laser, was used for the measurements of the sputtering of ZnS. The laser beam was apertured down and was telescoped to a small size (approximately 100μm) in the direction of the traveling atoms (see Figure 5.6). A Questek excimer laser was power locked at 35mJ/pulse and was operated at 50Hz. The 3keV Ar^+ ion beam pulse width was 500nsec, and the current measured with the Faraday cup was 2μA. The laser power was attenuated with glass plates to a different degree for each run. The signal was charge digitized for higher laser powers; at lower laser powers, the signal was detected by pulse counting. In the charge digitized mode, there were 10^4 laser shots per run, and in the pulse counting mode the number of averages was 100.

5.3.2 CdS

This sample was purchased from Eagle-Pitcher as a single crystal. The crystalline structure of CdS and ZnS is identical. The CdS sample was cleaned by the manufacturer and had a smooth finish. The final step of preparation (by the crystal growers) was to pass the sample through S vapor. Therefore, one side of the sample was

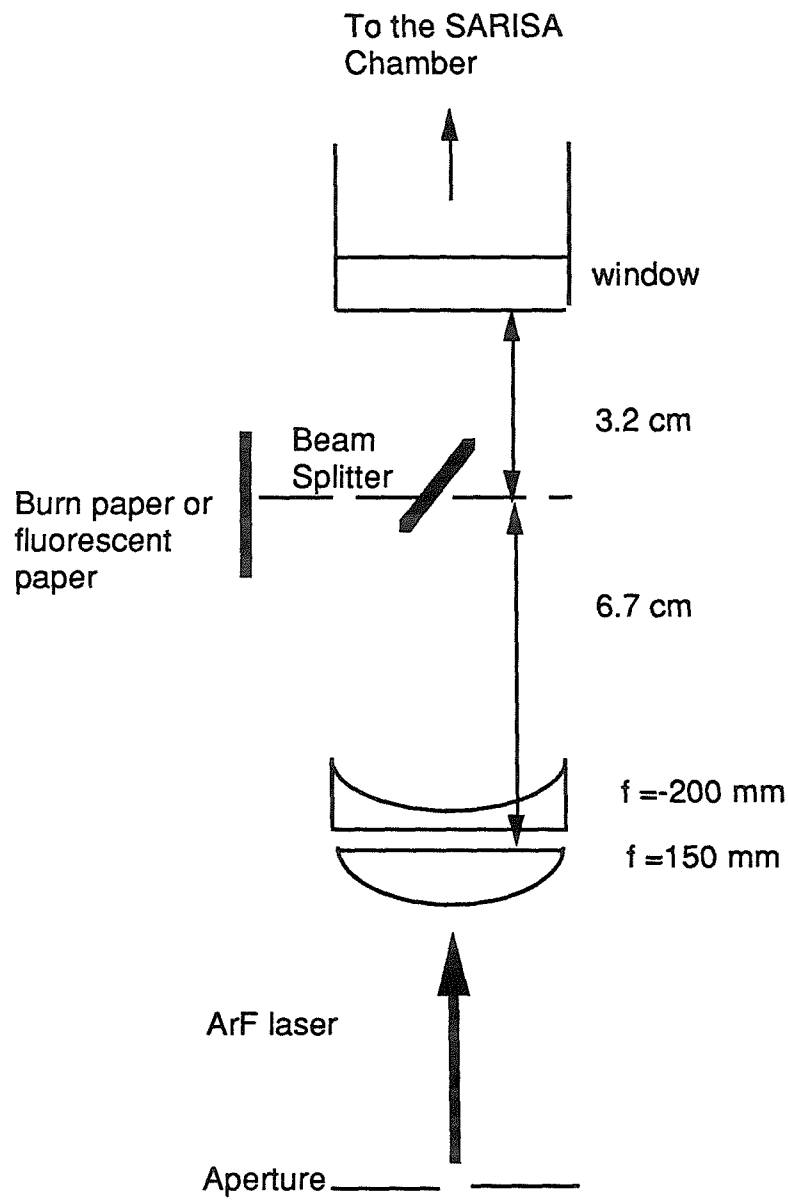

Figure 5.6 The lens system used to focus the ArF excimer laser beam. A burn paper is positioned approximately the same distance as the target. The impression of the beam burned on the paper indicates the size of the beam in front of the target. This size is about 100μm in the flight path. An aperture is positioned before the lens to reduce the size of the beam.

enriched in S, while on the other side Cd was exposed. This sample was sputtered with 3keV Ar^+, and examined by ArF laser ionization in the same fashion described for the ZnS sample. In these experiments the Cd side of the sample was bombarded by the ion beam. The ion beam pulse width was 500nsec and 2000 laser shots were used for each spectrum taken.

A KrCl (222nm, 5.6eV) laser was also used for similar nonresonant experiments. In this excimer laser, stable resonator optics were installed. The beam diverged enormously with this condition, and was only focused down to a 1mm diameter using the same optics as with the ArF laser with the appropriate coating. For these measurements, 10^4 laser shots were used for each run. For the S side of the sample, the ion current was 1.3μA and a total primary ion dose of $1.5x10^{16}$ ions/cm^2 was used in each set of experiments. For the Cd side, the ion beam pulse width used was 100nsec, and the total ion dose was $5x10^{14}$ ions/cm^2.

5.3.3 FeS_2

A natural single crystal of pyrite (FeS_2) was used for the experiments described below. The sample was cut from a face of the cube with a diamond saw, and cleaned ultrasonically in three stages with trichloroethylene, acetone, and methanol. This sample was examined by nonresonant ionization of the sputtered species using the same procedure for CdS. The crystal structure of this sample is different from the other two metal sulfides described above. FeS_2, in the form of pyrite, has an NaCl structure, where Fe replaces the Cl,

and Na is replaced by an S pair. The experiments with ArF laser were the same as described with CdS. This sample was also examined using a KrCl laser, as described above for CdS, as well as with the KrF laser (248nm, 5eV), but no power studies were done for the latter wavelength.

5.4 Results and Discussion

The results of ion bombardment of FeS_2, ZnS, and CdS are best understood by reference to their dissociation energies and ionization potentials (summarized in tables 5.1,2). The signal level of the sputtered species was studied as a function of the laser power for different excimer lasers (power study). The results of these studies are presented as the ratio of signal from the sputtered dimer to the signal obtained from the sputtered atom. Note that the powers plotted in the power studies is an average power measured at the exit window of the SARISA chamber. In all of the experiments, the primary ion beam was of 3keV Ar^+.

In ion bombardment of ZnS, we have observed sputtering of S, S_2, Zn and Zn_2 in neutral form (see Figure 5.7a). There is isobaric interference for S_2 and ^{64}Zn. As seen in Figure 5.7b, there are three more dominant isotopes of Zn with masses (in amu) of approximately 64 (48.6%), 66 (27.9%), and 68 (18.8%). The natural abundance of the isotopes is given in the parentheses. There also exists an isotope of mass 67amu (4.1% natural abundance), which is not resolved completely in these measurements. The major isotope of S (32 amu)

Molecules	D (eV)	IP (eV)
Cd_2	.09(D)	-----
CdS	3.9 ± .3	-----
Fe_2	1.1(C)	-----
FeS	3.3(C)	-----
FeS_2	-----	-----
Zn_2	.168	9.0 ± .2
ZnS	2.1(C)	-----
S_2	4.4(A)	9.4

Table 5.1 The ionization potential (IP) and dissociation energies (D) are the relevant parameters in the formation of molecules in sputtering. The data from Radzig[19] indicates the precision in the measurements by the letter in the parentheses. The letters A, C, and D mean 1%, 10%, and 30% accuracy in the measurements. The blanks in the table are values not found in the literature. The IP of Zn_2 and D of CdS were reported by other sources[20,21].

Element	Sublimation energy(eV)	Ionization Potential (eV)
S	2.88	10.36
Fe	4.34	7.9
Zn	1.35	9.39
Cd	1.16	8.99

Table 5.2 Sublimation energies of the elements from Nagoya Tables (Ref. 3.7). The surface binding energies of these elements from the elemental target is estimated to be equivalent to these values. The ionization potentials are from Radzig[19].

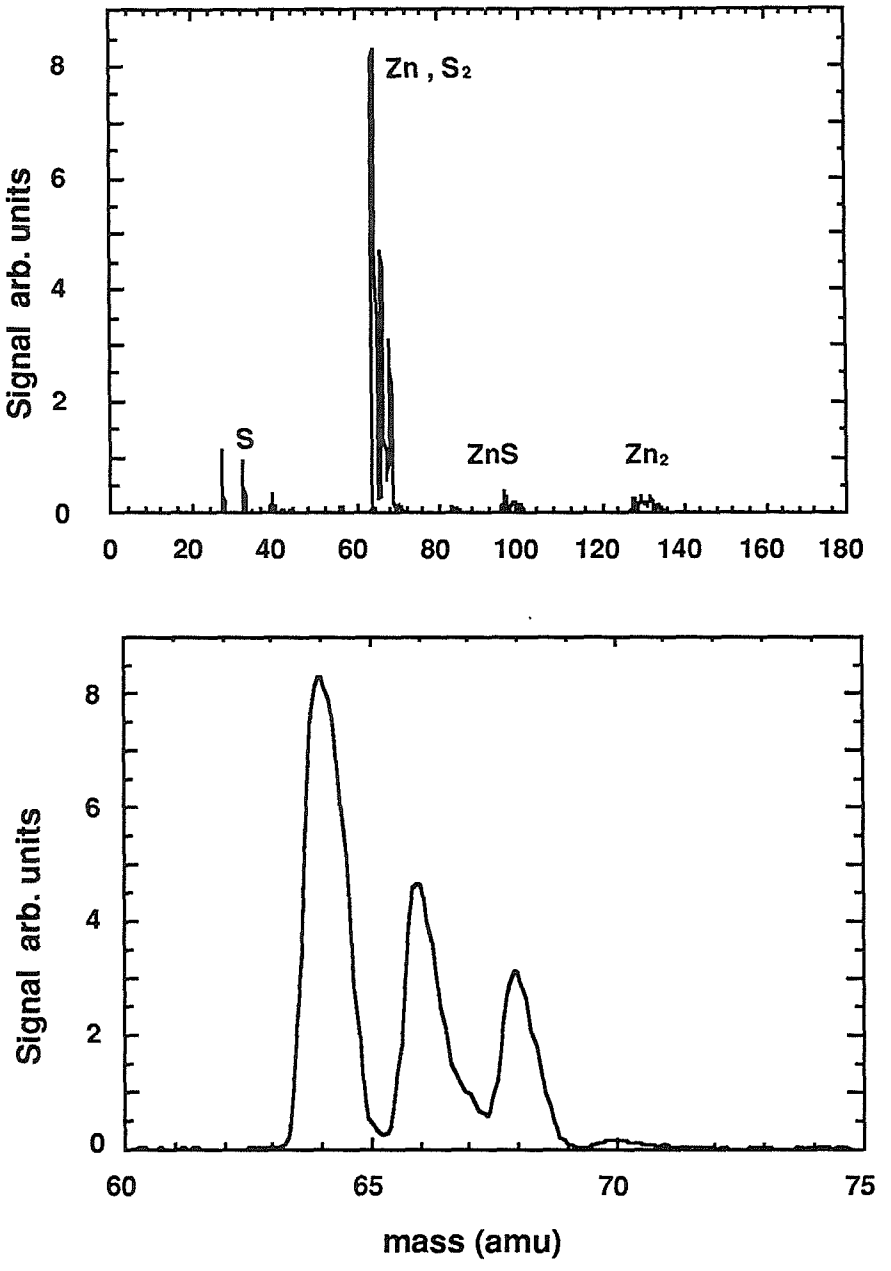

Figure 5.7 a) A NRIS spectrum of ZnS obtained with ArF laser. b) Higher resolution spectrum of the Zn isotopes from the same spectrum.

makes up 95% of S, thus the interference of S_2 with ^{64}Zn. One can use isotopic ratios of Zn to verify the existence of S_2. While the ratio of $^{68}Zn/^{66}Zn$ stayed the same with increasing laser power, the ratio of $^{64}Zn/^{66}Zn$ increased. Figure 5.8 shows the result of using the ratios of the Zn isotopes and subtracting the mass 64 signal from the natural abundance of ^{64}Zn. The subtracted signal is assumed to be the signal from the sputtered S_2, and is plotted as a function of the laser power (ArF). The increase of the S_2 signal with increasing laser power is a sign that the ionization is not saturated. The S_2 signal remains constant for a small range of laser powers, and the signal starts declining again. This trend suggests that the dimer is photo-dissociated at higher laser powers. The same effect is observed when the laser beam is de-focused. However, only the Zn signal is decreased with the attenuation of the laser power.

Among the other sputtered species from ZnS are two very interesting molecules, ZnS and Zn_2. The interest in the two molecules has different origins, but both contain information regarding sputtering and formation of sputtered molecules. They are both rare molecules (in the gas phase). The ratio of the molecules to Zn atoms was calculated by using the peak height of ^{64}Zn for the atom and the highest peak for each dimer. The maximum ratio of the dimer to atom for these two molecules has been measured to be 20% for $\frac{Zn_2}{Zn}$, and 10% for $\frac{ZnS}{Zn}$ (see Figs. 5.9,10). It must be noted that the measurements here are NRIS measurements, and the signal ratios cannot be used as a direct quantitative measure of the relative

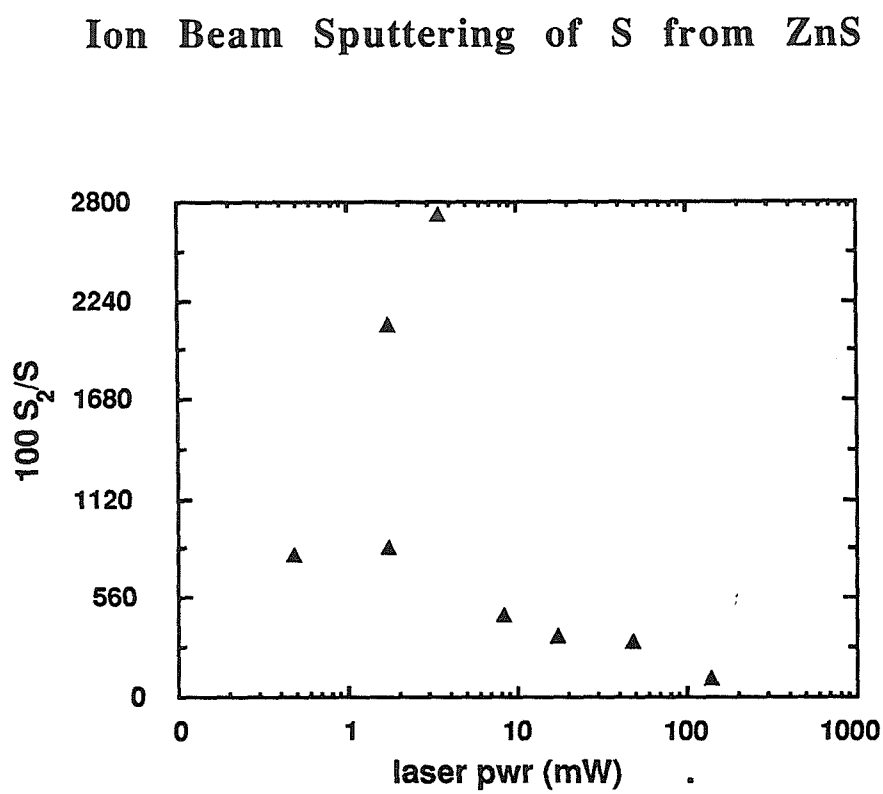

Figure 5.8 Ratio of the S molecule to the atom, sputtered from ZnS sample, as a function of the laser power. At higher laser power the photodissociation of the molecule is the more prevalent mechanism. The signal for S_2 is obtained by using the isotope ratios in the Zn signal. The laser used for ionization is an ArF laser. The laser power was measured at the exit point of the chamber and is not an absolute measure of the laser power, rather a relative scale.

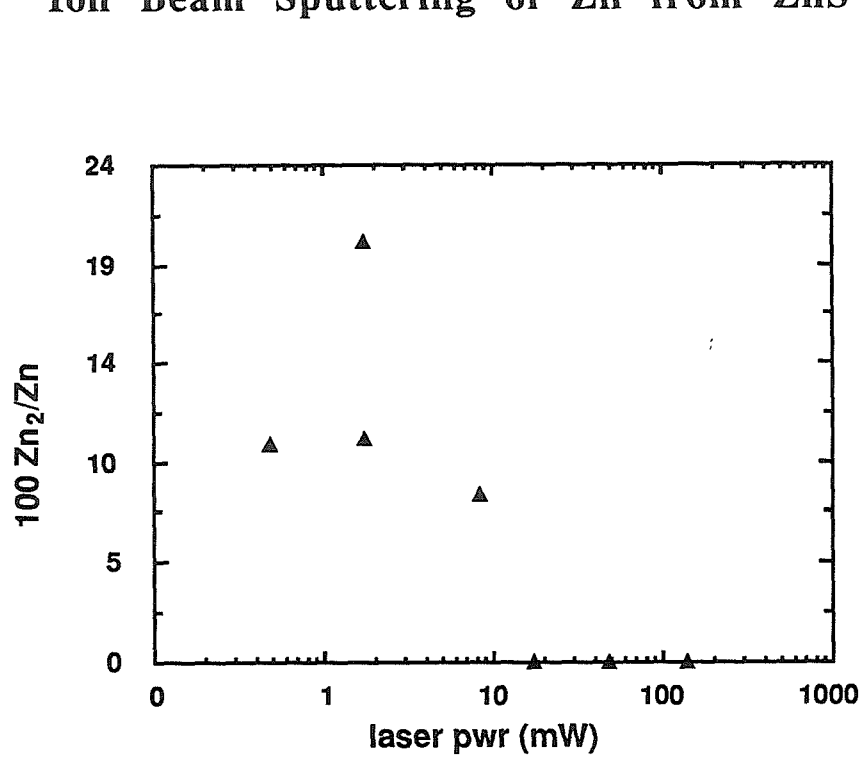

Figure 5.9 Ratio of the Zn dimer to the atom, sputtered from a ZnS sample, is plotted as a function of the ionization laser (ArF) average power. This diatomic has a lower dissociation energy than S_2 and at higher laser powers is completely photo-dissociated.

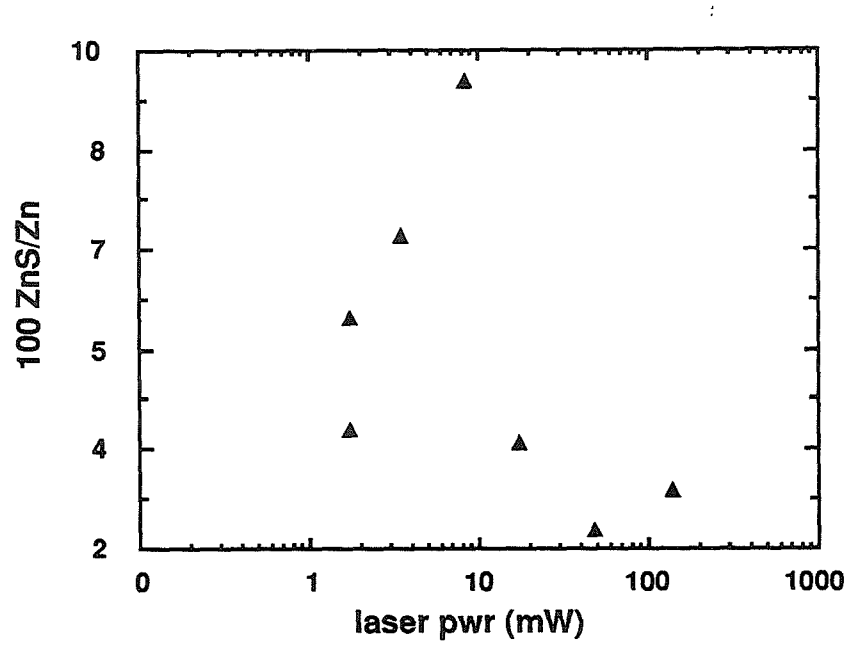

Figure 5.10 Ratio of the sputtered ZnS dimers to Zn, sputtered from an ZnS sample, is plotted as a function of the ArF laser average power. The laser power was measured at the exit window of the chamber. This ratio at lower laser powers is smaller than the Zn_2 to Zn ratio. This molecule has a higher photodissociation energy than the Zn dimer.

yields unless the ionization transition is saturated for all the species. Saturation of ionization of the molecules, however, is not trivial since the observed signal is a result of competing processes of ionization and fragmentation. The ionization efficiency of the different species is different as well as the dissociation energy of molecules. However, a lower limit for the molecular sputtering yields can be obtained from these studies.

In order to eliminate the isobaric interference with the metal, we also examined CdS. This material has the same crystal structure, and mass of Cd is ~114amu (eight isotopes). These experiments were done by 3μA ion beam with a pulse width of 400nsec. The number of laser shots used was either 1000 or 2000. An ArF NRIS spectrum of sputtering of CdS is shown in Figure 5.11. We started with the full laser power and attenuated the power by inserting glass plates in the beam path, making sure that the plates were perpendicular to the laser beam, so that the beam intensity profiles remained the same. This caution is taken because the velocity and angular distributions of the sputtered species may be different. The full average laser power at 20 Hz (the repetition rate at which the experiments were performed) was measured to be 40 mW (measured at the exit window of the SARISA chamber). The aperture, located in front of the lenses (Fig. 5.6), was open during these measurements. The laser power was attenuated to 7mW. The detector bias throughout the measurement was increased by 100V. The total ion dose to the crystal was about 1.6×10^{16} ions/cm^2. The preferential sputtering, mentioned in Chapter 3, is possibly stronger due to the larger mass

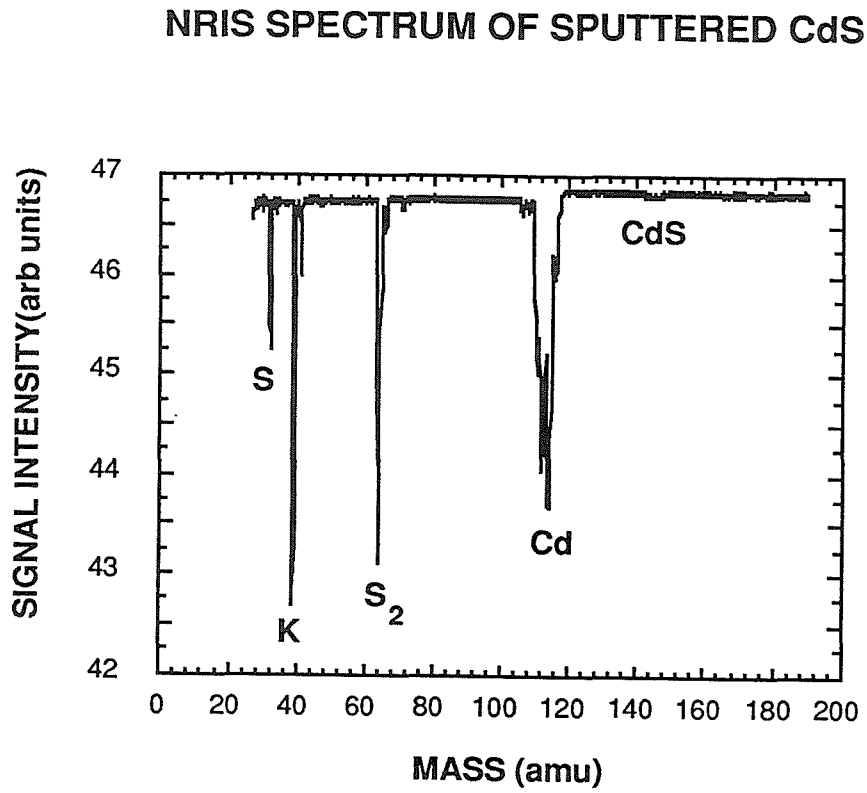

Figure 5.11 A NRIS spectrum of sputtered species from CdS. An ArF laser was used for nonresonant ionization.

difference of S and Cd. Preferential sputtering of S was previously reported by Moens et al.[22] The effect of competition between the two processes of photo-fragmentation and ionization is observed dramatically for S_2. The $\frac{S_2}{S}$ ratio of CdS, as a function of laser power, is plotted in Figure 5.12. The S_2 signal is almost always greater than S. The signal from CdS is not very strong, and the experimental conditions precluded the detection of Cd_2. On the average, the $\frac{CdS}{Cd}$ ratio is about 1.8%. To compare these experiments with ZnS, we did not observe Cd_2, as opposed to Zn_2. However, the laser power was only attenuated by almost an order of magnitude, and perhaps we would see Cd_2 at lower laser power. It should be pointed out that the dissociation energy of Cd_2 is even lower than that for Zn_2. It was shown in the experiments with CdS that our assumption about Cd_2 is correct, because at the lower power densities of KrCl, Cd_2 is observed with the same ratio to CdS as was observed when sputtering ZnS.

In the KrCl experiments, the Cd signal is again very strong. By blanking the Cd signal, we were able to detect Cd_2, CdS, and CdS_2. The signals obtained from these species were at most 2% of the Cd signal. Of the sputtered molecular species, the Cd_2 signal was the strongest, followed by CdS and CdS_2. The ratio of $\frac{S}{Cd}$, measured at the same laser power as the above species, is ~24%. The S/N ratio in these experiments was not as high as in the experiments performed with the ArF laser. The same qualitative trends in the change of the dimer signals as a function of the laser power were observed for these experiments, for both sides of the sample.

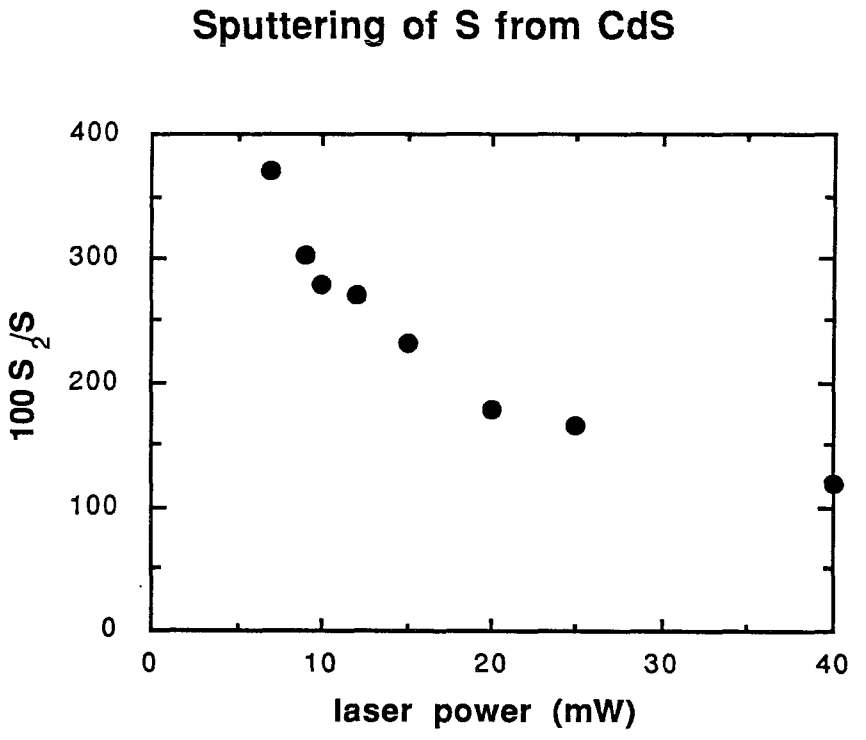

Figure 5.12 The ArF power study of sputtering CdS. The same qualitative behavior is observed for the ratio of sputtered S molecule to atom as for the sputtering ZnS in Fig. 5.8. The average laser power plotted here was measured at the exit window of the chamber.

A NRIS spectrum of sputtering of FeS_2 is shown in Figure 5.13. The ion beam current was 1.3μA, with 400nsec pulses. A laser power study was done as described above. The laser power was measured at the exit window of the SARISA apparatus, and was attenuated by an order of magnitude in several runs; the detector bias was increased by 200 volts throughout the measurements (thedetector gain increases by a factor of ~4 for every 100V increase in the bias, see Figure 4.4). The $\frac{S_2}{S}$ ratio is plotted as a function of the laser power in Figure 5.14. The ratio of $\frac{FeS}{Fe}$ was calculated using the signal from ^{56}Fe. The signal ratio is plotted as a function of the laser power that was measured during the experiments (see Fig. 5.15). In the case of both dimers, the ratio increases with laser power up to some intermediate laser power, and it decreases with further increase in the laser power. The $\frac{FeS}{Fe}$ ratio was at its maximum of 10% at laser power of 30mW. For the same laser power, a maximum of 400% was observed for $\frac{S_2}{S}$. At lower powers, a weak FeS signal was observed (<.1.8% for 10mW). The ratio of $\frac{S}{Fe}$ was from 0.6% to 6%.

The results of the KrCl laser ionization are simple to summarize: mainly Fe signal was detected. At lower laser powers some S and S_2 were observed. The same is true for the analysis with the KrF laser, but perhaps for different reasons. In the case of KrCl, the power density is too low to ionize these species, but in the case of KrF, the high laser power density is perhaps causing photo-dissociation of the

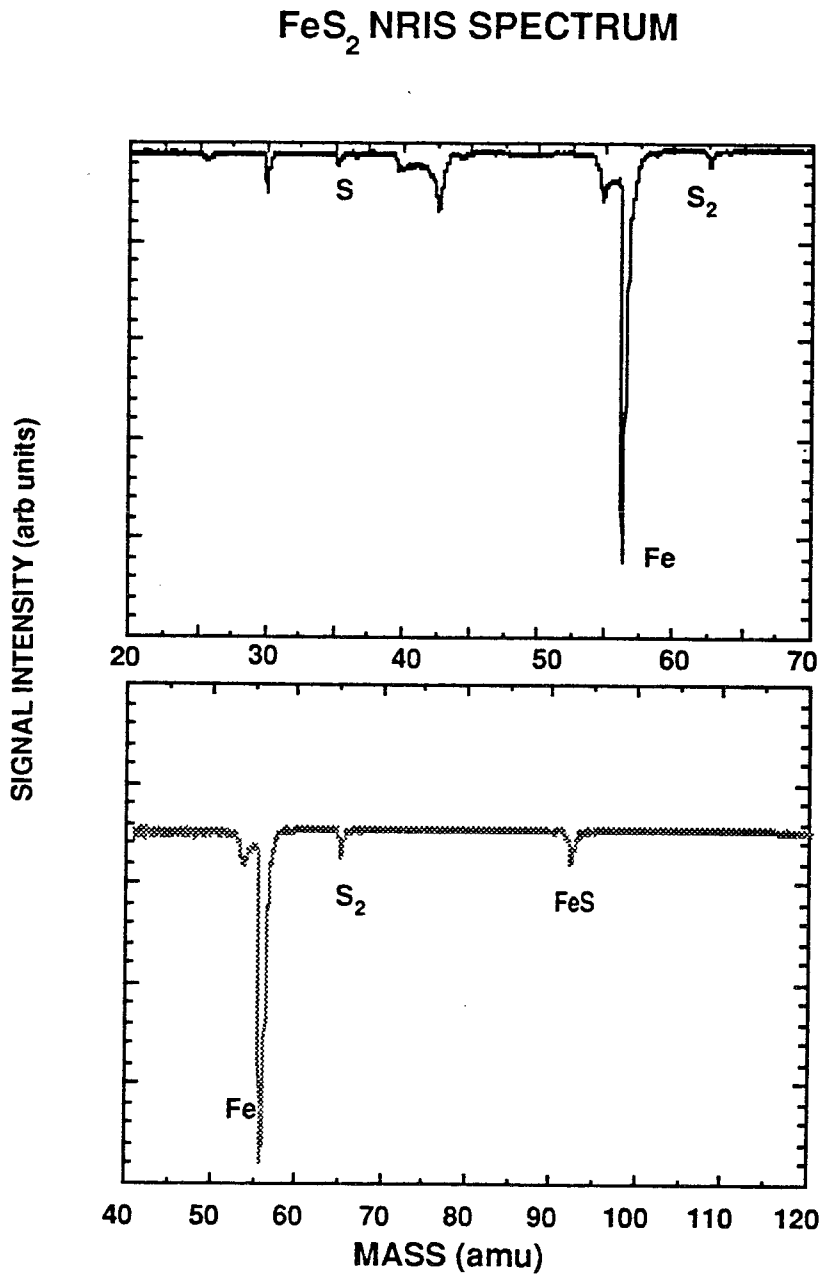

Figure 5.13 The NRIS spectrum of FeS_2 . The excimer laser used was ArF.

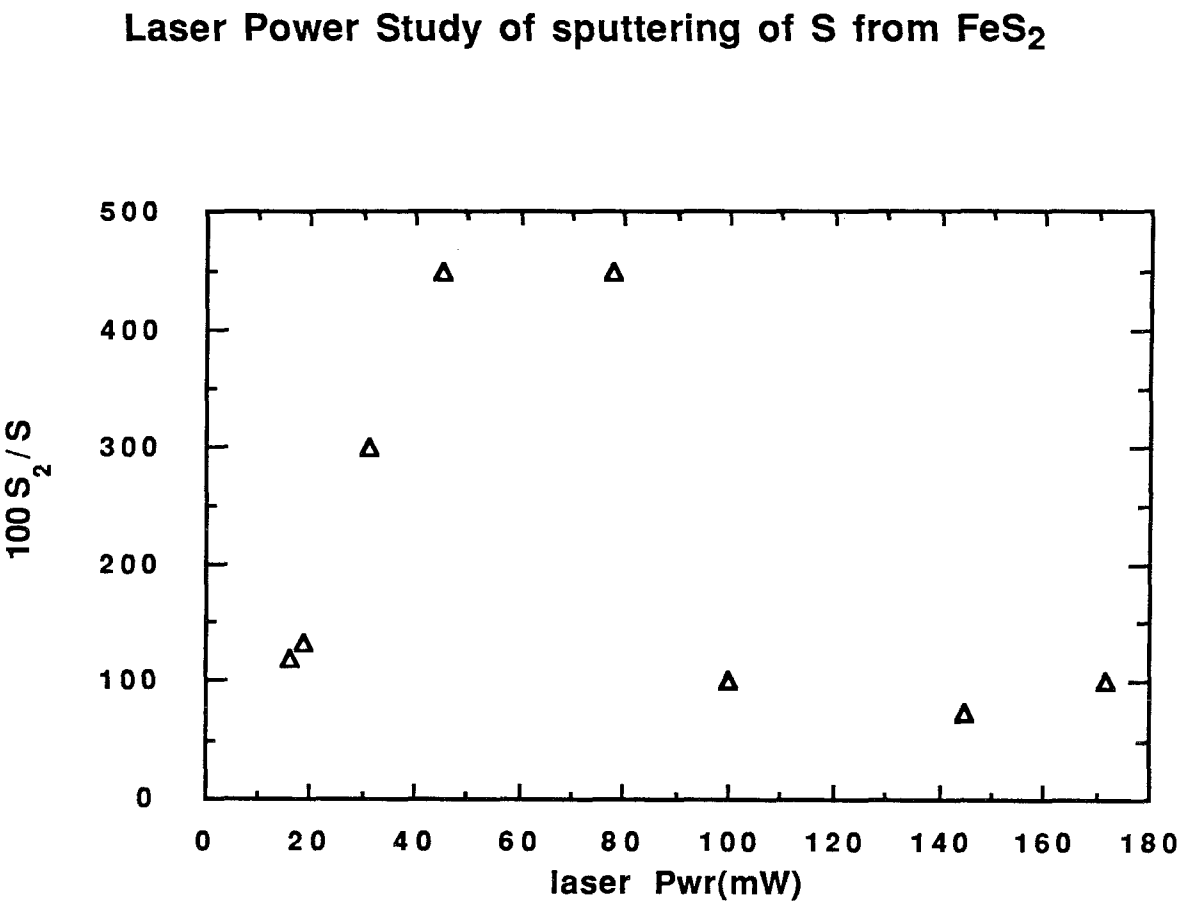

Figure 5.14 ArF laser power study of sputtering of FeS_2. The average laser power is measured at the exit window of the SARISA chamber. The ratio of sputtered dimer to atom has similar trends with the two other targets (CdS, ZnS)

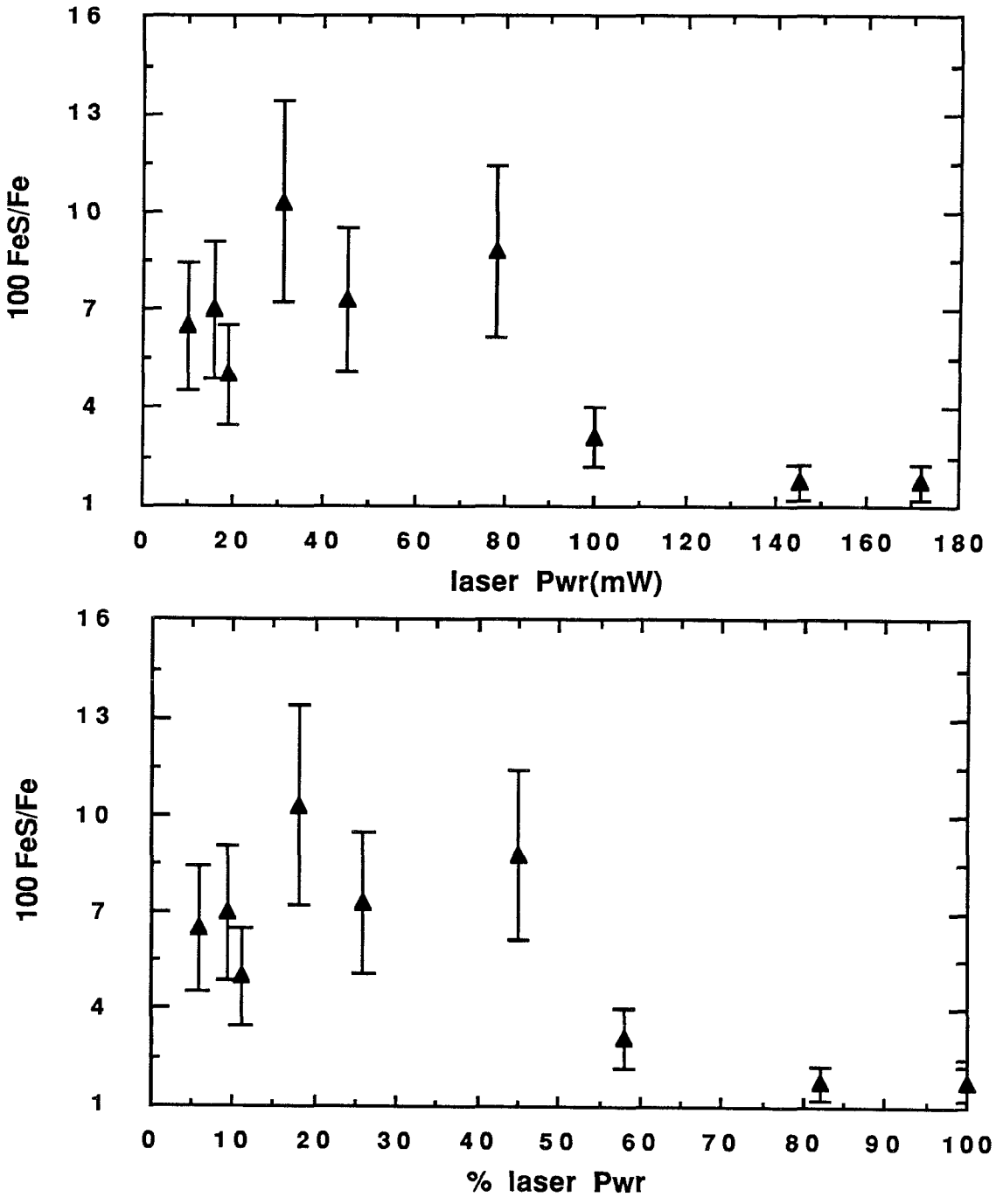

Figure 5.15 The ratio of the diatomic molecule of FeS to Fe sputtered from FeS_2 target. The NRIS was performed using ArF laser. The average laser power was measured at the exit window of the chamber.

molecule. The experimental results described above are all from the NRIS technique. The ionization efficiency of the species is different in this technique. The instrument in these runs is optimized to detect the sputtered metal element. However, this means that the ratios given above at least describe a lower boundary value. The metal sulfide (Metal=Fe, Zn, or Cd) is sputtered at a lower rate than S_2 and the metal dimer (in the case of Zn and Cd). This is a surprising result, because the metal-sulfur bonds are the only ones existing in ZnS and CdS. In the case of FeS_2, only sulfur-sulfur and metal-sulfur bonds exist. All of these species are ionized by two photon absorption. The mere presence of these molecules in the spectrum of the sputtered species suggests that the sputtered molecules form either above the solid surface after they have been ejected due to ion bombardment, or they form in the solid as a result of many collisions. Since the flux of sputtered atoms is not, in general, high enough for the first mechanism (recombination), the latter seems more plausible. It seems that the survival of the molecule depends on its dissociation energy and the binding energy of the molecule to the surface. One can assume, to first order, that the binding energy of the molecule is equal to the sum of the surface binding energies of the constituent atoms, and, further, the atoms' surface binding energy can be estimated by the elemental sublimation energy. This way the rate of survival of S_2 and metal dimer over metal-sulfide is a reasonable observation. Of course, these are suggestive trends, and resonant experiments of the molecule's internal energy could shed more light on the issue. One conclusion is definite: the formation of molecules is independent of

crystal structure. Through collisions, the atoms move in the solid, possibly forming dimers. The more stable molecules that are less strongly bound to the surface survive the ejection collisions, and can be detected as sputtered molecules. The detection with laser ionization is possible if ionization has a high probability and the molecule is not photo-fragmented. Fragmentation of the molecules also can occur by other mechanisms at any time within the flight path to the detector.

Because the sputtered molecules seem to form a significant percentage of the sputtered species, it is important for quantitative analyses to obtain an accurate measure of their sputtering yields. Another interesting result of these measurements has been the observation of the van der Waals molecules Zn_2 and Cd_2. These molecules are probably excimers. There is not much information on the spectroscopy of these molecules (the same is true for FeS), except for calculations, matrix isolation studies, and formation of the molecules from excited atoms. These facts make resonance measurements rather difficult.

We can summarize our observations with the explanation offered above as follows. We have observed sputtered molecules that their constituents do not have a bond in the solid. S is predominantly sputtered as S_2 . Since preferential sputtering of S seems to be present in all three samples, as the surface is depleted of S, moving S atoms in the cascade have less probability of encountering another S atom. Thus, the yield will consist of more

single atoms. The photodissociation energies for Zn_2 and Cd_2, tabulated in Table 5.1, are the values for the ground state molecule. These molecules are more strongly bound as excimers. Cd and Zn have surface binding energies that are smaller than that of S. It is conceivable to think of the metal sulfide as being more strongly bound to the surface than the metal dimers of Cd and Zn. This is one possible explanation for our observation. The results presented in this chapter also suggest some form of recombination mechanism (inside or outside the solid) is responsible for formation of molecules. We have also confirmed the importance of molecules in quantitative yield measurements. The bigger molecules, which could have also affect the yield measurements, were not observed, and their exact contribution remains for further investigations.

5.5 References

1 M.J. Pellin, W. Husinsky, W.F. Calaway, J.W. Burnett, E.L. Schewitzer, C.E. Young, B. Jørgenson, and D.M. Gruen, J. Vac. Sci. Technol. **B5**, 1477 (1987).

2 O. Oechsner and W. Gerhard, Surf. Sci. **44**, 480 (1974).

3 W.O. Hofer and H. Gnaser, Nucl. Inst. Meth. in Phys. Res. **B18**, 605 (1987).

4 R. De Jonge, T. Baller, M.G. Tenner, A.E. De Vries, and K.J. Snowdon, Europhys. Lett. **2**, 419 (1986).

5 H. M. Urbassek, Nucl. Instr. and Meth. in Phys. Res. **B18**, 578 (1987).

6 K.J. Snowdon, R. Hentschke, W. Heiland, and P. Hestel, Z Phys. A-Atoms and Nuclei **318**, 275 (1984).

7 G.P. Konnen, A. Tip, and A. E. De Vries, Rad. Eff. Vol. **21**, 269 (1974).

8 B.J. Garrison, N. Winograd, D.E. Harrison Jr., J. Chem Phys. **69**, 1440 (1978).

9 P. Sigmund, H.M. Urbassek, and D. Matragrano, Nucl. Instr. and Meth. in Phys. Res. **B14**, 495 (1986).

10 R. De Jonge, 1987, Ph.D. Thesis, FOM Institute.

11 R. De Jonge, K.W. Bensist, J.W. Major, A.E. De Vries, and K.J. Snowdon, Nucl. Instr. and Meth. in Phys. Res. **B28**, 214 (1987).

12 K.J. Snowdon, R.A. Haring, Nucl. Instr. and Meth. in Phys. Res. **B18**, 596 (1987).

13 E.A. Thomas and L. Efstathiou, Nucl. Inst. Meth. in Phys. Res. **B2**, 479 (1984).

14 R. Buhl and Preisinger, Surf. Sci. **47**, 344 (1975).

15 A. Aoki, Jap. J. of Appl. Phys. Vol. **19**, 1901 (1980).

16 M.A. Karolewski and R.G. Cavell, Surf. Sci. **210**, 175 (1989).

17 M. Grade and W. Hischwald, Z. anorg. allg. Chem. **460**, 106 (1980)

18 J. Berkowitz and J.R. Marquart, J. of Chem. Phys. **39**, 275 (1963).

19 A.A. Radzig and B.M. Smirnov, *Reference Data on Atoms, Molecules, and Ions* (Springer-Verlag, Berlin, 1985).

20 A.G. Gaydon, *Dissociation Energies and Spectra of Diatomic Molecules* (Chapman & Hill, London, 1968).

21 S.W. Buckner, J.R. Gord, and B.S. Freiser, J. Chem. Phys. **88**, 3678 (1988).

22 M. Moens, M. Van Craen, and F.C. Adams, Analytica. Chimica Acta. **161**, 53 (1984).

APPENDIX

TOTAL SPUTTERING YIELD MEASUREMENTS OF METAL SULFIDES

The total sputtering yield of FeS_2, CdS, and ZnS was measured using a profilometry technique. Each sample was bombarded for about 1-2 hours. The sputtering was with 3 keV Ar^+ in the raster mode of the ion beam operation in the SARISA apparatus. To calibrate these measurements, the same measurements were repeated for metallic targets of Fe and Zn. Also the total yield measurements were compared with TRIM calculations.

A.1 Sample Preparation

All the compound samples were single crystalline. The FeS_2 sample is a natural single crystal. ZnS sample was a polished sample provided by LLNL (Lawrence Livermore National Laboratory) and the CdS was polished by the manufacturer.

A.2 Profilometry Measurements

The profilometry measurements were done at Charles Evans & Assoc. The idea is simply to get a picture of the crater depth by moving a stylus over the crater and tracing the shape of the crater. The measurements of all of the samples were done at the two diagonals of the craters. The FeS_2 sample was sent back and the measurements were repeated in ten steps along each axis of the crater. For all the samples, two diagonal traces of the stylus were made. For the FeS_2 sample 20 traces were done, ten parallel to each side of the crater.

A.3 Analysis

The current on each sample was measured throughout the raster-sputtering. For samples, such as ZnS and CdS, in which charging occurs during sputtering due to the electronic nature of the samples, the reading of the currents changed throughout the measurements. To avoid introducing errors due to the nature of the samples, the current was measured through the Faraday cup before and after each measurement and that current was used for the calculation of the number of the primary ions impinging on the surface of the material. After the size of the crater was determined, the density of the material was used for finding the mass of the material removed and this number was converted to a total number of molecules removed for each primary Ar ion. This total yield

TOTAL YIELD MEASUREMENTS

Sample	This study*	Literature
Fe	2.4	3.1
FeS_2	1.1	----
Zn	14.5	15
ZnS	1.4	2.6
Cd	-----	20
CdS	2.8	---

Table A.1 *The samples were raster sputtered by 3 keV Ar^+ with 1 to 2 μA of current. The volume of the crater created by ion bombardment was then measured by profilometry to obtain the amount of material removed in sputtering. The uncertainty in these measurements is estimated to be about 20-30%.

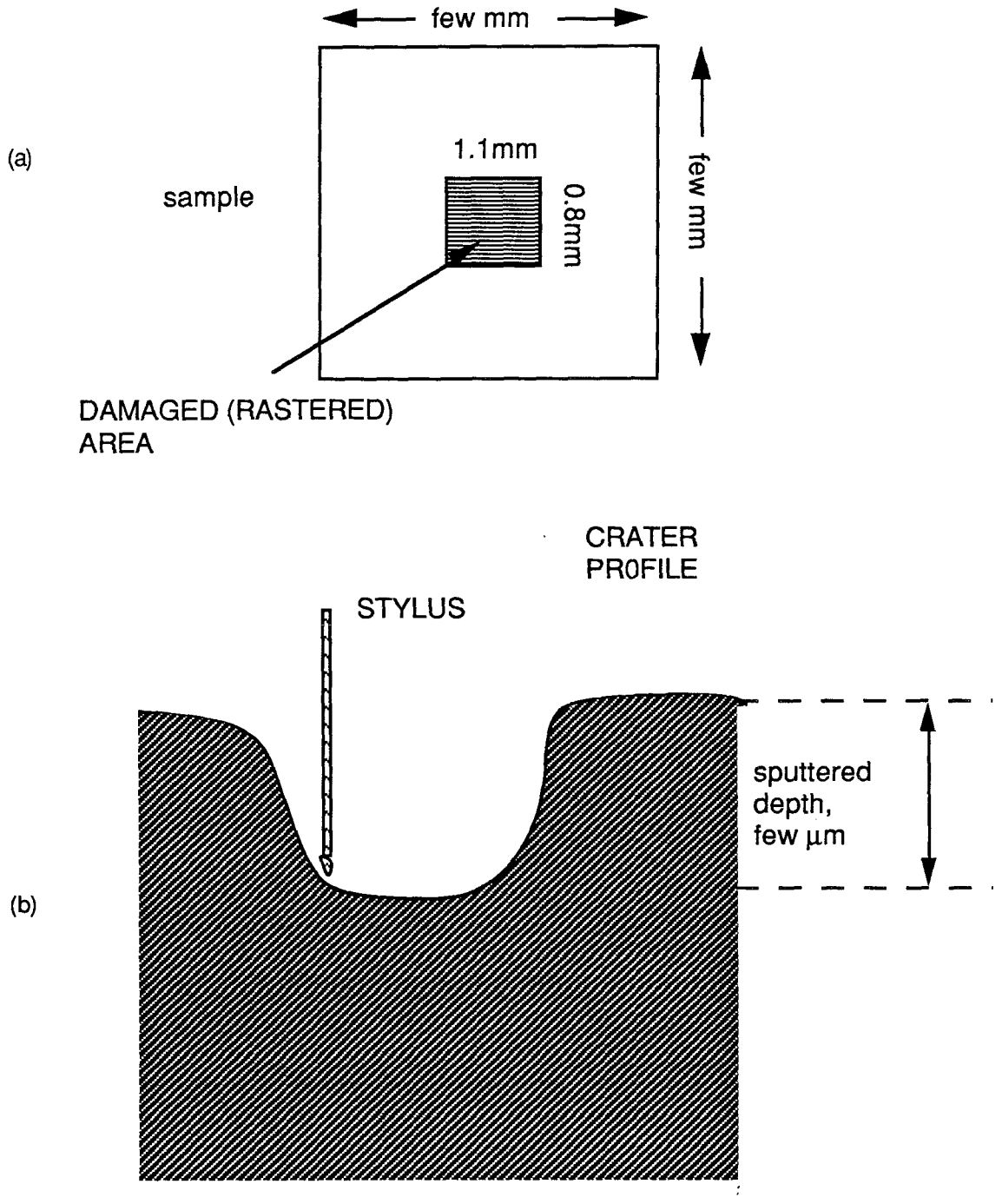

Figure A.1 a) Samples were sputtered with 3keV Ar+ ion beam, rastered over an area of approximately 1mm2. b) A Cross section schematic of the profilometry measurement of the sputtered sample.

therefore corresponds to the partial yield of metal from the compound material for all the metal sulfides examined here. For CdS and ZnS also this corresponds to the yield of the sputtered S. The values tabulated are estimated to have a 20% uncertainty.